Technische Universität München

Fakultät für Chemie

– Lehrstuhl II für Physikalische Chemie –

Electronic and Atomic Relaxation Processes in Pre-irradiated Rare Gas Matrices

Galyna Gumenchuk

Vollständiger Abdruck der von der Fakultät für Chemie der Technischen Universität München zur Erlangung des akademischen Grades eines

Doktors der Naturwissenschaften

genehmigten Dissertation.

Vorsitzender: Univ.-Prof. Dr. Johann P. Plank

Prüfer der Dissertation:

                1. Univ.-Prof. Dr. Vladimir E. Bondybey, Ph. D.
                   (University of California, Berkeley/USA), i.R.

                2. Univ.-Prof. Dr. Klaus Köhler

Electronic and Atomic
Relaxation Processes
in Pre-irradiated
Rare Gas Matrices

Electronic and Atomic

Relaxation Processes

in

Pre-irradiated

Rare Gas Matrices

Dissertation

Galyna Gumenchuk

To my Family

"The Frontiers of Knowledge (to coin a phrase) are always on the move. Today's discovery will tomorrow be part of the mental furniture of every research worker. By the end of next week it will be in be very course of graduate lectures. Within the month there will be a clamour to have it in the undergraduate curriculum. Next year, I do believe, it will seem so commonplace that it may be assumed to be known by every schoolboy."

<div align="right">

Cavendish Laboratory, Cambridge
"Principles of the Theory of Solids"

by

J.M. Ziman, F.R.S.
Melville Wills Professor of Physics in the University of Bristol

</div>

Contents

List of Figures

List of Tables

Introduction

When solid materials are exposed to high energy radiation, for instance, ultraviolet light or fast particle beams, a variety of defects may be produced, leaving part of the energy in the solid. If the energy of the incoming radiation, vacuum ultraviolet (VUV) light or electrons, exceeds the band gap energy E_g, atoms or molecules can be electronically excited or ionized, and localized charged defects may be produced in the solid. The presence of defects may change significantly material properties, and understanding of their formation, influence, and relaxation is, therefore, of a considerable interest not only for radiation physics and chemistry but also for material science.

Once the defects are formed, their relaxation can take place, resulting in a release of a part of the stored energy. This relaxation may be activated in a variety of ways, for instance, by heating, annealing of the solid, or by optical photons, and this forms the basis of the so-called activation spectroscopy. Studies of such relaxation processes may provide information about the properties and specific nature of the defects in the solid, and for this reason they have been extensively investigated in different classes of materials. Understanding of radiation-induced changes and relaxation paths are of high importance for development of new methods of material processing as well as for elaboration of effective methods of material protection from ionizing radiation in radiation physics and chemistry.

Rare-gas solids, atomic cryocrystals, represent, due to their simplicity, particularly suitable model of insulating materials. Because of their simple structure, weak inter-atomic forces, and strong electron-phonon interaction, they offer a suitable opportunity for studying radiation effects and different channels of the relaxation [16, 75, 158, 174].

The activation spectroscopy represents a powerful tool for investigations of relaxation in solids, with the the method of thermally stimulated luminescence (TSL) being the one most commonly used [169]. The TSL technique was employed for studies both of nominally pure [82, 83, 107] and doped [10, 30, 31, 40, 81, 150] rare-gas solids (RGS). The TSL may arise both from thermally stimulated reactions of neutral species (often called "chemiluminescence") and also from reactions of charged species.

Thermally stimulated mobility and recombination of neutral dopants or guests in matrices of inert elements is the well-known phenomenon, which is actively used in cryochemistry [2, 16]. Thermally induced reactions of neutral species (radicals)

1

were extensively studied in different matrices (see e.g. [2, 16, 19, 30, 38, 43, 81, 156]. Recent studies [134] of pre-irradiated rare-gas matrices revealed that thermally assisted chemical reactions may be involved in the relaxation cascades and influence charge dynamics.

While heating matrices previously exposed to ionizing radiation, another important process may take place, the thermally stimulated recombination of charge carriers, again often resulting in luminescence. Charge recombination obviously may release considerable amounts of energy, and the presence of charged defects has the strongest effect upon the properties of materials. In solid rare-gases, it was theoretically predicted [158] and experimentally found [58, 131, 132] that the positively charged carriers – holes – occur in the form of self-trapped rare-gas dimer ions, Rg_2^+. A large amount of data has been accumulated on impurity molecular ions in rare-gas solids. A detailed review of this subject is presented in review papers [16, 74] and monograph "Molecular Ions: Spectroscopy, Structure and Chemistry" (edited by T.A. Miller and V.E. Bondybey) [15].

Electrons in perfect RGS are essentially free [158], and they only can be trapped by some kind of imperfections (lattice defects or impurities with positive electron affinity). Gradual heating of pre-irradiated matrices results in release of electrons from successively deeper traps and in their promotion to the conduction band. Electrons mobilized in this way can then recombine with ionic centers of the opposite sign, resulting in the charge recombination luminescence. The energy of the charge recombination luminescence in RGS that is neutralization of intrinsic ionic rare-gas dimers Rg_2^+ by electrons falls into the vacuum ultraviolet (VUV) range. It is well-known as emission of the excited rare-gas dimers, Rg_2^* (the so-called M-bands) [50, 153, 158, 173].

Spectrally resolved TSL in the VUV range was studied both from atomic cryo-crystals pre-irradiated with X-rays in [82, 83], and from solids pre-irradiated with an electron beam in [128]. Based on TSL experiments, some analysis of photon yield in nominally pure and doped solid Ar was performed and parameters of the electron traps estimated [9, 82, 107]. However, analysis and interpretation of TSL data are hampered by its complex origin. As it was mentioned, TSL may accompany not only recombination of charge carriers but also thermally stimulated reactions of neutral species. As it appears from the above, in order to get reliable information on relaxation processes in pre-irradiated solids, a study of TSL should be complemented with measurements of thermally stimulated currents.

Another method for studies of ionic defect, the current activation spectroscopy, is based on monitoring of the charge carriers released from some traps and promoted to the conduction band. This can be registered as thermally stimulated conductivity (TSC) or alternatively as thermally stimulated exoelectron emission (TSEE). Experiments on TSC were performed with Ar solids doped with Au, Ag and O_2 [150]. The process of thermally stimulated exoelectron emission (TSEE) from solid into vacuum was found by our group in nominally pure solid Ar pre-exposed to low energy electron beam [133]. A use of TSEE method has some advantages in comparison to TSC activation spectroscopy. TSEE method does not require application

of strong electric fields and permits to (i) ascertain a sign of mobile charge carriers and (ii) differentiate between bulk and surface traps. Bearing in mind these benefits, we implemented TSEE complemented by TSL for the investigation of relaxation processes in cryogenic solids and charge centers stability [44]. This enables us to discriminate between reactions of neutral and charged species and find their interconnection. The special role of radiative processes in triggering relaxation posed the question on a part of photon-stimulated processes in pre-irradiated cryogenic solids.

Until recently, there was the only study (to our best knowledge) related to photon-stimulated relaxation processes in atomic cryocrystals [168]. In these experiments, samples were irradiated by pulsed synchrotron radiation. Between synchrotron pulses samples were exposed to laser pulses. Photoelectrons and photon-stimulated luminescence on the M-band of Xe and Kr were registered in these experiments. It was found that the characteristic lifetimes of photon-stimulated luminescence from solid Xe and Kr (1700 ns and 190 ns correspondingly) are very close to those for the spontaneous luminescence from Rg_2^* dimers on the well-known M-bands [158, 173]. The excitation spectra after laser irradiation were found to be identical to those for the spontaneous luminescence from atomic cryocrystals [158, 173]. However, the kinetics of photon-stimulated relaxation processes remained scantily understood.

The focus of our study is the final stage of relaxation, i. e., the processes occurring on completion of the irradiation, which are of special interest for understanding the radiation effects, dynamics of charge carriers, and stability of radiation-induced defects. As a typical simple solid we choose Ar matrix, pre-irradiated with low energy electron beam. The primary states of the relaxation cascades in the case under consideration are states of self-trapped or trapped holes (intrinsic ionic centers Ar_2^+) and trapped electrons, as well as metastable levels of guests. A stimulating factor for relaxation processes, as it was already mentioned, could be the heating of the sample or irradiation by visible light. Our study was concentrated primarily on poorly known photon-stimulated processes. Because the relaxation involves charges as well as neutral species, we combined different optical and current methods of activation spectroscopy: PSL, PSEE, TSL, TSEE. Our experiments, described in this Thesis, are published in [Appendix A: 2, 3, 5, 7–10, 13–15, 18, 19].

Our investigation was performed to contribute to the elucidation of some questions, where until recently the answers were missing:

1. On dynamics and kinetics of charge carriers under stimulation of pre-irradiated RGS with photon flux.

2. On the role of radiative transitions in relaxation cascades and possibility of their stimulation by chemiluminescent reactions. This question is closely related to the origin of some thermally stimulated peaks in TSL from pre-irradiated RGS, which was under discussion.

3. On interaction between atomic and electronic subsystems upon the relaxation of pre-irradiated solids.

4. In recent studies in our group, a new phenomenon was identified, an anomalous low temperature sputtering of particles from pre-irradiated solid Ar.

The presented Thesis is structured as follows: in the first parts, the theoretical background (Chapter 1) and methods of activation spectroscopy (Chapter 2) are described. The second part is devoted to the detailed investigation of the relaxation cascades in rare-gas solids. It consists of a description of our new experimental setup (Chapter 3), and presents results and their discussion (Chapter 4). The Sections 4.1 and 4.2 contain results of the relaxation cascades caused by photon source (laser light – "external" source for the sample – Section 4.1 and "internal" for the sample – Section 4.2). The Section 4.3 involves experimental evidence of the origin of thermally stimulated peak at 23K in luminescence and current curves. The last Section (4.4) is dedicated to the new phenomenon – anomalous low temperature sputtering from solid rare-gases, pre-irradiated with low energy electron beam. A brief summary completes the Thesis, giving a review of the main conclusions of the present work, as well as an outlook towards possible future studies.

Part I

Theoretical Background

1.1 Crystals structure

The rare-gas solids (RGS) belong to the simplest solids, forming regular, closely packed arrays of neutral atoms. The inert atoms, with closed shells of tightly bound electrons, are held together by weak Van der Waals forces, which act mainly between nearest neighbours in the lattice [85, 158]. The rare-gas crystals exist only at cryogenic temperatures, when the thermal energies kT become comparable to the weak interatomic interactions. The actual magnitude of these interactions depends on the size of the electronic shell and polarizability of the atoms being much stronger in xenon (54 electrons) than in helium (2 electrons). The theory suggests two alternative, closely packed and nearly isoenergetic possibilities for the RGS crystal structure: (i) the face centered cubic (fcc) and (ii) hexagonal (hcp), which are shown schematically in Fig.1.1 (fcc) and Fig.1.2 (hcp), respectively.
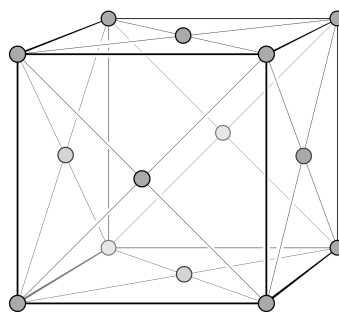
Figure 1.1: FCC lattice structure of solid Ar [84]

From the energy point of view, the difference between them is very small, but experiments indicate that under most conditions fcc is the preferred structure.

Interaction between atoms is described by the combination of attractive force at long ranges between the rare-gas atoms and arises mainly from induced dipole-dipole interaction and a repulsive force at short ranges (the result of overlapping
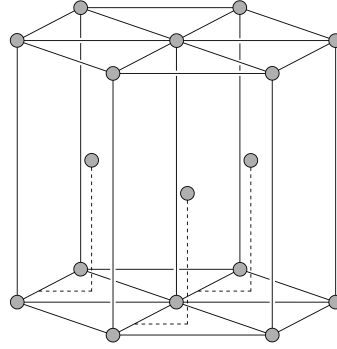
Figure 1.2: HCP lattice structure of solid Ar [84]

electron orbitals, referred to as Pauli repulsion). This interaction is often represented mathematically by the so-called Lennard-Jones potential [27]. This function describes relatively well dependence of the potential energy $U(r)$ on the interatomic separation r [27]:

$$U(r) = 4\varepsilon \left[A \left(\frac{\sigma}{r} \right)^{12} - B \left(\frac{\sigma}{r} \right)^{6} \right] \tag{1.1}$$

Here ε is the depth of the potential well, and σ is the equilibrium distance at which the repulsive and attractive forces in the gas phase compensate one another. The coefficients A and B take into account an interaction of surrounding atoms in RGS. For fcc lattice the value of $A = 12.13188$ and $B = 14.45392$ [49, 84].

The values of ε and σ for several RGS are given in the Table 1.1 [48,49,113,168]

	Ar	Kr	Xe
$\frac{a}{\sqrt{2}}$, [A]	3.758	3.992	4.337
ε, [meV]	10.3	14.2	19.4
σ, [A]	3.4	3.6	3.9

Table 1.1: Parameters of Lennard-Jones potential (ε and σ) for RGS. $\frac{a}{\sqrt{2}}$ is a distance between nearest beighbour [48, 49, 113]

Single rare-gases crystals of good quality can be grown under pressure by the method of Daniels et al. [29], for example. Large-grained polycrystalline bulk samples can be prepared by condensation at atmospheric or lower pressure [32]. The cells and gas handling system must be of ultrahigh vacuum construction to achieve pure samples by condensation.

The face centered cubic lattice is the stable structure for solid xenon, krypton, argon and neon [48, 85, 168]. In some cases of non-optimal crystal growth condi-

	T_m[K]	T_sb[K]	T_t[K]	a[Å]	ρ[g/cm^3]	β[10^4/K]	θ[K]	W_b[meV]
Ne	24.7	9 ± 0.5	24.55	4.46	1.4905	24.09	74.6	26.5
Ar	83.8	30 ± 0.5	83.81	5.32	1.7684	3.96	93.3	88.8
Kr	115.8	46 ± 0.4	115.76	5.65	3.090	4.08	71.7	123.2
Xe	161.4	60 ± 5	161.39	6.13	3.800	2.65	64	172.3

Table 1.2: Basic physical parameters of the rare-gas lattices. Melting temperature T_m, sublimation temperature T_sb, triple-point temperature T_t, lattice parameter a, density ρ, volume expansion coefficient β, Debye temperature θ, and binding energy per atom W_b are listed [48, 85, 173]

tion, a hexagonal close-packed phase may be found as a metastable admixture [6]. It has also been reported that the presence of impurities can result in formation of zones with hcp local structure [85]. For optical spectroscopy, it is often convenient to grow films on a cooled substrate by condensation from vapour. Films grown at a condensation temperature, which is higher than about 2/3 of the sublimation temperature T_sb, yield the best films, with fcc grains of about 100 nm size. The density of packing defects decreases as a function of increasing condensation temperature or film thickness. In contrast, films condensed at temperature lower than about $T_\mathrm{sb}/3$ exhibit grain size of about 10 nm, with a higher density of packing defects and evidence of the hcp minority phase [48].

The binding energy for an atom of RGS plays the most important role for defect formation.

Table 1.2 [48, 85, 173] summarises some basic structural and physical parameters of the solid rare-gas fcc lattices.

While the parameters in the above table give the static geometry of the lattice, actually the individual atoms are in perpetual, thermal motion around their idealized equilibrium positions. The physics of the lattice is determined by this thermal motion, which can be described in terms of phonons [172]. Because in the case of the RGS the elementary cell contains a single atom, the lattice phonon spectrum consists of only acoustic, but not optical branches [49]. This practically means that RGS are transparent for the infrared light (no IR adsorption occurs). The phonon spectrum of a lattice can be approximated by the so-called Debye model with the dispersion curves rising linearly with frequency up to some maximum value, so-called Debye frequency, or Debye cut-off. Brilouin zone in this case approximate also with Debye sphere of the same volume. Note that dynamics of the electronically excited states (excitons) in RGS strongly depends on their interaction with acoustic phonons.

1.2   Electronic states

All condensed rare-gases are insulators. In all of them except helium, the valence band derives from the highest occupied atomic p orbitals. The electronic structure

for solid Ar is illustrated in Fig.1.3 [49] where dependency of energy of the wave vector for different directions in Brillouin zone is shown. Consistent with weak binding, the valence band is relatively narrow as shown in Fig.1.3 and the hole mass is large. The conduction bands are wide and nearly free-electron-like (electrons are highly mobile). The energy gaps E_g are very large. Argon, neon and helium have gaps exceeding that of LiF, thereby claming title to the widest solid-state band gaps in the nature.
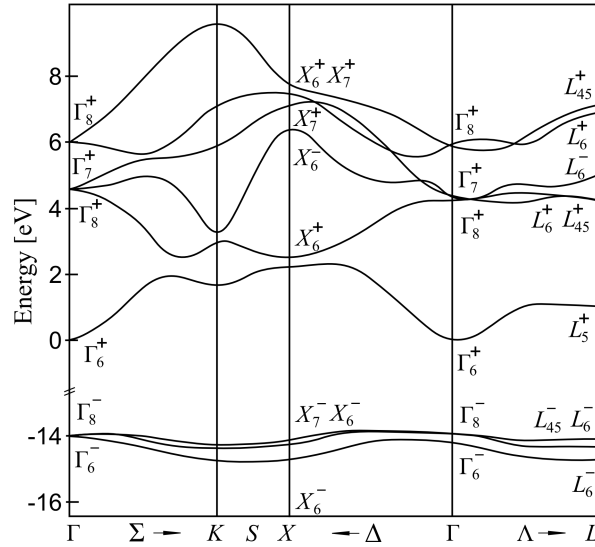
Figure 1.3: Energy band structure of solid Ar in the valence and conduction band region, including spin-orbit interaction. The structure is shown for different directions in Brillouin zone.

Parameters of the electronic band structure for all RGS are collected in the Table 1.3.

1.3 Excitons – excited electronic state

When RGS are excited with an energy little bit lower then E_g, excited electronic states within the energy gap are populated. The lowest excited electronic states in a regular lattice correspond to free excitons. One can present an exciton as a resonant transfer of atomic excitation through the lattice [172]. Frenkel model of excitons, elaborated by the example of solid Ar, considers an exciton with the wave-function, being mostly within a single unit cell [46]. Another presentation can be done in view of motion of bound pair – electron-hole (Wannier model) [170]. Differences of these models are the value of the radius of a bound pair (r_n) and the value of force, which binds electron with ionic host atom (g). Frenkel exciton is an exciton with a small radius (strongly bound exciton). Wannier exciton represents a weakly

	I[eV]	E_{g}[eV]	ΔE_{h}[eV]	Δ_{so}[eV]	χ[eV]	m_{e}^{*}	m_{h}^{*}	ΔE_{c}
								experiment
Ne	21.559	21.58	1.3	0.09	-1.3	0.83		
Ar	15.755	14.16	1.7	0.18	-0.4	0.48	5.3	2.35
Kr	13.996	11.01	2.3	0.69	0.3	0.42	2.1	2.2
Xe	12.127	9.33	3.0	1.3	0.5	3.35	2.1	2.0

Table 1.3: Some parameters of the electronic band structure of rare-gas solids. Ionization energy of the atoms, I, band gap at the Γ point E_{g}, valence band width E_{h}, spin-orbit splitting of the valence band edge Δ_{so}, electron affinity χ, effective mass of conduction electrons m_{c}^{*}, effective mass of valence holes m_{h}^{*} and width of electronic band ΔE_{c} are listed [49, 101, 122, 123, 152, 165, 173]

	Xe, $\Gamma(\frac{3}{2})$	Xe, $\Gamma(\frac{1}{2})$	Kr, $\Gamma(\frac{3}{2})$	Kr, $\Gamma(\frac{1}{2})$	Ar, $\Gamma(\frac{3}{2})$	Ar, $\Gamma(\frac{1}{2})$	Ne, $\Gamma(\frac{3}{2})$	Ne, $\Gamma(\frac{1}{2})$
g, [eV]	1.02		1.53		2.36	2.30	5.00	1.90
μ/m_0	0.37		0.40		0.48	0.47	0.56	0.55
R_1, [A]	3.18		2.49		1.83	1.87	1.17	1.19
ε_0	2.217	2.217	1.882	1.882	1.660	1.660	1.24	1.24

Table 1.4: Exciton parameters in RGS. Binding enerfy of exciton g, ratio of reduced exciton mass to free exciton mass μ/m_0, radius of the first excited state R_1, and static permittivity of the crystal ε_0. [49]

bound exciton of a large radius. In RGS, normally, one can describe an exciton as a combination of both types. The model of Frenkel exciton is more suitable for a light RGS as Ne or Ar and the model of Wannier exciton – for heavier RGS, such as Xe and Kr. For each model, an electron does not escape host atom completely, but stays slightly bound with the host atom. Binding energy g of excitons in RGS is given in a Table 1.4 [49].

A width of the lowest excitonic zone (B) can be represented by the simple expression [49]:

$$\frac{1}{2B} = \frac{1}{\Delta E_c} + \frac{1}{\Delta E_h} \tag{1.2}$$

where ΔE_c and ΔE_h are widths of the conduction and the valence band correspondingly. The calculated and experimental values of B are given in the Table 1.5 [49].

In accordance with ΔE_c and ΔE_h, one can expect that electrons in RGS, with an exception of He, are characterized by free-like behaviour. Emery and Song [39] found that for Ar and Kr, the free conduction electron state is a stable state at 0 K and at the melting temperature. In solid Ne, the free electron state is more stable than the electron bubble state at 0 K. So, the mobility of electrons in Ne, Ar, Kr and Xe are appeared to be high. In other words, it means that electrons are not self-trapped in

	Zone	Theory, B [eV]	Experiment, B [eV]
Xe	$\Gamma(\frac{3}{2})$	0.6	1.0
Kr	$\Gamma(\frac{3}{2})$	0.6	0.9
Ar	$\Gamma(\frac{3}{2})$	0.75	0.8
Ne	$\Gamma(\frac{3}{2}), \Gamma(\frac{1}{2})$	0.6	1.0

Table 1.5: Width of the lowest excitonic zone B (theory and experiment).

lattices of these RGS. In contrast to this, holes are self-trapped and their mobilities are 5 order of value lower than that of electrons. To illustrate the difference, a drift mobilities [cm^2/Vs] of carriers with charges $-e$ and $+e$ in solid (S) and liquid (L) condenced rare-gases are given in the Table 1.6 [26, 66, 94, 100, 151, 165].

	Temp.	μ_s^-	μ_L^-	μ_s^+	μ_L^+
Ne	25	600	•$1.6 \cdot 10^{-3}$	•$1.05 \cdot 10^{-2}$	•$1.6 \cdot 10^{-3}$
Ar	84	1000	475	•$2.3 \cdot 10^{-2}$	
Kr	116	3600	1800	•$4 \cdot 10^{-2}$	
Xe	161	4000	1900	$1.7 \cdot 10^{-2}$	

Table 1.6: Drift mobilities [cm^2/Vs] of carriers with charges $-e$ and $+e$ in solid (S) and liquid (L) condensed rare-gases. Mobilities, which exhibit thermally activated behaviour, are indicated by •. Data are given for solid and liquid at the triple point [26, 66, 94, 100, 151, 165].

Excitons can be self-trapped due to strong exciton-phonon interaction. Note that the phenomenon of self-trapping is of high importance for processes of electronically induced defect formation and desorption [14, 127, 158].

Mobile excitons or charge carriers cannot provoke lattice destruction immediately due to the fact that their lifetime at a lattice site $\tau_s \sim B^{-1}$ (B is the halfwidth of the corresponding band) is much less than the characteristic time of atomic displacement, $\tau_D \sim \omega_D^{-1}$ (ω_D is the Debye frequency). Self-trapping or trapping holes and excitons are in fact their localization within a volume of about that of a unit cell followed by an increase of excitation lifetime.

The role of the self-trappping mechanism in lattice defect formations will be discussed in more details in the next section.

1.4 Defects formation

Considering the key role of defects in relaxation processes, the short overview on the topic is given below. Two types of lattice defects will be discussed: pre-existing structural defects and radiation-induced ones.

1.4.1 Structural defects

Pre-existing structural defects are own defects of the lattice, formed during sample growing. If samples constitute the films, deposited on a cooled substrate by condensation from the vapour, such kinds of defects as vacancies, pores, interstitials, grain boundaries, leaps, twins appear in the sample. They are named primary defects of the matrix or initial defects of structure. For example, Ar matrix, deposited at 60K with special technique, contains minimum amount of primary defects, such as vacancies, and equilibrium concentration of such kind of defects at this temperature is $3 \cdot 10^{-7}$ (a. u.) [128]. Defects, named vacancy and interstitials, belong to the point defects of a matrix. In the Table 1.7 some parameters of point defects in RGS are listed.

	Ar	Kr	Xe
Crystal structure	fcc	fcc	fcc
E_d, Vacancy, [eV]		0.084 (experimental)	0.164 (calculated)
E_d, Interstitial, [eV]		0.321 (calculated)	0.582 (calculated)
E_d, Frenkel Pair, [eV]	0.5 (experiment)	0.435 (calculated)	0.746 (calculated)
E_{act}, Vacancy, [eV]	0.13 (experiment)	0.141 (experiment)	
E_{act}, Interstitial, [eV]	0.058 (experiment)		

Table 1.7: Energy of point defects creation E_d and activation energy E_{act} for RGS [168]

1.4.2 Radiation induced defects

Another kind of defects in cryocrystals are radiation induced defects, which are created under irradiation by light or particles of appropriate energy. Let us consider first a knock-on mechanism. It consists of shifts of atoms from the lattice site. For that, one has to transfer some energy to the lattice atoms that exceeds the threshold energy (E_D) of a defect formation. For each kind of the matrix, E_D can be calculated by the expression:

$$E_D = 4\varepsilon_c \tag{1.3}$$

where ε_c is binding energy. For example, in Ar matrix $\varepsilon_c = 80$ meV [158].

If a matrix is irradiated with electrons, the threshold electron beam energy, E_{th}, above which the lattice atom is displaced from the site due to the electron-atom head-on collision can be given as follows [90]:

$$E_{\text{th}} = 4\varepsilon_c \frac{(m + M_a)^2}{m M_a} \qquad (1.4)$$

where m and M_a are the electron and atom masses, respectively, ε_c is the binding energy. For Ar matrix the energy of the electron beam to create defects in Ar lattice via knock-on mechanism should exceed $E_{\text{th}} = 23.2$ keV.

Under irradiation by low subthreshold energy electron beam or VUV light, additional kind of defects can be created in the crystal via electronic subsystem. In this case, energy of electron beam is not high enough in order to directly displace the host atoms from their lattice sites. Defects in that case are created via excitation of electronic subsystem.

The electronic excitation energy relaxes by a numbers of radiative and nonradiative transitions followed by relaxation.

The nonradiative transitions are commonly followed by small (as compared to the lattice parameters) oscillations of a great number of atoms, i. e. by a heat release. There exists a special type of nonradiative transitions when a large displacement of a small number of atoms is accompanied by the creation of permanent lattice defects.

Note that radiative transitions of localized electronic excitation are of importance for defect formation.

1.4.2.1   Neutral defects formation

The electronically induced defects were first observed spectroscopically in neon matrix containing impurities of heavy RGS atoms [124, 125]. It was found that permanent lattice defects are created on excitation of both the electronic subsystem of an impurity atoms and own atoms of the matrix.

Let us consider in more details mechanisms of stable lattice defect formation. Defect formation means that own matrix atoms or impurity atoms are displaced from their regular sites to defect positions. The basis of the physics of this phenomenon is the transport of energy from electronic to atomic subsystem. The mobile band excitation (free electrons, holes, excitons) cannot create directly defects in the lattice because their lifetime (as it was mentioned in the Section 1.3) at a lattice site $\tau_s \sim B^{-1}$ (B is the halfwidth of the corresponding band) is much less than the characteristic time of atomic displacement, $\tau_D \sim \omega_D^{-1}$ (ω_D is the Debye frequency). On trapping, the situation changes essentially and τ_s becomes equal to the total lifetime τ_e of the trapped electronic excitation in the cryocrystal. If the energy released in the vicinity of the trapped excitation on its decay or transformation is higher than the threshold energy E_D, sufficient for the atom to be displaced to an interstitial position, a stable long-lived defect may be generated in the matrix. Note that only point defects are formed on electronic excitation trapping (via electronic subsystem). Thus,

the energy and time criteria of the electronically induced stable long-lived defects are [95]:

$$\Delta E > E_D, \text{ and } \tau_s \gg \tau_D. \tag{1.5}$$

From this point of view, localization of electronic excitation or self-trapping process are of high importance for electronically induced defect formation. Irradiation of RGS by electrons or photons with the energy less than E_{th} leads to excitation of electronic subsystem from the ground state. Strong exciton-phonon interaction in RGS results in self-trapping of excitons into atomic-type (A-STE) and molecular-type (M-STE) states. A self-trapping of excitons into the atomic and molecular states is accompanied by a considerable energy release to the lattice. Also, free band excitation, such as free excitons, can be trapped by an impurity or by own defects of the RGS due to breaking of translation symmetry. Atomic and molecular self-trapped and trapped states can be considered as short-lived defects which annihilate via radiative transitions. A part of them can convert to stable long-live defects in the lattice [130]. This kind of defects can stay in the matrix as long as no additional energy is transferred to the matrix via heating or photon irradiation. Since the energy of electronic excitaton is transferred into the kinetic energy of atomic motion over the unit cell, formation of point radiation defects (Frenkel pair, which consists of vacancy and interstitial) becomes possible in the bulk of the crystal.

Two channels of the exciton self-trapping in RGS are known: self-trapping into atomic type states (A-STE) and molecular type states (M-STE). It was found that in Ne matrix, excitons are self-trapped into the atomic centers [125]. Recently, biexcitons (excitonic molecules) in solid Ne were carefully investigated by [171]. The role of biexcitons in desorption from Ne films on a metal substrate by one-photon processes was analysed. In Xe and Kr solids, excitons are self-trapped into the molecular type M-STE states [79] and in Ar matrix – both types (A-STE and M-STE) of self-trapping states exist [128].

Schematic drawing of these processes is shown in Fig.1.4

Note that free excitonic states and self-trapped ones coexist in RGS under the condition that the relaxation energy of the lattice is larger than a halfwidth of the exciton band [49, 158, 174]. Potential barrier H_m separates states of free excitons from states of self-trapped excitons. The value of this potential barrier depends on the halfwidth of exciton band (B) and relaxation energy of the lattice (E_{rel}) and is given by the expression [48]:

$$H_m = \frac{4B}{27E_{\text{rel}}^2} \tag{1.6}$$

The Table 1.8 [48] gives the estimated values of H_m for atomic and molecular states of RGS.

Relaxation of excited states is also shown in Fig.1.4 [168] by FE (corresponds to free exciton luminescence), M, W and A lines. M line corresponds to the radiative transition of M-STE, so-called M-band. For Ar matrix, this band is situated at 9.72 eV and stemmed from the transition $^{3,1}\Sigma_u^+ \to {}^1\Sigma_g^+$ [49, 158]. W line indicates radiative transitions of the vibrationally hot M-STE (transition at 11.38 eV
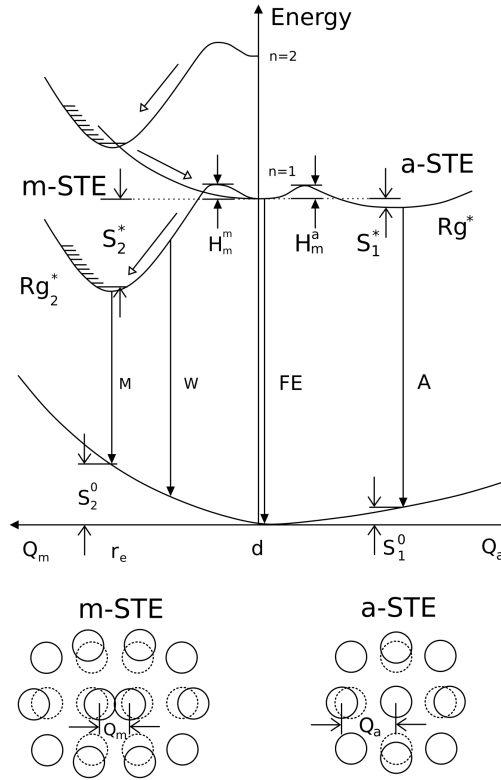
Figure 1.4: Schematic representation of potential curves (on the top of the figure) and geometrical structure (on the bottom) for molecular (left side) and atomic (right side) STE.

	Ar	Kr	Xe
H_m (A-STE), [eV]	0.01	0.03	(5.6)
H_m (M-STE), [eV]	0.002	0.01	0.02

Table 1.8: Potential barrier H_m separates states of free excitons from states of self-trapped excitons [48]

[78, 120, 126] in Ar). And A line (11,54 eV [126] in Ar) indicates an atomic STE radiative relaxation ($^3P_1 \rightarrow {}^1S_0$).

Note that, for example, a singlet lifetime of M-STE ($^1\Sigma_u^+$) is about few nanoseconds, and a triplet one ($^3\Sigma_u^+$) falls in a microsecond range [158]. Typical spectrum for solid argon under excitation of low energy electron beam is given in Fig.1.5 [158].

The mechanism of point defect formation via exciton self-trapping into A-STE states was proposed theoretically in [88] and developed in [47] and consists of a microcavity formation around the atomic excited center due to predominant repul-
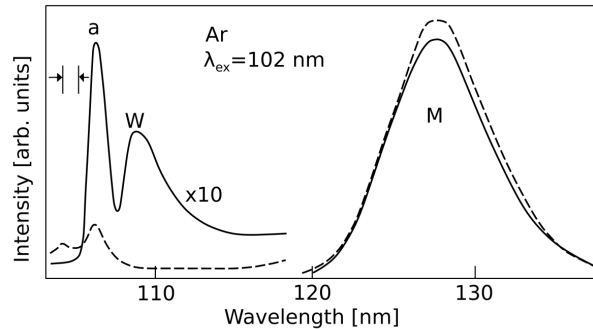
Figure 1.5: Luminescence of solid Ar under excirtation. The full curves are obtained from uncoated sample. The broken curves are from a sample, coated with a thin layer of Ne. Bands labelled 'a' and 'M' are from A-STE and M-STE in relaxed excited states. The band W is attributed to vibrationally hot M-STE at the surface [158].

sive forces. The occurrence of a bubble around a conduction electron or an exciton is associated with negative electron affinity in condensed phases of the light RGS. The value of electron affinity is given in Section 1.2 [Table 1.3]. Electron affinity E_a of a solid designates the vacuum energy level relative to the conduction band minimum. A negative value of E_a means that a conduction electron will experience a finite increase of kinetic energy when it exits the surface. In a broader context, the surface could be internal, such as the bubble interface. In this case, electron affinity (absolute value) will not appear as kinetic energy, but as the repulsive part of the distortion energy to create the bubble.

A local deformation of the lattice around the microcavity relaxes through the formation of Frenkel pairs. This mechanism is typical for light RGS with negative electron affinity. Experimental evidences of defect formation, induced by the exciton self-trapping into A-STE states, were presented in [124, 125, 130, 139]. In more details, A-STE states are associated with the $^3P_1 \rightarrow {}^1S_0$ and $^1P_1 \rightarrow {}^1S_0$ transitions. Their spectrum consists of two components: high-energy component A_2, stemmed from A-STE in a regular lattice, and a low-energy component, A_1, which is associated with structural defects. The pronounced enhancement of the defect related A_1 component was found while A_2 component associated with the A-STE in the regular lattice remained unchanged. Such a behavior clearly indicates the formation and accumulation of the permanent lattice defects generated via self-trapping of excitons into A-STE states [124, 125, 130]. The elastic deformation is followed by the primary "bubble" formation because of the negative electron affinity of solid Ne [2] and hence prevailing repulsive forces between the excited atomic center and surrounding atoms occurs in a short-time scale. High local stresses in the lattice can induce some plastic deformation during the lifetime of the excited state. The analysis of possible plastic deformation [47] revealed the microscopic structure of the exciton-induced defects formed via A-STE in solid Ne. The structure appeared to

present the second-nearest neighboring vacancy-interstitial pair. The experimental study of the exciton induced defects, performed using activation spectroscopy methods [59], confirmed the model suggested above. An important feature of the model is the formation of defects in an excited state.

In the case of exciton self-trapped into M-STE states, relaxation energy is transferred to the surrounding atoms at both stages – in the excited state of the M-STE and in the ground state by the reaction:

$$R^0 + R^*_{\text{exciton}} \rightarrow R^*_2 + \Delta E^*(\text{M-STE}) \rightarrow h\nu(R^*_2) + R^0 + R^0 + \Delta E^0(\text{D}) \qquad (1.7)$$
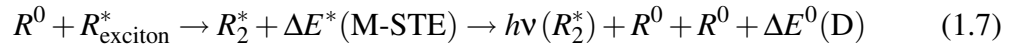
In the specific case of solid Ar, the energy release during the M-STE vibronical cooling $\Delta E^*(\text{M-STE})$ is about 1.25eV [49, 109] that is higher than the binding energy per atom in solid Ar (80meV [158]). After the radiative transition ($h\nu(R^*_2)$) of the relaxed M-STE to a repulsive part of the ground state potential, the excess energy $\Delta E(\text{D}) = 1.1$eV is shared between two dimer atoms, in other words, there appear the two "hot" atoms with a 0.55eV kinetic energy available for the defect creation. In accordance with this consideration, the mechanisms of exciton-induced defect creation can be classified as an "excited state' mechanism and a "ground state" mechanism [125, 142].

The self-trapping, occurring during the lifetime of the excited state, results in the formation of a molecular dimer aligned along the $\langle 110 \rangle$ crystallographic directions. This stage followed by the M-STE formation in the on-center position is shown in Fig.1.6 (a and b). The formed center resembles a "dumb-bell" configuration of
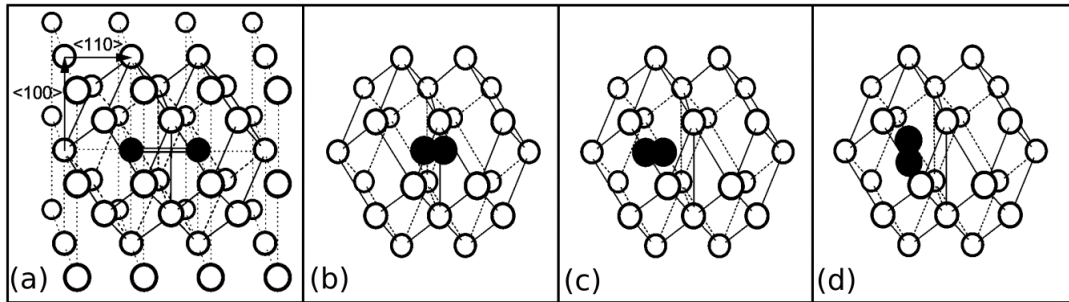
Figure 1.6: Scheme of the "excited state" mechanism of Frenkel pair formation, induced by exciton, self-trapping into M-STE state.

the interstitial atom. Its displacement along the $\langle 110 \rangle$ direction to an off-center configuration (position c in Fig.1.6) cannot stabilize the center. It was shown [33] that the split $\langle 100 \rangle$ "dumb-bell" form is the only stable form of the interstitial atom in the RGS lattice. One can assume that the short-lived defect of the off-center configuration can be stabilized by the reorientation of the dimer axis to the $\langle 100 \rangle$ direction (d in Fig.1.6).

The Frank-Condon transition of this dimer to the ground state will correspond to the transition of the molecular center to the permanent defect level with almost

no change in the interatomic distance. The energy, needed for the reorientation, can be released in the lattice in the course of the vibronic relaxation. As the theory shows [68], in a system with a strong local vibration, the energy release proceeds in a jump-like multiphonon process. It seems to be the case for the M-STE relaxation that offers the basis of the development of the "excited state" mechanism.

The model of defect creation by the "ground state" mechanism is not so straightforward as it may seem at the first sight. The matter is that during self-trapping, Rg atoms are brought closer together, displacing along the $\langle 110 \rangle$ direction, as shown in Fig.1.6b. However, there are no stable interstitials of the "dumb-bell' configuration aligned along the $\langle 110 \rangle$ crystallographic direction [33]. Recent theoretical studies [103, 104] showed that in the fcc lattice of RGS, the weak coupling between close-packed atomic rows and the crystal matrix may give rise to an interstitial atom of a specific configuration – a smeared clump, called a crowdion. The vacancy also becomes delocalized, forming a smeared sparse region (anticrowdion).

1.4.2.2 Charged defects (STH)

To create charge centers in RGS, an excitation energy should be higher than ionization energy E_g. It was shown [36] that electron-hole pairs (Ar^+–electron) are created more efficiently under low energy electron beam with energy of about 120 eV. Ionisation cross-section σ for solid Ar is shown in Fig.1.7 [36]
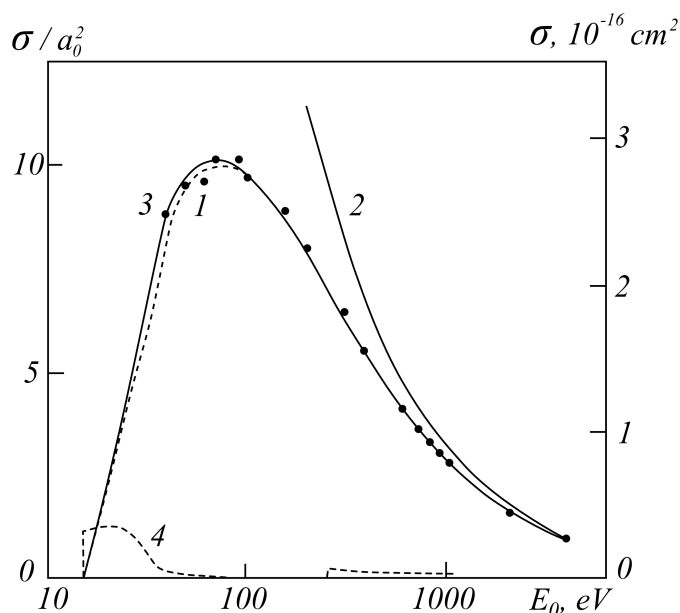
Figure 1.7: Ionisation cross-section of Ar atoms with electrons (1 – experimental value, 2 – calculated value, according to Born approximation, 3 – calculated value, assuming a semi empiric approximation [36] and 4 – Ionisation cross-section of Ar atoms with photons [97].

Rare-gas solids He, Ne, and Ar have negative electron affinities because the filled-shell rare-gas atoms represent net repulsive pseudopotentials for a conduction electron. For light RGS with negative electron affinity, only point defect, such as vacancy or pore, can play a role of own matrix trap for an electron. Besides this, electrons can be trapped by guest atoms with positive electron affinity – so-called "electron scavenger", such as oxygen or, taking into account polarization energy of about 1 eV for argon matrix, nitrogen. In the case of positive electron affinity, a question is steel not clear – of which kind of traps electrons survive in.

From the beginning, the theoretical treatment of self-trapped holes in rare-gas solids, introduced by Druger and Knox [34], was based on the model "molecule in a crystal". They considered self-trapped holes in solid argon, using the potential energies obtained for Ar_2^+ in free space. By minimizing the total energy of Ar_2^+, embedded into the lattice with regard to various lattice relaxations, they found that stability derives almost entirely from the molecular bond between the two atoms and that the equilibrium bond length is almost unchanged in the crystal. This work also included an examination of the self-trapped hole in Kr and Xe.

More recent calculations, based on another model [158], yield similar results. In this model, the energy of the perfect crystal, containing no hole, is represented by the usual form of lattice energy with terms in quadratic or higher order for lattice point displacements. The total energy of a crystal, containing a hole, is the above energy minus the energy of the missing electron. Additional terms take into account the energy change due to the relaxation of the lattice points from the perfect crystal equilibrium position and the polarization energy due to the presence of a charged particle in the lattice. The energy of the total system is a function of two variable parameters: the hole wave function and the lattice relaxation. It was found that the lattice relaxation can be taken as a variable parameter to minimize the total energy because the extension of the hole wave function beyond two atoms is small and can be neglected for the ground state. Using a representation of the hole simpler than that of Druger and Knox, Song [157] and Umechara [166] have studied self-trapping holes and reached similar conclusions.

Summarising a representation given above, one can make a conclusion that in condensed rare-gases heavier then helium, holes self-trap in the configuration of rare-gas dimmer, R_2^+, due to strong interaction with phonons [49, 158]. In another words, hole Ar^+ can be caught by host atom of Ar with creation of Ar_2^+ (STH) within 10–12sec. Self-trapped hole Ar_2^+ is localized in the lattice and can be considered as charged defect of RGS matrix.

Research group, headed by Prof. V.E. Bondybey at the Department of Chemistry of TUM, performed a series of experiments [58, 132] that confirmed that: (i) stable ionic centers in the RGS lattice are formed in a configuration similar to the molecular ions Rg_2^+, and (ii) trapped holes resemble that configuration of the dimer ions. The influence of the lattice defects, which act as traps for charge carriers, was examined and condition of the stability of ionic centers was discussed. High thermal stability of charged centers (STH) of solid Ar at low temperatures was found [133].

1.4.3 Defects stability. Annealing.

The term "annealing" is used to denote the process of disappearance of defects. It thus occurs in materials containing defects in concentration larger than the thermodynamic equilibrium concentration. Thermodynamic driving forces reduce the concentration of the defects to the equilibrium concentration characteristic of the material at some fixed temperature [158]. An excess of defects disappears because: (i) the defects become mobile. They migrate to surfaces, grain boundaries, they recombine with their counterpart (for instance, an interstitial recombines with a vacancy) or they form new defects by association between themselves or with other types of defects (or impurities); (ii) they dissociate when they are complex. Each of the processes: migration, recombination, complex formation and dissociation, is characterized by an activation energy. For example, for argon matrix, Frenkel pairs are annealed efficiently at 15 K and activation energy is about 30-80 meV [4].

Defects in rare-gas solids are metastable. As long as we will keep temperature low enough (up to 10 K for Ar matrix, for instance), as long defects stay immobile. The stability of a vacancy-interstitial pair depends on the elastic and Coulomb interactions that exist between the elements of the pair [90]. Increasing temperature, one can stimulate annealing of the defect. For the Frenkel pair, it means that interstitial goes back to the lattice site and vacancy disappears. If electron was trapped by this vacancy, it gets freedom and again can move throw the crystal. In this way, positively charged defects (STH) can be neutralised by recombination with electrons. Note that the electron in rare-gas matrix has higher mobility than the hole by factor of 10^5 [158]. In another words, one can improve crystal structure under heating, reducing amount of defects toward to the thermodynamic equilibrium concentration.

1.5 Desorption as surface analogy of defects formation via electronic subsystem in the bulk of the sample

The ejection of atoms or molecules from the surface of a solid in response to primary electronic excitation is referred to as electronic sputtering or desorption induced by electronic transitions (DIET). Primary electronic excitation may be stimulated either with charged energetic particles or with photons.

First, we shall summarize the experimental situation briefly. Sputtering of atoms and molecules from the surface of solid Ne, Ar, Kr, and Xe has been studied under excitation by energetic electron or ion beams [76, 110, 154, 160]. Particularly, desorption of Ar has been investigated upon excitation by ions [119, 120], electrons [25, 37] and photons [41, 87]. In most experiments [37, 41, 119], the total yield of neutral atoms was measured. The partial contribution to desorption of excited atoms was singled out in Ref. [25] and [87], where it was shown to be directly stimulated by the primary excitation of excitons. It was found that both surface and bulk

excitons take part in this process [87].

Let us consider a short description of sputtering mechanism. The sputtering process consists of four steps: (i) primary excitation, (ii) electronic relaxation into electron-hole pairs, (iii) energy transport to the surface, (iv) ejection process. In an insulator, electronic relaxation processes create a certain number of free and bond electron-hole pairs. A free pair consists of a hole in the valence band and an electron near the bottom of the conduction band. Their motions are uncorrelated in the case when Coulomb interaction is negligible. If the motion is correlated via stronger Coulomb interaction, the pair is bound and named exciton. The average energy E, needed to create one electron-hole pair, is proportional to the band-gap energy of the respective material [121]. Then this energy can be transferred to the surface of the sample, yielding the sputtering. An important condition of the electronic sputtering or DIET is localization of electronic excitation as in the case of electronically induced defect formation.

Main channels of energy localization in RGS are self-trapping of excitons and self-trapping of holes (STH) or formation of the intrinsic ionic centers. As it was described in Section 1.4, excitons in RGS may be self-trapped into atomic type (A-STE) and molecular type (M-STE) states. Relaxation of A-STE, M-STE and STH goes with energy excess, which can be spent on defect formation in the bulk of the sample or on a sputtering of host atoms (desorption) if process occurs on the surface. In view of this, the models of DIET, suggested above, are based on relaxation of these three types of localized electronic states in RGS.

"Cavity-ejection mechanism" and "dissociative-recombination mechanism" were suggested to explain the sputtering phenomenon.

"Cavity ejection mechanism" was suggested for the first time by Coletti et al. [24]. This mechanism is connected to atomic self-trapped excitons (A-STE type) and can be described by the reaction:

$$R^* \rightarrow R^* + \Delta E^*(\text{A-STE}) \rightarrow h\nu(R^*) + R^0 + \Delta E^0 \tag{1.8}$$
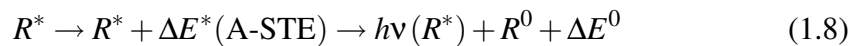
where R^* is excited atom or exciton, R^0 – atom in ground state, $\Delta E^*(\text{A-STE})$ is the energy release under exciton self-trapping into A-STE and ΔE^0 – the energy release at transition to the ground state, $h\nu(R^*)$ denotes the radiative atomic transition.

This mechanism prevails in solid Ne and partially in solid Ar, where repulsion due to negative electron affinity is strong enough, resulting in a cavity formation around an excited atom [174].

The radius of the cavity is 0.4 nm for the Ne [88], which has to be compared to the nearest-neighbour distance, 0.316 nm. Trapping can occur either in the bulk or at the surface of the sample, as it shown in Fig.1.8(a). At the surface, short-range repulsion is no longer spherically symmetric, like in the bulk, but effectively directed outside the surface, resulting in the ejection of the excited atom [174]. Excited atoms can be ejected due to relaxation of both surface excitons and bulk excitons trapped into the A-STE configuration near the surface.

The second mechanism of atom ejection in the ground state, illustrated by Fig.1.8(b), is connected to molecular self-trapped excitons (M-STE). This type of
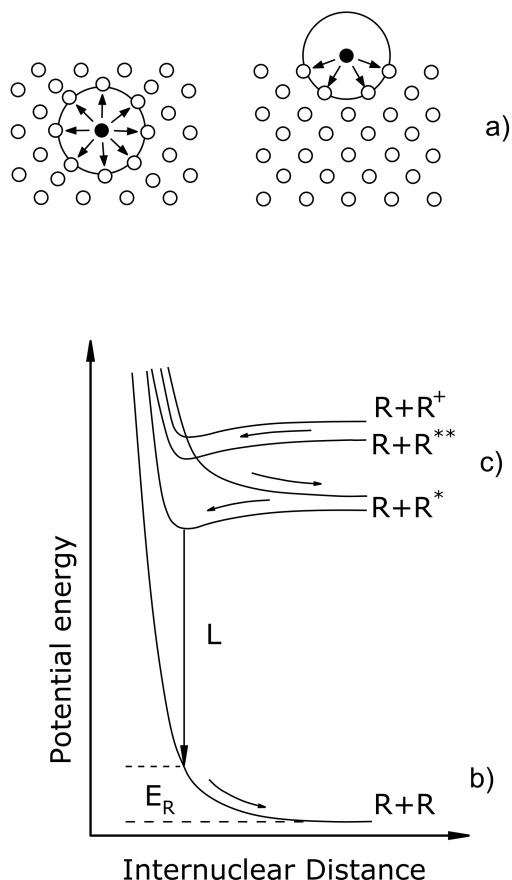
Figure 1.8: Schematic presentation [174] of
a) an A-STE formation cavity and how it leads to ejection of an excited atom.
b) molecular-type desorption model.
c) dissociative recombination model, leading to the ejection of fast excited atoms.

excitons exists mostly for heavy rare-gases such as Xe, Kr and partially Ar. In general, M-STE is equivalent to a rare-gas eximer molecule embedded in a matrix of the same kind of atoms. An eximer has a strongly repulsive ground-state potential energy curve and bound excited states. Excimers are well-known from the gas phase [22]. The M-STE decays radiatively, yielding emission bands according to the reaction:

$$R^0 + R^* \to R_2^* + \Delta E^*(\text{M-STE}) \to h\nu\left(R_2^*\right) + R^0 + R^0 + \Delta E^0(\text{D}) \qquad (1.9)$$
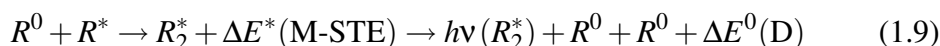
the symbols are similar to those used in (1.8).

For RGS, this emission falls into VUV range (so-called M-bands). The radiative decay terminates at the repulsive part of the ground state potential energy curve. Therefore, the two atoms, constituting the eximer, are accelerated after radiative decay, and the potential energy in the ground state E_R (in Fig.1.8(b)) is converted into the kinetic energy.

The third possibility (Fig.1.8(c)) for the desorption is dissociative recombination of self-trapped holes (R_2^+) with electrons, which is accompanied by the energy release $\Delta E(\text{DRec})$, which may result in the desorption of excited atoms and atoms in the ground state according to the reaction:

$$R^0 + R_{\text{H}}^+ \rightarrow R_2^+ + \Delta E^+(\text{STH}) \rightarrow R_2^+ + e \rightarrow R^0 + R^* + \Delta E(\text{DRec}) \qquad (1.10)$$
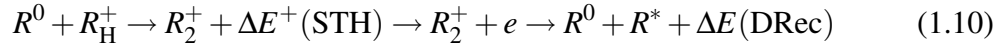
It is essential that in reactions (1.8), (1.9), (1.10), the energy is liberated at the localization stage as well as at the annihilation of the localized state. According to the reactions (1.9) and (1.10), molecules R_2^* and R_2^+ ions can also be the products of electronically induced desorption. Sputtering of eximers Ar_2^* and Ne_2^* was observed spectroscopically by emission from plum of desorbing species under the sample surface in Refs. [120] and [67, 129] correspondingly.

For desorption mechanism, the question of energy transfer from the bulk to the surface is quite important. In sputtering experiments, information concerning the transport of electron-hole pair to the surface is obtained, measuring the sputtering yield as a function of the sample thickness. A variety of experiments have been performed with different projectiles (protons, heavier ions, electrons) [77,86]. It was found that with increasing of the sample thickness d, the yield of desorbing particles increases until saturation is reached at rather large value of d. This is a proof of the important influence of energy transport to the surface. It was accepted [174] that the transport arises from diffusion of electron-hole pairs. Schou [149] compared the diffusion length l_0 obtained with different methods like sputtering, photoelectron and photoluminescence spectroscopy [153, 173]. Severe discrepancies were found. They were attributed to the influence of sample preparation conditions and their quality. For solid Ar the diffusion length was about 21 nm [77, 173]. For solid Xe and Kr, error of l_0 reaches a 3rd order of magnitude (l_0 varies from 30 nm [149] to 1000 nm for solid Xe) because the dynamics of excitons of these RGS dramatically depends on the sample quality.

A much more detailed insight into the microscopic mechanism has been obtained with a tuneable photon source for excitation purposes. In the first experiment of this type, P. Feulner et al. [41] measured the desorption yields for rare-gas atoms, desorbed from monolayers and multilayers of Ar and Kr on Ru (001) as a function of photon energy. Experiments performed by Zimmerer's group with synchrotron radiation, that were summarized in [174], contributed a lot to understanding the excitonic mechanisms of DIET.

A highly informative (as to DIET) mechanisms appeared to be time-resolved mass-spectroscopy methods. Employing them, it was found that the kinetic energy of ejected species ranges from 0.1eV to 0.8eV, that is much higher than thermal energies. The energy spectra of ejected neutral atoms under keV electrons and He^+ beams have been presented for Ar, Kr, and Xe by O'Shaughnessy et al. [154]. The spectra, exhibited two well-defined peaks for all RGS, are studied.

Let us discuss in more details the data on DIET from Ar with a focus on the higher energy peak. The energy distributions have either a peak around 0.5eV [160]

or a shoulder [110, 154]. The peak is due to excimer emission, $Ar_2^* \left(^{1,3}\Sigma_u^+ \right) \rightarrow Ar_2 \left(^1\Sigma_g^+ \right) + h\nu$, followed by its decay with the 1.1eV energy release, which is sheared between two atoms as shown in Fig.1.9 [129]. Since their energies are much larger than the cohesive energy (80 meV), a low energy collision cascade is generated, resulting in ejection of particles.
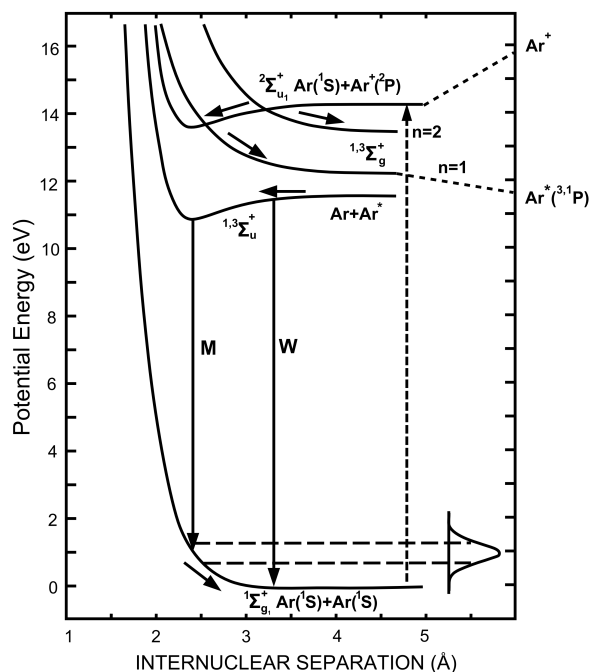
Figure 1.9: Potentials for Ar-pair in solid Ar. The luminescence bands M and W are indicated. The W band is an ejected dimmer [118]. Vertically dashed line indicates excitation to a hole state. The solid arrows indicate a relaxation pathway.

At the end of this Section, we should mention high-resolution kinetic-energy distribution curves of metastable Ar atoms, combined with angular distribution analysis, following excitation of a monocrystalline Ar (111) film condenced on Pt (111) [91, 92]. Primary excitation was performed with monochromatic slow electrons (14.5eV). A fine structure of the kinetic-energy distribution with several maxima was identified and analysed. The most energetic maximum (345meV) has a very broad angular distribution and originate from the "dissociative-recombination mechanism".

CHAPTER 2

Activation Spectroscopy

2.1   Introduction

What is meant by "activation spectroscopy"? Exposure of solids to a high energy, vacuum ultraviolet (VUV) light or charged particles results in part of the energy being absorbed by the matrix. While some of this energy is rapidly reemitted or dissipated in the solid as heat, part of the absorbed energy is stored in the solid. This energy can then be released for instance by subsequent heating of the sample, or by its irradiation by photons. The methods of activation spectroscopy are based on such a release of energy stored in the pre-irradiated solids. These methods are generally recognized as a useful tool for investigations of different classes of materials, and the area of activation spectroscopy has developed into a very lively field and topic for studies of cryogenic solids. The interest in this problem is motivated both by questions of fundamental interest, as well as by practical applications, such as dosimetry, cryochemistry, astrophysics etc.

The specific properties of the rare-gas solids, such as their small binding energies and simple electronic and crystal structures make them very suitable for studies by the methods of activation spectroscopy, and offer a good opportunity for gaining insights into various phenomena common to solids, and gaining their understanding on a microscopic, molecular level. This understanding is then valuable in helping in the development of promising technical applications in areas such as solid-state photochemistry, laser techniques, radiation physics, and material science. A further advantage of the rare-gas solids for studies of both charge carriers and neutral species (radicals) are their very large band gap energies E_g, especially in Ne (E_g = 21.58 eV) and the resulting transparency of these materials over a wide spectral range, and the location of the lowest excitonic levels of RGS at high energies, in the VUV range. This advantage makes it possible to produce in the lattice a variety of ionic species with ionisation potentials below the onset of ionisation continuum of the matrix and of easily observable neutral fragments (radicals). The transparency of rare-gas matrices from the far infrared (FIR) to the vacuum ultraviolet (VUV) makes it easy not only to produce, but also to detect these species spectroscopically

27

in absorption, but provides also a very favourable medium for their observation by means of stimulated emission.

Intensive spectroscopy studies have yielded a lot of new information about configuration and chemistry of a number of ionic guests in cryogenic solids, their electronic structure and dynamics. A large amount of data has been accumulated on impurity molecular ions in rare-gas solids – the widest band gap insulators. A detailed review of this subject is presented in review papers [16, 74] and monograph "Molecular Ions: Spectroscopy, Structure and Chemistry" (edited by T. A. Miller and V. E. Bondybey) [15].

Until recently, however, little was known about trapped electrons in RGS matrix. The main question is which kinds of traps exist in the matrix for electrons. Activation spectroscopy is very convenient tool to clear up this question. A combination of current and luminescence measurements gives a possibility to separate processes which involved charged and neutral species. Charged centers formed by rare-gas atoms themselves in the lattice are intrinsic ionic centers. Note that the self-trapped holes (STH) are in fact intrinsic ionic molecular centers formed in the lattice because of strong electorn-phonon interaction. They are also of great importance in view of the prominent role of holes in electronically induced phenomena like the desorption of atoms and molecules from the surface of solids and the lattice rearrangement followed by a production of point defects [35, 71, 98, 108].

Activation spectroscopy is the most adequate method of studying ionic states as well as neutral ones because this technique provides us with direct information on the electronic structure and dynamics of these species and also defects structure. In this chapter, we describe shortly an activation spectroscopy technique and method of analysis of underlying phenomena with an accent on the photon-stimulated specroscopy.

2.2   Photon-stimulated current spectroscopy and luminescence. Method of analysis.

First, let us consider a photon-stimulated relaxation path, which consists of exo-electron emission and radiative recombination of positively charged species with electrons. To get knowledge about phenomena underlying the exoelectron emission as well as luminescence, we need to analyse trapping parameters for charge carriers within the forbidden band.

The analysis of defect energy levels in insulators and semiconductors has received considerable attention [20, 65, 80, 89], with possibly the greatest effort being concentrated on evaluating the energy and the concentration of traps in these classes of materials. The method which has been most widely adopted has been that of thermally-stimulated current analysis for semiconducting materials [105]. In general, however, considerable difficulties are encountered in evaluating trapping parameters from thermally stimulated data and many different analytical treatments

have been developed [106].

The technique which we call photon-stimulated current spectroscopy (PSC) is the optical equivalent of thermally-stimulated one and can be used to evaluate the trapping parameters such as characteristic lifetime for the process of detrapping, trap energies, densities and cross-sections of interaction charged species with photons from the experimental data.

2.2.1 Measurement methods

The technique involves first of all cooling of the sample to a low temperature and then filling the traps with, for example, photo-injection, or band-to-band photo-excitation, or irradiation with charged particles. Important for this case is that we should cool the sample to the temperature which is low enough to inhibit thermal release of the charge carriers from the traps. Another part of the technique consists of (i) system for photon stimulation relaxation (laser source) of the pre-irradiated sample and (ii) system for electron collection and detection (including a PC registration). One can register either simply current in the sample or emission of charge carriers from the sample in vacuum.

For the measurements of photon stimulated luminescence, we can also use a cooling system and a system for the sample excitation. This part of experimental devices allows to excite an RGS sample at low temperature. In addition, we have to use a system for photon stimulated relaxation of the pre-irradiated sample and a monocromator or a spectrometer with photo-multiplier connected to a PC for registration of light emission. One possibility is a registration of total yield of the photon stimulated luminescence. But the most informative way is to register spectrally resolved relaxation emission. For example, if one choses a line of neutral oxygen or nitrogen (for doped RGS samples), it is possible to get information about characteristic lifetime for these lines in pre-irradiated RGS matrix. Or selecting a line of luminescence of self-trapped excitons, one can analyse characteristic lifetime for the relaxation processes formed by this irradiation.

2.2.2 Method of analysis

In our investigation, we consider the relaxation process which consists of several paths. One of them is a photon-stimulated path. It includes first of all detrapping of electrons from their traps. It leads to a direct escaping of charged particles from the sample or their recombination with charged centers of opposite sign. In the following analysis, we consider N_c – concentration of released charged particles (electrons in our case). If they will escape the sample directly, we will register a photon-stimulated current and one can analyse a decay curve according to the considered model. The photon-stimulated recombination reaction of positively charged species with released from their traps electrons is a concurrent with exoelectron emission process and leads to the VUV luminescence.

Because intensity of reaction of recombination yielding a VUV luminescence also depends on the concentration of free electrons (N_c), we can take the same method for the analysis and extracting the characteristic lifetime of the recombination luminescence from the decay curves.

For the analysis of PSC we consider the most simple model illustrated in Fig. 2.1

Conduction band

E_{t}

Valence band
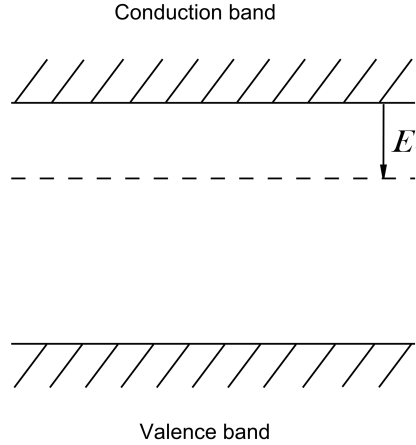
Figure 2.1: Schematic presentation of a band model for solids with a single trap level at E_t marked with a dashed line

We have a single level of trapping centers (electron traps) at E_t below the conduction band (CB). The density of these traps will be N_t, their capture cross-section S_t and n_t will represent the density of these traps which are occupied by electrons. The analysis of the energy of the traps is straightforward and can be obtained directly from the spectrum. In general, for wide-band materials, the trap depth corresponds to the long-wavelength cut-off of the peak, whereas in narrow-band materials, the peak of the spectrum corresponds closely to the trap depth. But in order to evaluate the density of the traps and their capture cross-section an auxiliary experiment is required.

For the evaluation of characteristic lifetime of the process of detrapping after deposition of the sample under electron bombardment at low enough temperature, one have to measure a time decay of the current intensity. It has an initial sharp rise in conductivity followed by a much slower decay as the traps are emptied. Because intensity of current is proportional to the density (n_t) of free-carriers (electrons) one can consider a decay curve for free electrons. This process is shown on Fig.2.2 where a variation of free-charge density with time during traps empting is shown.

After the charge has been photo-released from the traps, it may stay in the CB until it recombines with a carrier of opposite sign or until it is removed at one of the electrodes in the case of a sample containing a substantial space charge. There is also the possibility that once excited into the conduction band, the carrier may be retrapped, and in the following analysis we consider the simplest situation where no
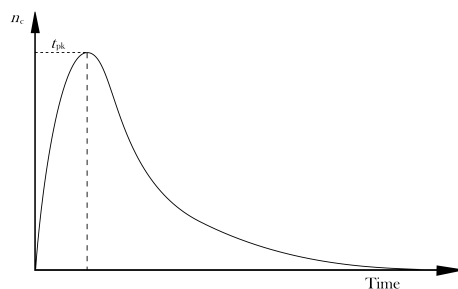
Figure 2.2: A decay curve for the density of free-carriers (electrons)

retrapping occurs. For the case where retrapping is neglected, the decaying portion of the curve may therefore be represented by the following expression [21]:

$$N_c = N_0 g(t)\tau_c \exp(-gt) \qquad (2.1)$$

where N_c is a free-carrier (electron) density, g is the product of the density of photons irradiating the sample (photons/cm^2) and the effective interaction cross-section of the photons and the electrons in the traps, τ_c is the effective lifetime of the electrons in the conduction band. N_0 – the initial concentration of electrons in the traps. Characteristic lifetime for the detrapping is $\tau = \frac{1}{g}$ and can be easily extracted from the decaying curve of the current.

In our analysis, we will consider a special case when the density of photons follows an exponential decay $g = g_0 \exp\left(-\frac{t}{\tau}\right)$. Then the density of free electrons N_c can be expressed by [135, 137]:

$$N_c = N_0 g_0 \exp\left(-\frac{t}{\tau}\right)\tau_c \exp\left(-t g_0 \exp\left(-\frac{t}{\tau}\right)\right) \qquad (2.2)$$

Current measurements give us a time dependency of current intensity $I(t)$. Intensity of current is proportional to the concentration of free electrons. That is why extracting lifetime from this curve gives us the information about characteristic time of the relaxation process.

2.3 Thermoluminescence.

Thermolumunescence (TL) in solids is the light emission that takes place during heating of a solid following an earlier absorption of energy from radiation [169]. The essential condition for TL to occur in an insulator or a semiconductor is that the material must have been previously exposed to radiation. Once TL emission has been observed, the material will not show it again after simply cooling and reheating. The material should be reexposed again to radiation to obtain TL. Heating in this process is not an exciting agent but a stimulant.

Urbach [167] is usually credited with suggesting TL as a potentially useful research tool for trap-level analysis. The basis of mathematical treatment of TL was first given by Randall and Wilkins [116] and Garlick and Gibson [53], after which it started gaining favor for applications in archaeology, geology, health physics, medical science, radiation dosimetry as well as for analysing defect structures in solids (Townsend) [163]. Daniels et.al. [28] were the first to use TL as a technique for radiation dose measurements in radiation dosimetry. Their proposal also led to its use in determining the age of archaeologic and geologic speciments.

A large number of dielectric materials (amorphous, single-crystal and polycrystalline semiconductors, insulators, organic compounds, biological materials and biochemicals) exhibit TL emission. Here we present a short description of the physical and mathematical treatment of TL emission and the methods of their analysis.

2.3.1 Thermolumunescecne measurement methods

TL measurements can be made with a very simple and relatively inexpensive experimental setup, which can be easily assembled in a research laboratory. The TL intensity can be recorded in two ways: (i) measurements of total yield TL versus T and (ii) spectrally resolved yield of TL versus temperature, which is much more informative. In the second case (ii), recording of spectral distribution of the emitted light corresponding to each glow curve can reveal in detail relaxation paths. Different mechanisms leading to emission, such as band-to-band transition, transition involving trapping via tunnelling, or simultaneous trapping and annihilation of electrons and holes at the recombination centers, can also be interpreted. The TL spectrum can be obtained simultaneously in a wide wavelength range using CCD-camera. An investigation of TL intensity versus temperature is done to measure also the radiation dose. The experimental setup in this case consists of (i) a heating system with controlled variation of the temperature, (ii) system for light collection and detection and (iii) a system for recording the signal and PC. In this case measurements of total yield of TL or spectrally resolved one can be done. It gives us a possibility to get more information about mechanism of each TL peak formation and also get thermo-activation parameters such as an activation energy for each kind of traps.

2.3.2 Thermoluminescence mechanism

A diagrammatic representation of an energy-band model of thermoluminescence is shown in Fig.2.3:

During irradiation, the luminescent center C can be excited to its excited state C'(transition 1) followed by fluorescence (transition 2). At the same time, ionising radiaton produces free electrons via transition 3 (from valence band) and transition 4 (involving the impurity center C). The electron then moves through the lattice and is trapped with a high probability in the state T (transition 5). The electron may spend some time in the trap before being thermally released to the CB (transition 6),
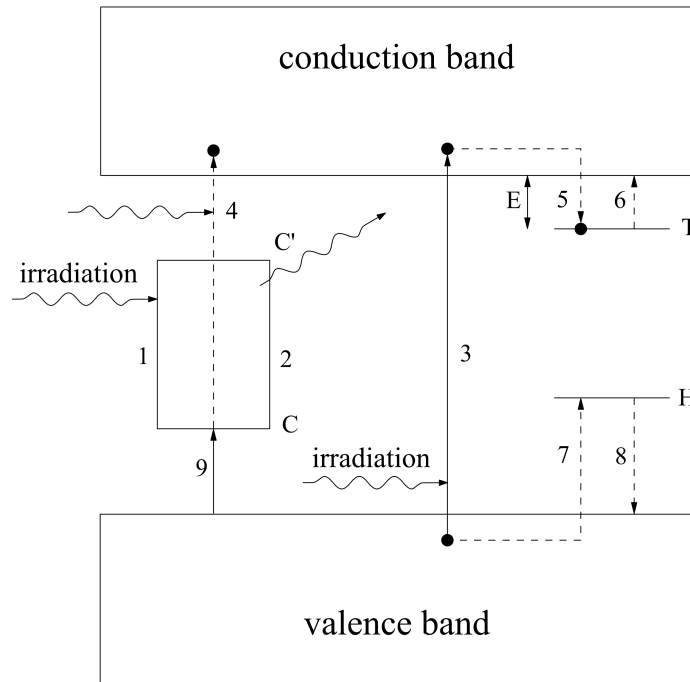
Figure 2.3: The diagrammatic representation of an energy-band model

followed by radiative recombination with the luminescent center C. Note that the direct recombination of free electrons and holes across the band-gap is a less likely process than the indirect process described above. The intensity of thermoluminescence, the so-called "glow curve", increases with the raising temperature because more trapped electrons are released per time interval. The intensity reaches a maximum and starts to decrease as the traps (or recombination centers) are depleted. The temperature at which the glow curve exhibits a maximum depends on the trap depth E below the bottom of CB. More than one maximum in the glow curve points to the fact that the traps are distributed in separate groups at different depths and each maximum represents a particular set of trapping levels.

The release of charge carriers from the trapping levels by heating depends on the probability of their escape [169]. The charge carriers released from the traps recombine radiativelly via the conduction (CB) band or valence (VB) band, giving rise to TL intensity I_t. I_t at any time is proportional to the rate of recombination of holes and electrons at the recombination center level C (Fig.2.3) and is given by [169]

$$I_t = I_0 \exp(-pt) \tag{2.3}$$

Where I_0 is initial intensity at $t = t_0$, and $p = s \exp\left(-\frac{E}{kT}\right)$. The frequency factor s varies slowly with temperature and can be considered as a constant for a particular

trap.

In practice, released charge carriers have a finite probability of getting retrapped. In the case of second-order kinetics (bimolecular), released free carriers have an equal probability for going to recombination centers or returning to the trap (re-trapping). The simplest case is no-retrapping case when all charge carriers released from their traps recombine radiatively. In this case intensity of TL, I_{TL}, will be proportional to the rate of a release of trapped carriers, and is given by

$$I_{TL} = N_{t_0}\, s \, \exp\left(-\frac{E}{kT}\right) \exp\left[-\left(\frac{s}{\beta}\right) \int_{T_0}^{T} \exp\left(-\frac{E}{kT}\right) dT\right] \qquad (2.4)$$

Where N_{t_0} is the number of electrons trapped at the initial temperature T_0 and β is the rate of heating. This expression is Randall and Wilkins [116] equation for the no-retrapping case of the first order kinetics.

We will consider this simplest case. Analysis of the equation (2.4) shows us that I_{TL} builds up as the temperature increases as the second exponential term in eq. (2.4) approximates unity; then I_{TL} reaches a maximum at particular intermediate temperatures as the second term starts decreasing; then I_{TL} falls of for any further insrease of temperature as the second exponential decreases rapidly to reduce I_{TL} to zero.

By setting $\frac{dI_{TL}}{dT} = 0$ at $T = T_m$ one can obtain:

$$E = kT_m \ln\left(\frac{skT_m^2}{\beta E}\right) \qquad (2.5)$$

At low temperature, however, one gets:

$$I_{TL} = N_{t_0}\, s\, \exp\left(-\frac{E}{kT}\right) \qquad (2.6)$$

From the equation 2.6 we can obtain the value of the trap depth E from the initial portion of the TL curve (the co-called initial-rise method) without determining s.

From the equation 2.5 it is obvious that: (i) with the increasing of β (heating rate), the T_m shifts to higher temperatures for a given trap (Braunlich) [17]; and (ii) for a constant value of β, T_m shifts toward higher temperatures as E increases or s decreases.

Generally, in practice, a material does not exhibit a single TL peak but a multipeak curve. Before starting any analysis, the peak under study has to be isolated from the neighboring overlapping peaks. This method of isolation, the so-called cleaning technique, has been proposed by various researchers (Hoogenstraaten [70], Gartia and Ratnam [54]). With this technique, a proper thermal treatment is chosen to remove all temperature peaks lower than the peak under study [70]. The TL peak can be also isolated by high-temperature irradiation, optical bleaching, or photostimulation with an appropriate frequency. Methods of analysis developed for obtaining TL parameters will be briefly discussed below.

2.3.3 Methods of analysis

2.3.3.1 Initial-Rise Method

This method is most common in use [169] for obtaining E values when frequency factor s is not known.

The initial-rise method can be used when the sample has a single glow curve or when there is no overlapping of glow peaks belonging to different trapping states. The method is based on the fact that as the glow curve initially begins to rise, the density of unoccupied recombination centers and the density of trapped electrons remain approximately constant, and hence the TL intensity is strictly proportional to $\exp\left(-\frac{E}{kT}\right)$.

In the case where the factor s is temperature dependent, by the factor T^{α}, the actual trap depth will be $E - \alpha kT$.

2.3.3.2 Isothermal Decay Method

Isotermal decay is a general technique for determining E and s and does not employ any particular heating cycle. The pre-excited TL material is quickly heated to a particular constant temperature and the light emission, which decays exponentially as a function of time, is monitored. The slope m of the linear plot between $\ln\left(\frac{I_t}{I_0}\right)$ and t will be equal to $s\exp\left(-\frac{E}{kT}\right)$. The decay is observed at several temperatures and their respective slopes m are calculated. The slope of the linear plot of $\ln(m)$ vs. $\frac{1}{T}$ will be $\frac{E}{k}$ and the intercept is $\ln(s)$, from where E and s are calculated [169].

2.3.4 Thermally stimulated exoelectron emission (TSEE)

TSEE is also considered to be an effective technique for interpreting the effects underlying TL and for understanding the nature and distribution of the trapping states that the electrons are released from when a pre-irradiated sample is heated. These released electrons (so-called exoelectrons) get raised to the conduction band (C-band). After they reach energy high enough to overcome the potential barrier at the surface, they leave the solid sample. They can be collected by a detector with a positive potential electrode in place above the sample. The curve obtained as a function of temperature is also called a glow curve [169]. The same thermally detrapped electrons might recombine radiatively at a recombination center giving rise to TL emission. A correlation between a TL peak and TSEE peak at the same temperature may indicate the presence of electron traps contributing to the TL at that temperature (Becker) [8]. TL-TSEE correlation studies have been done by various researchers (Fukuda et al. [51], Tomita et al. [162], Holzapfel and Krystek [69], Spurny and Kaambre [159], Uchrin [164]). Any absence of correlation between TL and TSEE, could be due to the fact that TSEE is a result of surface traps (arising from adsorbed atoms-molecules and or surface imperfections) as well as volume traps (existing within the solid), whereas only volume traps contribute to TL emission. Also, if TL

emission occurs via detrapping of carriers and their subsequent radiative recombination through tunnelling process, TSEE will not occur along with TL without the carriers entering the CB.

When TL and TSEE occur simultaneously the same methods of analysis can be applied to the TSEE curves.

Part II

Experimental Setup

3.1 Experimental chamber

3.1.1 Cryostat and vacuum system

To create and investigate rare-gas solids one needs low temperatures and a high vacuum environment therefore a refrigeration system (cryostat) with temperature monitoring and a vacuum-pumping system with pressure monitoring.

Our experimental setup based on the closed-cycle helium refrigerator. In this type of cryostat the helium is compressed by the compressor unit connected to a compact head module (expander) by high pressure (feed) helium flex line. The cooling effect is obtained by means of the helium expansion within the head module in two stages after which helium gas returns through the low pressure line to the compressor unit. The components of the system are listed in the Table 3.1

Cold head	Compressor unit	Substrate	Temperature controller	T_{min}	Temperature sensor
Leybold RGD 5/100	Leybold RW 6000	Mirror: Cu coated by Ag/MgF$_2$ or Au	Leybold LTC 60	6 K	Two Si diodes

Table 3.1: Cryostat system with temperature control unit used in experiments

The LEYBOLD cryostat allows us to reach a temperature around 6K and this system is equipped with two temperature sensors, one mounted directly on the cold finger (5.9 – 5.5K lowest value) of the cryostat and the second at the substrate holder (6.4 – 6.6K). The temperature of the matrix is assumed to be the average of these two

values. The LEYBOLD vacuum system is based on standard, O-ring sealed ISO-K components and the cryostat chamber is pumped by $190\,\mathrm{ls}^{-1}$ turbo-molecular pump. The base pressure under cryo-pumping reaches $6 \cdot 10^{-8}$ mbar ($1.5 \cdot 10^{-6}$mbar at the room temperature).

Another kind of cryostat was used to investigate a spectrally resolved vacuum ultraviolet (VUV) luminescence from pre-irradiated RGS. In this type of cryostat liquid He should be very slowly put into the cryostat chamber which consists of two parts separated by a needle valve. The upper one which serves in fact cryopump is filled in first, when pressure decreases to its lowest limit the needle is opened and second volume connected to the substrate is filled in with liquid He. In order to diminish He losses because of room temperature radiation from the experimental chamber walls a heat shield connected with liquid nitrogen volume is used. This cryostat allows us to reach the temperature about 4.5K. That is well suited for an investigation of all RGS including solid Ne. But because we have a metallic substrate spectroscopic methods can be used along without current measurements. Temperature sensor is mounted on the substrate nearby the sample. Other sensors are used to get an information on the temperature distribution inside the experimental chamber.

Vacuum-pumping system in this case consists of two pumps. First is a forvacuum pump and when we reach the pressure around 10^{-4}mbar another pump – NORD (ionisation pump) – is switched on. This system guarantees the base pressure P in the deposition chamber under cryo-pumping $P \approx 10^{-7}$mbar at the pumping speed of about $100\,\mathrm{ls}^{-1}$.

3.1.2   Sources of electrons

To irradiate the sample by a low energy electron beam two types of electron gun were used. To produce the electrons with energy around 200eV heated tungsten filament was used. It was maintained at a constant negative potential – in the range 100-600V with respect to the grounded substrate. The electrons ejected from the filament were focused by a cylindrical electrostatic lens (L_3 – tube-shaped lens) on the sample. Fig.3.1 shows a procedure of a low energy electron beam formation using the tungsten filament.

L_3 is located at about 5cm distance from the substrate and held at slightly higher negative potential than the filament. Energy of electron beam was changed in the range $100 - 500$ eV. The electron current can be varied from 1 to 12μA and the electron density in the range of $0.2 - 2.4\ \mu\mathrm{A\ cm}^{-2}$.

Another kind of an electron gun was used in experiments performed to investigate the spectrally resolved VUV luminescence. This gun has a construction of the so-called "Pirss' guns. To focus the electron beam special lens is used. Note that in the Pirss geometry electron beam divergence is very small. The electrons ejected from oxide cathode are accelerated by anode which is kept at the same potential as the substrate (grounded). The operating range of this electron gun is $100\mathrm{eV} - 10\mathrm{keV}$. As a rule we used the beam of comparatively high electron density – $1\ \mathrm{mA\ cm}^{-2}$.
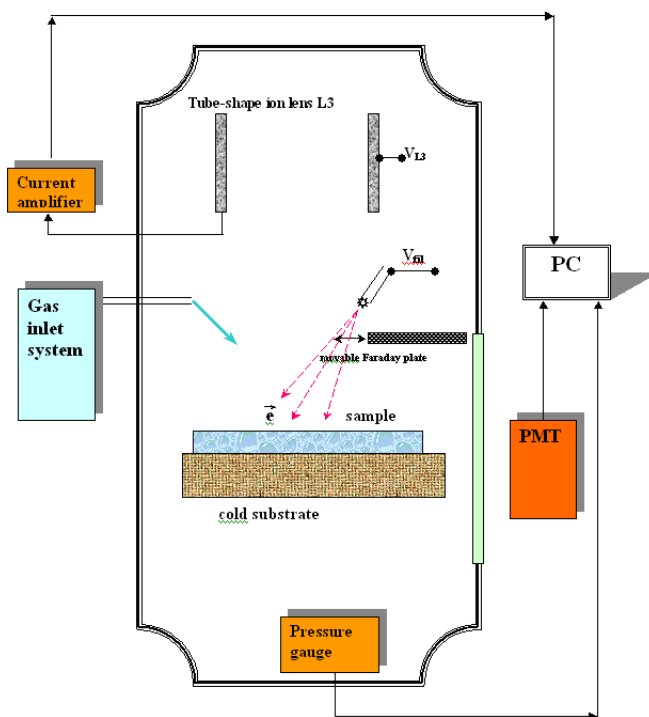
Figure 3.1: Schematic drawing of the sample preparation process.

3.2 Sample preparation

3.2.1 Deposition

Samples of RGS were grown from the gas phase by condensation on a silver-coated metal substrate over-coated by very thin insulator layer (MgF_2) cooled by a closed-cycle refrigerator (Leybold RGD 580). The structure of samples and therefore charge trap levels and their distribution within the energy gap were varied by changing deposition temperature and gas flow parameters such as a flow speed. For the most part we used continuous deposition. A typical deposition rate was kept at about 2ml per min. The sample was deposited during 30min and a typical sample thickness was $50 - 100 \mu m$. High-purity (99.999%) Ar gas was used to form a matrix. The N_2, O_2 and Xe_2 were used as dopants. The gas-handling system was degassed by heating under pumping before the experiment. The base pressure in the deposition chamber was $6 \cdot 10^{-8}$ mbar and was monitored using a Compact BA Pressure Gauge PRB 260. The presence of impurities such as N_2, O_2, H_2O, CO_2 was smaller than 10^{-4}. The deposition rate and the sample thickness were determined by measuring the pressure decrease in a known volume.

For the spectrally resolved VUV spectroscopic measurements we deposited a sample very fast (during 5min) on the cold substrate. In this case a typical sample

thickness was about $50 - 100\mu m$ and was determined by measuring the pressure decrease in the known volume of a bulb in the gas inlet system. High purity Ar (99.999%) gas was used. The content of impurities such as O_2, N_2, CO_2, and H_2O did not exceed 10^{-4}. The base pressure under cryopumping was about 10^{-7}mbar and was monitored by vacuum ionization gauge. During deposition the temperature was kept low enough (6K) to prevent all thermally stimulated processes. The temperature of the samples was measured by a calibrated GaAs diode fixed on the substrate.

3.2.2   Charge center generation and formation of metastable centers as atomic N or O

To ionize samples we used an electron beam because the ionisation cross-section in this case is larger than that at photoionization (see [36] and Fig.1.7 in the thesis). Charged centers were generated in two ways: (i) by irradiation of the grown neutral sample and (ii) by deposition from the gas phase under electron bombardment. In the case (i) the thickness of the subsurface layer containing charged centers depends on the electron beam energy and can be easily varied. Using the (ii) way it was possible to generate charged centers across the whole sample. A hot tungsten filament served as a source of electrons when we used slow electrons with energy up to 500eV. The electrons were accelerated to the needed energy and focused by a cylindrical electrostatic lens placed in front of the substrate and held at -200V potential deflected the electrons toward the sample (see Fig.3.1). In another case (i) we used 1keV electrons and irradiate the sample after deposition from the gas phase. In both cases we used slow electrons of energy 200eV (close to the maximum of ionisation cross-section) in case (ii) and up to 1keV in case (i). Note that threshold energy for electrons which can produce defects via the so-called "knock-on mechanism" in Ar matrix is estimated to be of about 23.2 keV (see Section 1.4.2). So electrons of lower energy cannot create defects via "knock-on" mechanism because their kinetic energy is insufficient to displace the lattice atoms from regular sites via elastic collisions. However, even low energy electrons are able to create point lattice defects via excitation of the electronic subsystem [130,139]. The current density of the electron beam was kept at about 1 mA cm^{-2} in case (i) and 0.03 mA cm^{-2} at the deposition under the electron beam.

It should be noted that in rare-gas matrices containing dopant or guest molecules neutral metastable centers – atoms and radicals – are created quite efficiently under electron bombardment. N atoms are formed under electron bombardment of RGS matrices [99, 137], forming the well-known forbidden transition $^2D \rightarrow {}^4S$ on the wavelength 523nm. The green spot onto the sample can be seen in that case. Interesting to note that life-time of this transition is about 20s in Ar matrix [63]. And one can also expect an appearance of a recombination emission due to N_2 formation under heating of the matrix, when diffusion of the N atoms becomes significant. In similar way atomic oxygen can be formed under irradiation the sample by the

electron beam yielding the $^1S \rightarrow ^1D$ emission. The characteristic life-time for this transition does not exceed 1 second. Heating of the oxygen-containing samples also results in the diffusion of oxygen atoms and creation of molecule O_2^* followed by emission of the well-known Herzberg progression indicating radiative transition of excited oxygen molecule into the ground state.

3.2.3 Annealing procedure

To investigate an influence of the sample structure on the relaxation process we performed experiments with annealed samples. During annealing the lattice imperfections such as interstitials can be shifted to their regular position in the lattice and vacancy-interstitial pair will be annealed. Also vacancies diffuse to some kind of sinks as dislocations, grain boundaries etc. In this way we get more perfect structure of the sample. For the purpose Ar samples were prepared as was described above. After the irradiation completing samples were warmed up with a constant rate to some fixed annealing temperature, kept at this temperature for a definite time (for example $5 - 10$ min) and then were slowly cooled down. Another way to get a more perfect structure is deposition at a higher temperature [128, 158].

Moreover, Ar matrix deposited at 60K with special technique contains minimum amount of primary defects such as vacancies and equilibrium concentration of such kind of defects at this temperature is $3 \cdot 10^{-7}$(a. u.) [128]. Hence if we need to create a maximum amount of defects in the Ar matrix, the deposition temperature should be lowest one. In our case the lowest temperature was of about 6K. In this case under following heating of the pre-irradiated matrix we will get a luminescent, current or pressure curves containing a lot of peaks, which correspond to different kind of defects [115]. To separate some peak for the analysis we used some version of the special so-called cleaning technique [169]. This technique is used in order to remove all temperature peaks lower than the peak under study. If we will deposit a sample of Ar at 18K, for example, surface related defects (annealed at 12K in Ar matrix) or radiation stimulated Frenkel pairs (annealed at temperature around 15K) will not be formed in the matrix.

3.3 Measurements

3.3.1 Activation spectroscopy

In our study we employed both optical and current activation spectroscopy technique using stimulation by heating and by photons. Several relaxation processes in pre-irradiated samples were studied: a release of electrons from the traps and their transport and recombination with intrinsic and extrinsic ionic centers along with the found in our studies desorption or sputtering from pre-irradiated solids. Under heating the processes mentioned above were monitored by measuring of thermally stimulated exoelectron emission (TSEE) as well as recording yields of thermally

stimulated luminescence (TSL) due to recombination of charged and neutral species and anomalous low temperature sputtering [135–138, 140, 141, 143].

For the photon-stimulation we used an external source – laser light in the visible range as well as the internal source – luminescence of dopant atoms or molecules formed in the pre-irradiated Ar matrix [62–64]. Photon-stimulated recombination luminescence (PSL) was monitored for the intrinsic and extrinsic charged centers. Because the range of recombination emission of positively charged guest centers depends on their level location within the band gap PSL study of doped solids involves wide range of spectra from visible to vacuum ultraviolet. In addition to the PSL we detected photon-stimulated exoelectron emission (PSEE) to monitor both electron transport and charge recombination.

3.3.1.1 Description of experimental devices

The experiments were performed using different apparatus (i) with He-flow cryostat for spectrally resolved PSL measurement in VUV range (at the department of Crogenic System Spectroscopy, Verkin Institute for Low Temperature Physics & Engineering NASU in Kharkov, Ukraine) and (ii) with a closed-cycle refrigerator Leybold RGD 580 (at the Matrix Isolation Spectroscopy, Department of Chemistry, Technical University of Munich, Germany) for PSEE, TSEE, and TSL measurements in wide range of spectra.

Fig.3.2 shows an experimental chamber (i) with liquid He cryostat and measurements devices for spectrally resolved intrinsic and extrinsic VUV luminescence from pre-irradiated by an electron beam rare-gas solids. For the excitation of solid argon the electron gun with energy 1keV was used. He-Ne laser was used to stimulate the recombination luminescence after electron bombardment. The luminescence spectra of solid Ar were recorded under exposure to the electron beam and immediately after excitation using a normal-incidence VUV monochromator with a dispersion of 1.6nm/mm.

All current measurements and registration of the total yield of thermally stimulated luminescence as well as detection of electronic sputtering were performed with another setup (ii) schematically shown in Fig.3.3

In this case as a source of slow electron (100-500 eV) a tungsten filament served. As a source of photons stimulating relaxation processes Ion Argon Laser in combination with a tunable Dye Laser was used. The thermally or photon-stimulated currents of electrons emitted by pre-irradiated sample were detected with a movable Faraday plate or with L_3 electrode correspondingly. In order to register the total luminescence yield the cryostat was turned (by 90grad) to the optical quartz window to collected photons by PMT sensitized to the VUV light. The geometry for TSL measurements is shown in Fig.3.3. Simultaneously with current or luminescence we registered a pressure in the experimental chamber as a function of temperature in experiments on thermally stimulated phenomena or as function of time for photon-stimulated relaxation at fixed low temperature. More detail description of the devices and the data acquisition is given below.
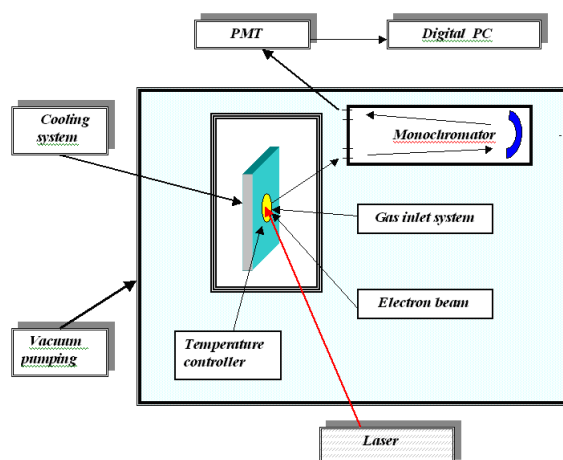
Figure 3.2: Schematic drawing of the experimental chamber for spectrally resolved measurements in VUV range using cryostat with liquid He.

3.3.2 Laser stimulated measurements

As it was mentioned in order to initiate the relaxation processes in the pre-irradiated matrix we used as a source of photons the laser light in the visible range. The laser light was switched on after completed irradiation of the sample with an electron beam and photon-stimulated exoelectron emission as well as recombination luminescence of self-trapped with electrons were monitored.

In the PSEE experiments to cover the whole visible range a coherent Ar Ion Laser (Innova 70) and a Coherent CR-599 Dye Laser operating with Rhodamine 6G and pumped with Argon Ion Laser and a Coherent 899-05 Dye laser using Stilbene 3 and pumped with a Coherent Argon Ion Laser (Innova 70) were used. A continuous mode for the measurements was used. The laser light was introduced into the sample chamber with an optical fiber. The laser power was varied in a range 10 – 75mW (the power was measured in front of the sample) and laser beam was defocused to the diameter of about 3cm to cover the whole the sample. The rise of the indicated temperature value did not exceed 0.2K under excitation by the most powerful laser light – 75mW, when a sample had the most imperfect structure and hence had less transparency for the visible light.

Fig.3.4 shows examples of the temperature increase under exposure to the laser radiation of different power. It is clearly seen that the laser even at maximum power could not heat the sample up to the threshold temperature for thermally stimulated processes in Ar matrix (10K) and the data obtained are not perturbed by any thermally stimulated processes.

Other kind of laser was used to investigate a recombination luminescence on the M-band of pre-irradiated by low energy electron beam Ar. A He-Ne laser of low power (2mW) in the CW mode was used with a 1:4 neutral attenuator. The laser beam was defocused to a diameter of 2.5cm to cover the whole sample. The
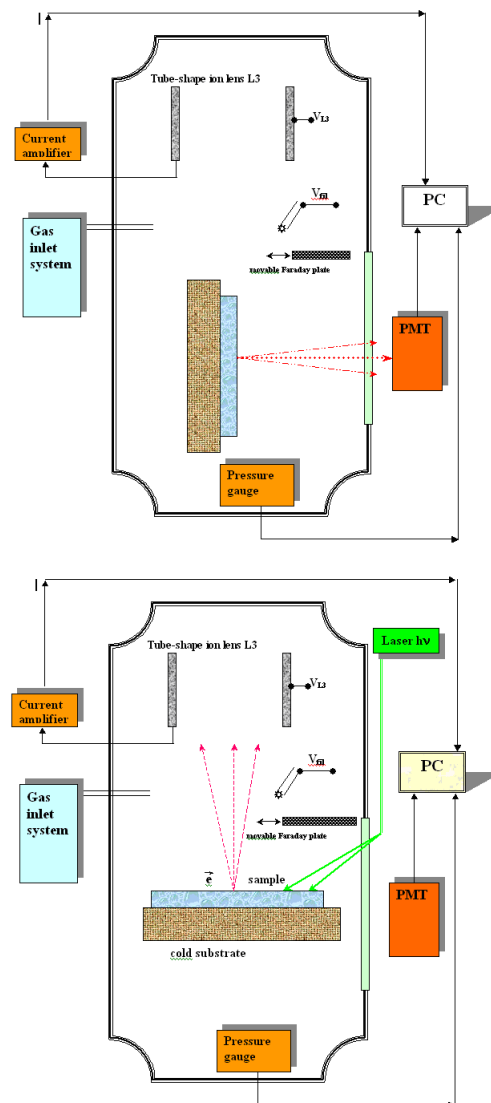
Figure 3.3: Schematic drawing of the experimental chamber for (a) current measurements together with pressure monitoring and (b) for total yield of TSL simultaneously with pressure.

indicated temperature value did not change when the laser was switched on. All measurements were made at temperature (6K) lower than the threshold temperature for the thermally stimulated processes.

Concerning the reproducibility of the data it should be underlined that only strict maintenance of experimental conditions yields reproducible results. Yields of photon-stimulated processes only slightly depended on a number of experiments per day. The substrate was heated up to 100K after each cycle of measurements. TSEE yields appeared to be more sensitive to the conditions of the sample prepa-

Figure 3.4: Temperature control of the sample heating under laser irradiation with different laser power.

ration, e.g. to a number of experiment performed at the same day. Fig.3.5 shows differences in TSEE curves for the first, second and third experiment which were done in the same day.

One can see that for first experiment low temperature peaks from 10 up to around 20K are dominate in TSEE curve. For the second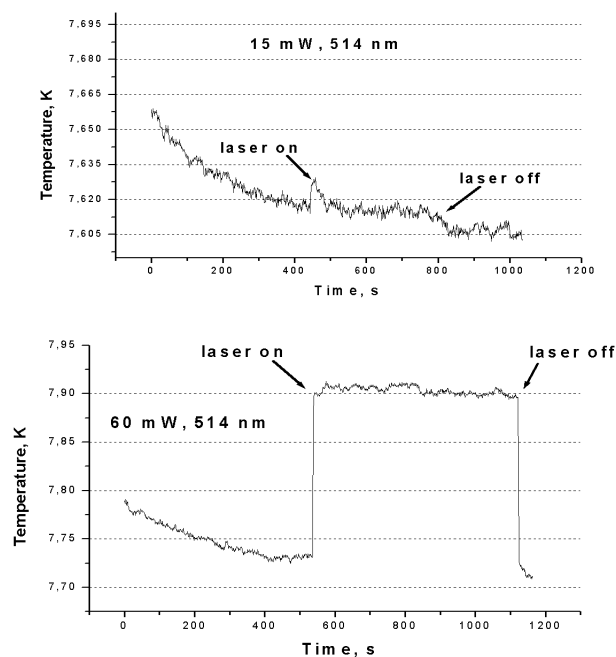 experiment low temperature peaks and high temperature peaks around 40K have a comparable intensity and for the third experiment high temperature peaks are dominated in the TSEE curve. We suppose that such a tendency appears due to an influence of the residual gases accumulation in the samples with time. To keep the conditions of the experiments later on we performed one cycle of the measurements per day at the same vacuum after annealing of the substrate up to 350K under pumping over 10hours or more.

3.3.3   Registration of spontaneous and stimulated luminescence

Relaxation process in pre-irradiated samples can be monitored by measuring a total and spectrally resolved yield of visible and VUV light. The total yield of luminescence in both range (visible and VUV) was detected with a conventional and solar-blind PMT (Fig.3.3). By introducing a convertor of vacuum ultraviolet irradiation into visible light we were able to extend the available wavelength and detect luminescence from 800 up to 10 nm. Spectrally resolved luminescence of dopants as well asTSL from pre-irradiated Ar matrix was measured by the Multichannel S2000
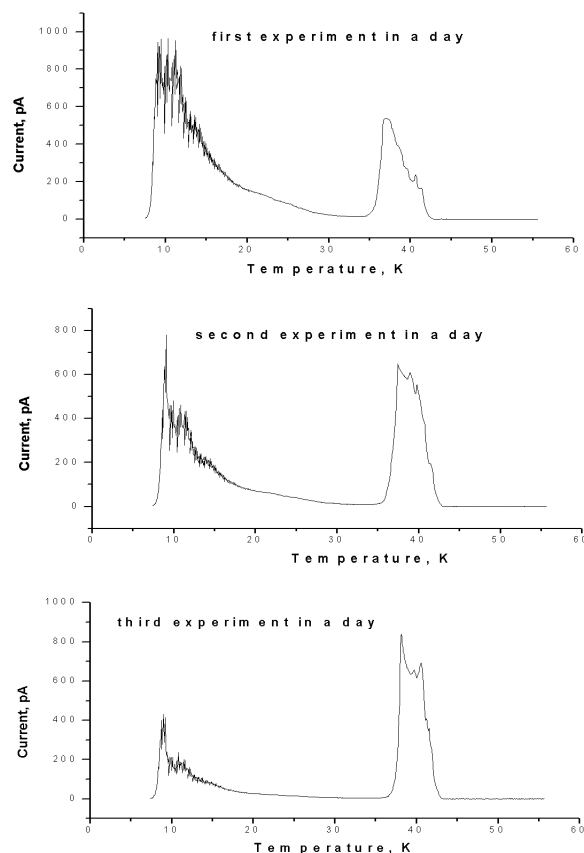
Figure 3.5: TSEE from pre-irradiated solid Ar for first, second and third experiment which were made in the same day.

Spectrometer Ocean Optics based on CCD detectors operating in the range 170 – 1100 nm. It enabled us to monitor generation of species of interest and TSL from recombination of dopants. This spectrometer was applied as a new part of our experimental setup and the scheme of new set up will be given below in a Section 3.4.

In addition, we measured yields of spectrally resolved emissions at the wavelength of the intrinsic and extrinsic recombination luminescence for RGS matrixes in VUV range. For the purpose a normal-incidence VUV monochromator (1.6nm/mm dispersion) was used with a PMT sensitized to VUV (Fig.3.2).

3.3.4   Registration of exoelectron emission

The emission of electrons from pre-irradiated samples was detected with a movable Au-coated Faraday plate kept at a small positive potential (+9V). It was positioned at a distance of 5mm in front of the sample grown on a grounded substrate. When we measured a current stimulated by a laser light introduced into the chamber via fiber optics we collected electrons by L_3 electrode hold also at a small positive potential.

As the substrate we used a silver-coated copper mirror with a thin layer of MgF_2. The substrate temperature was measured with a calibrated silicon diode sensor. A programmable temperature controller permitted us to keep the desired temperature and heating regimes. In most experiments we used a linear heating with the rate of 3.2 K min^{-1}.

The current from the Faraday plate was amplified by a FEMTO DLPCA 100 current amplifier. The converted voltage was reversed in the polarity by an inverter and digitised in a PC. Currents as low as 100fA can be easily detected. Fig.3.3 illustrates exoelectron current measurement procedure.

3.3.5 Registration of the anomalous low temperature sputtering

To monitor the desorption yield from the preliminary irradiated films, we measured the pressure in the chamber as a function of temperature (under heating with a constant rate of 3.2 K min^{-1}) simultaneously with exoelectron current measurements or luminescence detection. Pressure in the vacuum chamber was monitored using a Compact BA Pressure Gauge PBR 260. The position of the gauge in the chamber is shown in Fig.3.3. In order to distinguish the radiation effect in pressure rise upon heating the pressure was measured for nonirradiated and then from irradiated sample. As it will be demonstrated further the pressure rise at low temperatures from nonirradiated sample is quite low but still detectable. Irradiation enhanced the pressure rise nearly by an order of magnitude [See section 4.5 – anomalous low temperature sputtering].

3.4 New experimental setup for simultaneous measurements of the the relaxation process: TSL, TSEE and anomalous low temperature desorption.

Because all relaxation processes are sensitive to the sample structure, its purity and prehistory it is a nontrivial task to keep identical condition of sample preparation. Certain advantage can be gained monitoring simultaneously a number of relaxation processes at the same sample. With this in mind a new low-temperature modification of activation spectroscopy technique – real time correlated study of relaxation processes in cryogenic solids with simultaneous measurements of the exoelectron emission, spectrally resolved luminescence and detection of the total sputtering yield was developed [114]. The first results obtained with this technique are published in [115, 143, 145–147].

The procedure of sample growing and charge generation was described above. After sample preparation substrate was turned to the position for measurements. We measured yields of the thermally stimulated exoelectron emission (TSEE) from pre-irradiated samples, thermally stimulated luminescence (TSL) and total sputtering

yield (by pressure monitoring) simultaneously. Before this modification we were able to measure only TSEE simultaneously with pressure monitoring or integrated yield of TSL along with pressure. The exoelectron yield was measured with an Au-coated Faraday plate of modified configuration kept at a small positive potential +9V and connected to the current amplifier FEMTO DLPCA200 A centrally located hole in the Faraday plate permitted to detect spectra from the sample though an optical window simultaneously with current detection. The modified setup includes a wide optical range Multichannel S2000 Spektrometer Ocean Optics ($170 - 1100nm$) equipped with CCD detectors. Spectra were recorded with the resolution not worse than 1.3nm in ms time window. This enabled us to monitor simultaneously the temporal and temperature evolution of all spectral features in the whole operating range of the spectrometer. The sputtering yield was detected by measuring the pressure change in the chamber using Compact Full Range BA Pressure Gauge PBR 260. In contrast to our previous records [135, 138] which were done point by point in the new modification of experimental setup pressure above the sample was monitored steadily. For calibration we used the flow-rate controller. The temperature was measured with a calibrated silicon diode sensor, mounted at the substrate. The relaxation processes in Ar samples were studied in the temperature range from 7 to 42K. The programmable temperature controller LTC 60 allowed us to maintain the desired temperature of deposition, irradiation and heating regimes. In the experiments on PSEE the laser light was introduced into the experimental chamber by fiber optics through the special hole in the center of the Faraday plate.

The program developed permitted to detect synchronously spectra over entire operating range, TSEE or PSEE current, temperature and pressure in the chamber [114].

Fig.3.6 shows the latest modification of the experimental setup for correlated in real time measurements of relaxation emissions.
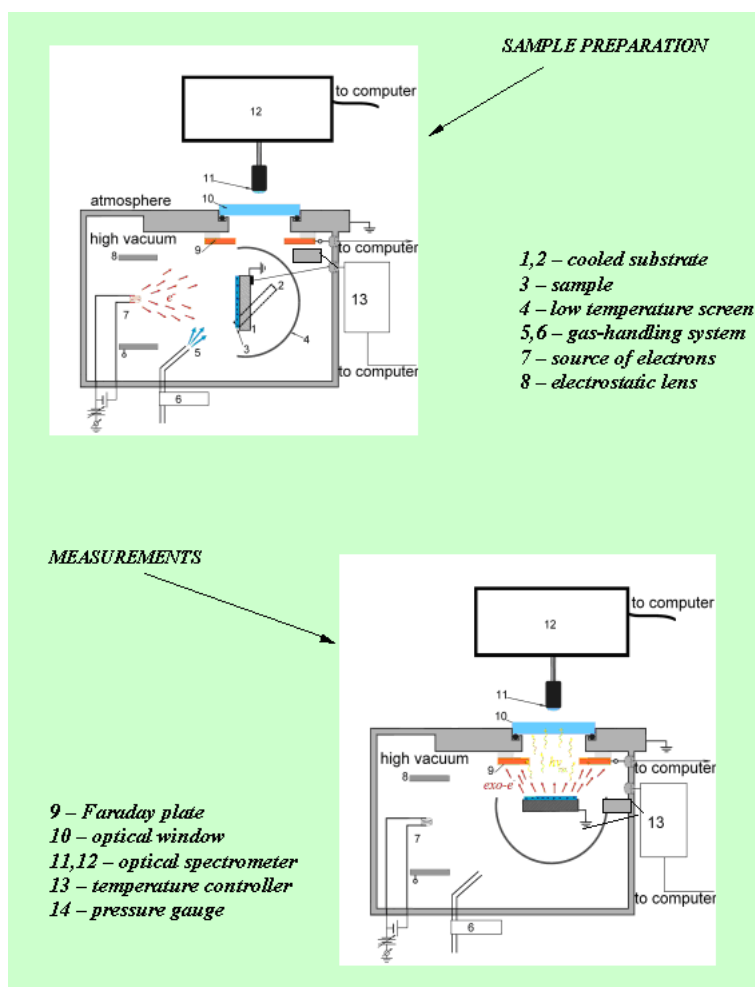
Figure 3.6: New modification of the experimental setup for the "real-time correlated" study. Simultaneously measurements of a luminescence, current and desorption yields.

Experimental Results and Discussion

4.1 Energy-band model and relaxation channels in RGS

Before discussing the results of the thesis, let us consider first the energy-band model as applied specifically to solid Ar (Fig.4.1). The conduction band CB and the valence band VB are relatively narrow as compared with band gap energy E_g. On the other hand, the CB appears to be nearly twice wider than the VB. In line with this, holes being generated in matrix have less mobility than electrons by factor 10^{-5}. Holes are self-trapped in matrix within 10^{-12}s due to interaction with phonons forming STH levels nearby the VB ("STH" in Fig.4.1). Similar levels can be formed by other rare-gas "guests". Electrons characterized by free-like behaviour cannot be self-trapped in solid Ar. They only can be trapped by shallow traps (lattice defects) or by deep traps (impurity atoms or molecules of positive electron affinity χ). Schematically these traps are shown in Fig.4.1 as TE levels. Note that the STH levels are quite deep with respect to the VB and holes cannot be released by heating. In contrast to this, trapped electrons under heating or photon irradiation are promoted to the CB and become mobile. In the CB electron has two possibilities:

  i) to recombine radiatively with intrinsic (STH) or extrinsic (guest) centers (yielding the VUV radiation),

 ii) to directly escape the sample due to a negative electron affinity E_a of Ar matrix.

Channels i) and ii) are concurrent channels. An electron releases from a trap and then either escapes the sample or recombines radiatively with positively charged centers. Let us consider relaxation channels in more details.

4.1.0.1 Relaxation channels

Pre-irradiated doped Ar matrix contains stable point defects – charged and neutral ones. The formation of long-lived charge centers is a possible way to store energy.
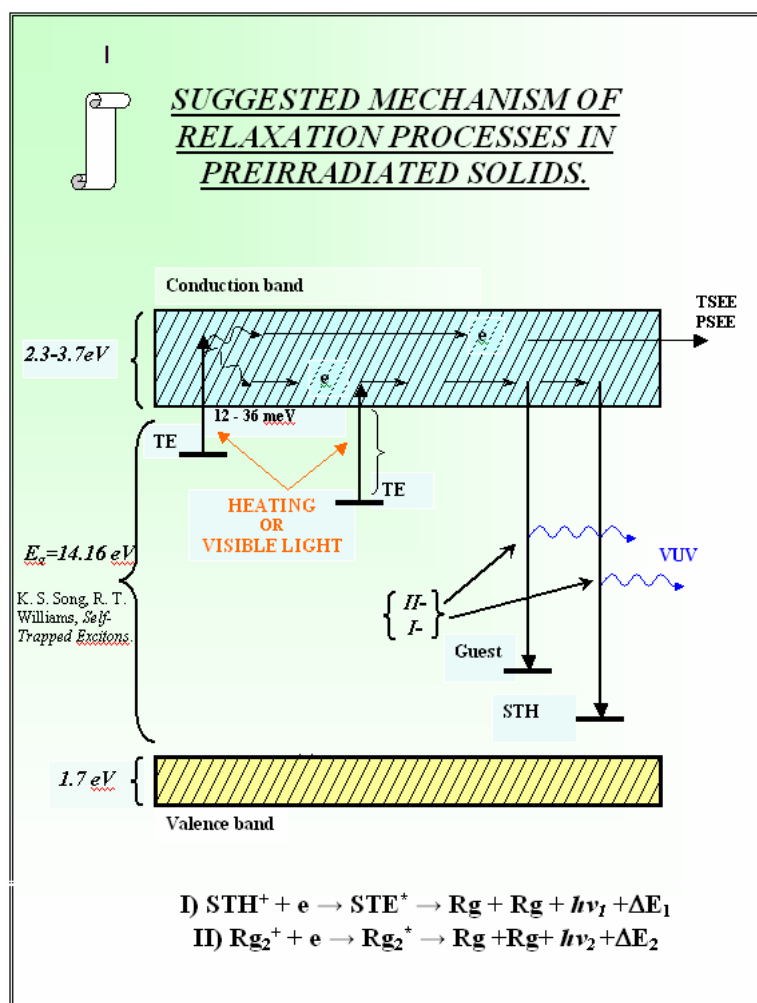
Figure 4.1: Energy-band model for relaxation channels of pre-irradiated solid Ar.

Time span of this storage is determined by the stability of charge centers. As long as the centers of opposite sign are localised and spatially separated in the lattice, they are stable. As it was already mentioned, relaxation processes in RGS are in fact driven by release of electrons and their mobility.

To release electrons from shallow traps, it is sufficient to heat the sample to a specific temperature. Under heating, electrons stored by the sample in shallow traps during e.g. electron bombardment, get additional portion of energy, sufficient for de-trapping. Estimated in Ref. [128] activation energy for shallow traps in solid Ar is of about 12 – 36 meV. Being mobilized, electrons eventually reach positively charged centers and neutralize them yielding luminescence in the M-bands at a decay of Rg_2^* centers (9.7eV for Ar and e.g. 7.1eV for Xe). These processes correspond to (i) relaxation path and were observed in [77, 82, 128].

We found a new relaxation channel – anomalous low temperature desorption (ALTD) [135, 138, 140, 141, 144] which appears if the charge recombination under

heating in pre-irradiated sample occurs near the surface. The mechanism of ALTD is supposed to be based on the energy release (of about 1eV [77]) at the transition of Ar_2^* to a repulsive part of the potential curve of the ground state.

Detrapped electrons can leave directly the sample without any barrier in solid Ar because of its negative electron affinity ($\chi = -0.4$eV), yielding a thermally stimulated exoelectron emission (TSEE) [63, 64, 135, 138, 143, 147]. This is a relaxation channel which corresponds to (ii) relaxation path. All these processes do not start if one keeps a sample at low temperature (up to 10 K for Ar matrix). Energy stored by a sample during pre-irradiation stays "frozen" in the matrix as long as low temperature is kept.

From deep traps electrons can be released by irradiation with photons of appropriate energy. Such a deep trap can be atomic or molecular oxygen with binding energies $E_b = 2.61$ eV for O^- and $E_b = 1.6$ eV for O_2^- if take into account polarization energy of Ar matrix [135], and, correspondingly, only irradiation of the sample with the light of suitable energy is sufficient to promote the electron from such a kind of deep, so-called "thermally disconnected" trap, to the CB. Stimulating factor to release electrons from their traps and trigger the relaxation in this case is irradiation by photons. Note that in that way we can release electrons not only from deep traps but also from shallow ones. Relaxation in this case also consists of several paths – photon-stimulated exoelectron emission (PSEE) and recombination of electrons with charge centers with following radiation in the VUV range [62–64].

Schematically, both type of processes – thermally and photon-stimulated relaxation paths – are shown in Fig.4.2. In other words, the triggering mechanism for the whole relaxation can be both heating as well as irradiation by photons.

In the next two sections, we will discuss dynamics of the photon-stimulated relaxation paths and give experimental proves that this channel consists of the radiative recombination of charged species as well as of the exoelectron emission from pre-irradiated solid Ar. Section 4.2 involves an analysis of relaxation channels, stimulated by an external source of photons (laser light). Section 4.3 deals with the study of relaxation paths, stimulated by some kind of "internal source' – irradiation by atomic nitrogen "afterglow" (N radicals were produced in Ar matrix under electron bombardment). Sections 4.4 and 4.5 are devoted to the thermally stimulated relaxation. A focus of Section 4.4 is interconnection between atomic and electronic relaxation processes. A solid evidence of the 23K peak origin in TSL and TSEE yields from pre-irradiated solid Ar is given also in Section 4.4. A new phenomenon found – anomalous low temperature desorption – belongs also to the relaxation paths is discussed in Section 4.5.
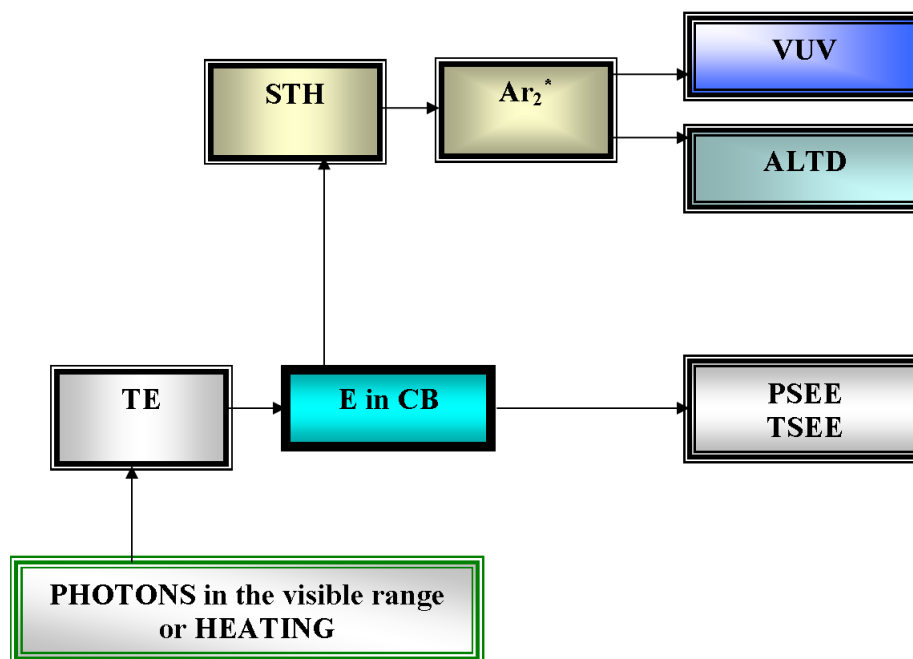
Figure 4.2: Schematic presentation of relaxation processes caused by photons in the visible range or heating of solid Ar preliminary irradiated with electron beam.

4.2 Recombination of self-trapped holes with electrons and exoelectron emission from pre-irradiated solid Ar stimulated by external photon source

4.2.1 Introduction

Excitation and ionization of dielectrics with vacuum ultraviolet (VUV) light, X-rays or with fast particles essentially affect properties of solids. Excited states, their dynamics and relaxation have been under extensive investigation in different classes of materials [16,128,158,174]. Rare-gas solids formed from identical atoms bonded by weak interatomic forces offer the unique opportunity to study radiation effects and different relaxation channels due to their simple structure (preferable fcc lattice), and strong electron-phonon interaction results in a high quantum yield of electronically induced processes.

The processes occurring on completion of the irradiation at the final stage of relaxation are of special interest for deeper understanding the radiation effects, dynamic of charge carriers, and stability of radiation-induced defects. The primary states of the relaxation cascades in this case are states of self-trapped or trapped holes, namely intrinsic ionic centers Rg_2^+, and trapped electrons, as well as metastable

levels of guests. Relaxation processes in pre-irradiated solids could be triggered by heating of the sample or by irradiation with photons.

Charge recombination is one of the most energetic processes with strongest effect on the material property. That is why radiative recombination is important relaxation channels responsible for the carrier concentration and local electric fields in irradiated solids, which influences a number of processes such as emission of photons and electrons, energy conversion, desorption etc. Methods of activation spectroscopy are commonly accepted for investigation of relaxation in solids.

In this chapter, we present first results on the study of exoelectron emission and radiative recombination of STH with electrons released by external source of photons in the visible range (laser light) from atomic Ar cryocrystals pre-irradiated by a low energy electron beam. In order to study kinetics of relaxation processes we used the laser operated in continuous mode. Analysis of the data obtained shows that the photon-stimulated relaxation processes are branched into the several paths: the main of them is the radiative recombination of intrinsic ionic centers (self-trapped holes) of dimer configuration Ar_2^+ with electrons released from the traps by a visible light, and other one is photon-stimulated exoelectron emission (PSEE).

Experiments for the detection of first relaxation channel (radiative recombination of STH with electrons) were performed with solid argon using method of conventional cathodoluminescence spectroscopy in a combination with the technique of photon-stimulated luminescence (PSL). In this case we used the laser light as external source for triggering the relaxation channels in pre-irradiated solid Ar. The characteristic lifetimes for the decay of photon-induced intrinsic recombination luminescence observed under continuous laser emission were analysed.

Here are also presented new results on influence of the parameters of external light source (laser) on the characteristics of the relaxation channel. An influence of the laser power and wavelength on the characteristic lifetime of the exoelectron emission was investigated.

4.2.2   Experimental

First we will describe important details of the experimental procedure for measurements of photon-stimulated by laser light the intrinsic recombination VUV luminescence from pre-irradiated solid Ar.

The samples of nominally pure Ar (99.999%) were deposited during 5 min in the way desribed in Sections 3.2.1 and 3.2.2. The temperature during deposition was kept low enough (6 K) to prevent all thermally stimulated processes. All films were irradiated by 1 keV electron beam during 30 min after deposition (see Section 3.1.2).

The luminescence spectra of solid Ar were recorded during the irradiation as depicted in the Section 3.3.3. After irradiation we tuned the monochromator to the wavelength of the M-band of solid Ar to register spectrally resolved intrinsic recombination luminescence from samples under laser irradiation (He-Ne laser, 2 mW, CW) (Section 3.3.2). The indicated temperature value (6 K) did not change when

the laser was switched on. Stimulated by photons in the visible range spectrally resolved luminescence in the M-band was registered.

For the detail investigation on the influence of the laser power and wavelength on such characteristics of the relaxation path as lifetime of photon-stimulated exoelectron emission (PSEE) and interconnection between photon- and thermally-stimulated processes another kind of experiments was performed.

In view of the fact that the relaxation can be triggered by photon irradiation or heating we combined methods of thermal and optical activation spectroscopy in order to investigate the whole set of relaxation paths and their interrelation. The general sequence of experimental procedures was as follows: (1) sample deposition under electron bombardment, (2) irradiation with a laser light after completing an electron bombardment and measurement of the photon-stimulated exoelectron yield, (3) after completing of the laser irradiation samples were heated with a constant rate and thermally stimulated exoelecron emission (TSEE) was monitored. Details of the experiments are given below and in the Chapter 3.

The samples of nominally pure solid argon (99.999%) were grown under irradiation of electron beam with energy 500 eV as was described in Section 3.2.1 and 3.2.2. It enables us to generate charged centers across the whole sample. During deposition the temperature was kept at 6 K to minimize possible thermally stimulated processes.

To initiate the relaxation of the pre-irradiated matrix we used as source of photons the laser light. To cover the whole visible range a combination of coherent Ar Ion Laser (Innova 70) and a Coherent CR-599 Dye Laser (Section 3.3.2) were used. The laser power measured in front of the sample was varied in the range 10 – 75 mW measured in front of the sample and laser beam was defocused to the diameter of about 3 cm to cover the whole the sample. The rise of the indicated temperature value during irradiation did not exceed 0.2 K under excitation by the most powerful laser light – 75 mW (see Section 3.3.2, Fig.3.4). The programmable temperature controller LTC 60 permitted to keep the maintained temperature during sample preparation, as well as to control the desirable heating rate. For the measurements on the pre-exposure of the sample to laser light on the following TSEE we used a continuous heating with a constant rate of 3 Kmin^{-1}. The TSEE yield was measured in a range 6 – 45 K.

The emission of electrons from pre-irradiated samples was detected as described in the Section 3.3.4. To investigate an influence of the sample structure on the lifetime of the relaxation processes we performed experiments with annealed samples. For the purpose Ar samples were prepared as was described above. After irradiation with laser light each sample was annealed at 25 K during 5 min and then cooled down to 6 K. On cooling the sample was irradiated once again with the electron beam. The laser was switched on again and exoelectron emission from the annealed sample was measured. Then we repeated the cycle of the annealing and laser irradiation with measurements of the exoelectron emission.
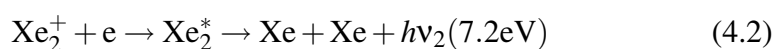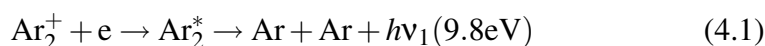
4.2.3 Results and discussion

Frenkel pairs – interstitials and vacancies can be created in atomic cryocrystals via excitation of the electronic subsystem by a low energy electron beam [128].

Electron-hole pairs are generated under electron beam quite efficiently because the ionization cross-section for electrons exceeds in several times the value of ionization cross-section for VUV photons (see [36] and Fig.1.7 in the Thesis). Holes generated under irradiation are self-trapped in the lattice within 10^{-12} s [158] due to electron-phonon interaction and become immobile at low temperature. As it was suggested theoretically [158] and proved experimentally [131, 132] the self-trapped holes (STH) have the configuration of dimer ion and could be considered as Rg_2^+ centers in own matrix. In contrast electron could not be self-trapped in solid Ar and characterized by free-like behavior [158]. Because of a negative electron affinity $E_a = -0.4$ eV [158] and therefore prevailing repulsive forces electron can be trapped only by such a kind of the lattice defects like vacancies, vacancy clusters or pores. These traps are thought to be relatively shallow but nevertheless trapped electrons remain stable at low temperatures at least up to 9 K. STH have the mobility much less than electrons (by factor $10^{-4} - 10^{-5}$) and high binding energy therefore they cannot be released in that way [158].

An activation energy needed to release and mobilize electrons could be transferred by heating as well as by photon irradiation. Solid Ar is a wide-band material with the conduction bandwidth of about $2.3 - 3.7$ eV [49] and the long-wavelength cut-off of the photoexcitation curve is defined by the trap depth. A depth of the most shallow trap was estimated to be of about 12 meV [128]. The strongest peak at 15 K in TSL of nominally pure Ar related to the exciton-induced defects is characterized by the activation energy of 15 meV according [128] and 36 meV according [150]. The deep thermally disconnected trap could be a guest atom or molecule with positive electron affinity. A typical example of so-called "electron scavenger" is oxygen. The oxygen atom has binding energy 2.61 eV and for molecular oxygen that value is 1.59 eV as one can estimate taking into account polarization energy E_p of an Ar matrix ($E_p = -1.15$ eV) [135, 137]. In fact photons in the range $3 \cdot 10^{-3}$ eV could be used to release electrons from their traps and promote them to the conduction band. Note that the intense exoelectron emission from pre-irradiated solid Ar was observed under excitation by laser light of 2.76 eV energy [134].

When the electron starts to move through the lattice there are two possibilities:

1. to recombine radiativelly with positively charged intrinsic Ar_2^+ and extrinsic (for example Xe_2^+) centers by the following reactions [62,63]:

$$Ar_2^+ + e \rightarrow Ar_2^* \rightarrow Ar + Ar + h\nu_1(9.8eV) \tag{4.1}$$

$$Xe_2^+ + e \rightarrow Xe_2^* \rightarrow Xe + Xe + h\nu_2(7.2eV) \tag{4.2}$$

2. to go to the surface and escape the sample (as it was observed in [134–136, 138] for nominally pure and doped solid Ar).

4.2.3.1   Photon-stimulated intrinsic VUV luminescence.

To verify a first relaxation channel (i) – radiative recombination of detrapped electrons with charged centers in Ar matrix, we performed an experiment on photon-stimulated luminescence (PSL) in combination with cathodoluminescence spectroscopy.

Fig.4.3 shows a typical spectrum of solid Ar recorded under 1 keV electron beam. The main feature of the spectrum is the well-known M-band at 9.8 eV, stemmed from the radiative decay of Ar_2^* center – transition from the $^{1,3}\Sigma_u^+$ state to the repulsive part of the ground state $^1\Sigma_g^+$. Note that the radiative state could be populated via the exciton self-trapping and in the process of recombination of the STH with electron.
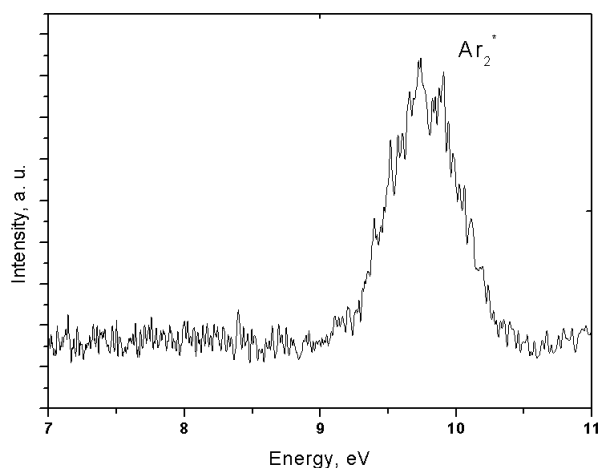
Figure 4.3: Luminescence of solid argon, excited with an electron beam at 1 keV at 4.5 K. The main feature of the spectrum is the M-band at 9.8 eV.

Pre-irradiated sample of solid Ar was exposed to the laser light of 1.96 eV energy and power 2mW. An intensity of the intrinsic recombination emission (the M-band) due to reaction (4.1) was monitored during the exposure. To prevent thermally stimulated release of electrons from the traps the sample was kept at the temperature of 6 K. The result is shown in Fig.4.4.

We observed an initial sharp rise in the VUV recombination intensity after the laser was switched-on followed by a much slower decay as the traps were emptied. No such a kind of effect was observed neither from the substrate nor from samples, which were not subjected electron beam irradiation. The experiment clearly demonstrates high efficiency of the VUV recombination luminescence stimulation by low

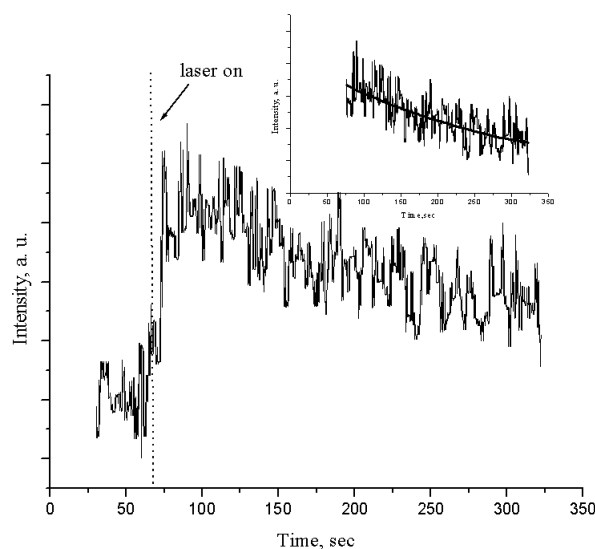Figure 4.4: Spectrally resolved luminescence from pre-irradiated solid argon in the M-band, excited with laser light ($h\nu = 1.96$ eV). The decay part of the curve shown in the inset is approximated by a first-order exponential curve with a characteristic time of 280 ± 50 s.

energy photons. Note that the energy of these photons is sufficiently high to release electrons also from such a deep impurity trap as for example O_2^-. A binding energy of electrons E_b at these centers is estimated to be $E_b = 1.6$ eV if take into account a correction to the O_2 electron affinity $E_a = 0.44$ eV [93] due to the polarization energy of Ar.

After the electron has been released from the trap it can stay in the conduction band until the recombination event or until it will escape the sample surface. According to [21] the decay of the free-carrier density N_c if consider the case of no-retrapping can be represented by a simple exponential expression:

$$N_c = N_0 g(t)\tau_c \exp(-gt) \tag{4.3}$$

where g is the product of the density of photons irradiating the sample and the effective interaction cross-section of the photons and the electrons in the traps, τ_c is the effective lifetime of the electrons in the conduction band. N_0 – the initial concentration of electrons in the traps. When we use the laser light of a constant intensity as a source of photons $g(t)$ can be described as the product of laser power P and effective interaction cross-section σ of the photons and the electrons in the traps. In that case $g(t)$ has a constant value and $g(t) = g = P\sigma$. The expression for the density of free carriers in this case could be written as follows [62]:

$$N_c = N_0 P\sigma\tau_c \exp(-P\sigma t) \tag{4.4}$$

The decay of the recombination luminescence stimulated with the laser light can be described by (4.4) with the characteristic time $\tau = g^{-1}$, which characterizes the interaction cross-section of the photons and electrons and describes the kinetics of the radiative relaxation.

The observed in our experiment behavior of the laser-induced intrinsic recombination luminescence is quite similar to that measured in the experiments [134–136, 138] on photon-stimulated exoelectron emission (PSEE) from nominally pure and doped solid Ar. Taking into account these findings and the results of our experiments one can see two channels of relaxation processes in pre-irradiated solid Ar films. Absorbed and stored in solids energy can be released by visible range photons via direct escaping of electrons from the sample (PSEE) or by recombination with positively charged centers accompanied by luminescence.

4.2.3.2 Photon-stimulated exoelectron emission. (influence of the laser power and wavelength on the parameters of relaxation)

To check the influence of visible-range photons on the direct escaping of the electrons from the sample (channel (ii)) we performed an experiment on photon-stimulated exoelectron emission. The yield of exoelectrons stimulated by laser of wavelength $\lambda = 514$ nm and power $W = 25$ mW is shown in Fig.4.5 as an example. Switching on the laser light results in a sharp signal rise with the following slow decay.

As was shown in [21, 63] the decay can be described in a no-retrapping case by the expression (4.3). Note that the intensity of the current is proportional to the concentration of electrons in the conduction band. Because a rate of the exoelectron emission and recombination luminescence on the M-band depends on the concentration of electrons in the conduction band the same expression (equation 4.3 or 4.4 depends on the source of photons) can be applied to describe both decays: photon-stimulated recombination luminescence (see reactions 4.1 and 4.2) [63] as well as PSEE. Note that the characteristic lifetime for the decay of recombination luminescence (several tens of seconds) exceeds the "intrinsic" M-band lifetime (1.8 ns for singlet and 1200 ns for triplet in Ar matrix [158]) by many orders of value [62, 63]. When we use the laser light as a source of photons $g(t)$ has a constant value and $g(t) = g = P\sigma$ (see equation (4.4)). Fig.4.5 shows the temporal evolution of PSEE signal. From the beginning after completing irradiation with an electron beam one can see slow decay of the signal, but after the laser was switched on a sharp increase of the exoelectron current was observed following its slow decay. The decay shown in Fig.4.5 can be described by (4.4) with a time $\tau = g^{-1}$, which characterized time needed for electrons passage into the conduction band and escaping the sample without any barrier because of the negative electron affinity of Ar (-0.4 eV).

An advantage of using the laser as a source of photons is the possibility change easily the laser power P at the fixed wavelength in order to clear up an influence of the laser light power on the lifetime τ. For this purpose we performed a series of experiments on PSEE with different laser power. The results are demonstrated in Fig.4.6.
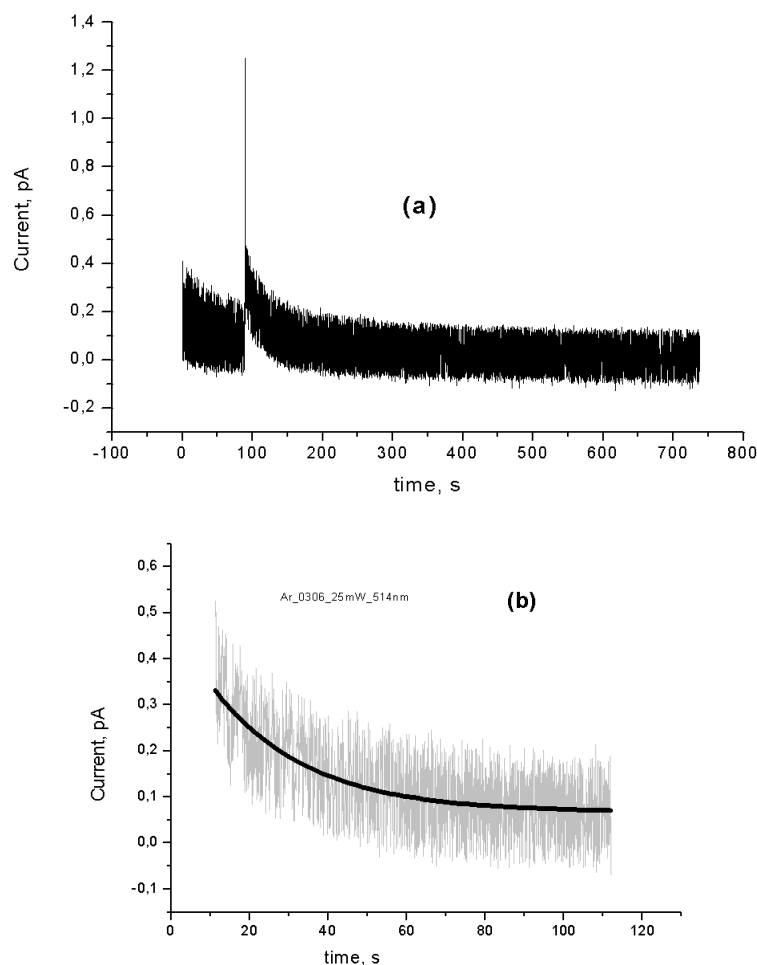
Figure 4.5: Exoelectron emission from pre-irradiated with e-beam solid Ar, stimulated with the laser light (514nm, 20mW) (a). (b) shows enlarged initial portion of the decay curve.

At the laser power 15 mW extracting from the decay curve lifetime τ is about 42 s. When we increase the laser power one can clearly see a decreasing of the lifetime. And at the 75 mW the lifetime became about 23 s. Note that the temperature rise during irradiation with the most powerful laser did not exceed 0.2 K and we can be sure that any additional thermally stimulated processes did not occur. Quite a large error in the value of the characteristic lifetime can be caused by some differences in the sample structure. We found that the experiment on determination of the lifetime is quite sensitive to the quality of the sample. In Fig.4.7 one can see the results of the PSEE experiment performed with 2 cycles of annealing.

After completing the electron beam irradiation the laser was switched on and exoelectron emission from the sample was measured. In that case we used the laser with power 20 mW and wavelength of the laser light was 514 nm. After a cycle
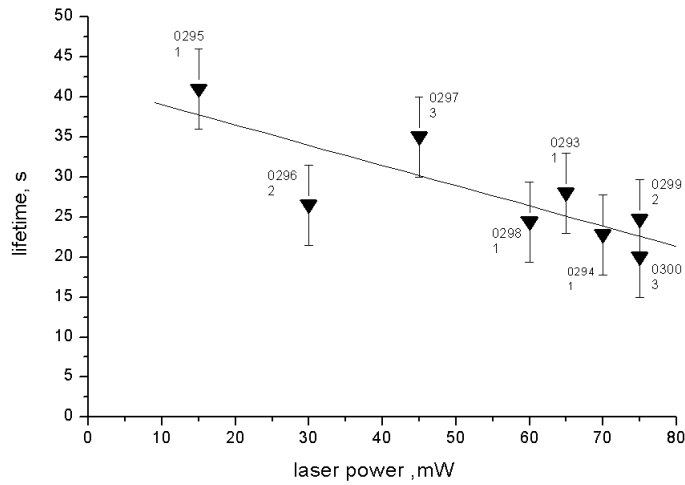
Figure 4.6: Dependence of the lifetime of the exoelectron emission from the laser power at the fixed wavelength (514 nm).

of laser irradiation the sample was annealed at 25 K during 5 min and then was cooled down to 6 K and irradiated once again by the electron beam. On completed irradiation the laser was switched on again. The lifetime extracted from the curve of the exoelectron emission is of about 13 s after first cycle of annealing and after second cycle of annealing – 8 s. The annealing procedure improves the sample structure and the effect of the electron scattering on defects of structure becomes less pronounced. This results in shortening of the time which electrons need for the escaping from the sample. And indeed τ is shortened with each following annealing cycle.

The lifetime depends on the two factors: (i) the lifetime is inversely proportional to the density of photons (laser power) irradiating the sample, (ii) the effective interaction cross-section of the photons and the electrons in the traps. That is why the lifetime of the photon-stimulated exoelectron emission is expected be dependent on the wavelength of the laser light. To check this assumption we performed a series of PSEE experiments with tunable laser. In this case Coherent Ar Ion Laser (Innova 70) and a Coherent CR-599 Dye Laser operating with Rhodamine 6G and pumped with Ar ion laser were used to cover the range from 450 to 640 nm. In Fig.4.8 one can see the decay curves of the current from pre-irradiated samples stimulated by the laser light with wavelength: 622 nm (a), 514 nm (b) and 476 nm (c).

Laser power in all these experiments was fixed and in front of the sample its value was 25 mW. The lifetimes extracted from these curves are: 36 s for the curve of exoelectron emission stimulated with the red laser (622 nm), 24 s – green laser (514 nm), and 10 s – for the blue laser (476 nm). Fig.4.9 shows the dependence of PSEE lifetime on the wavelength of the laser light at the fixed laser power. The lifetime is seen to rise as the laser wavelength increases. Thus we can say that laser
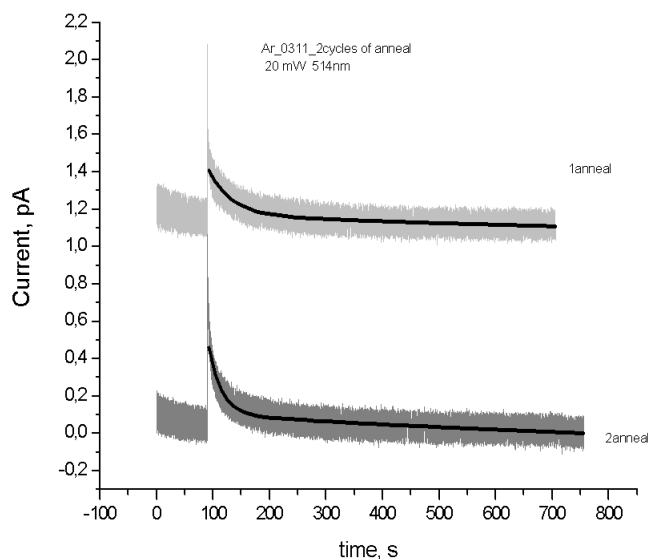
Figure 4.7: Two cycles of annealing for the sample of solid Ar pre-irradiated with e-beam. Black solid lines are the exponential fitting curves for the first cycle of annealing (a) and second one (b).
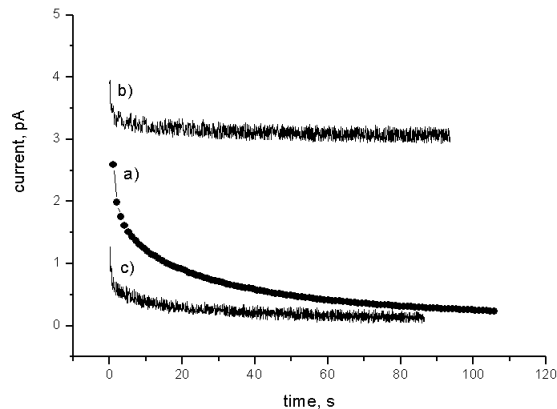
Figure 4.8: The decay curves of pre-irradiated solid Ar stimulated by the laser light with different wavelength at the fixed laser power 25 mW.
a) $\lambda = 622$ nm, b) $\lambda = 514$ nm, c) $\lambda = 476$ nm.

light with shorter wavelength shortened the lifetime for the relaxation process. A change of the laser wavelength can result in some change of the effective interaction cross-section and hence also the lifetime τ of the relaxation processes. Moreover the photons of higher energy create more "hot" electrons in the conduction band and provide a preference for the PSEE with respect to the charge recombination processes.
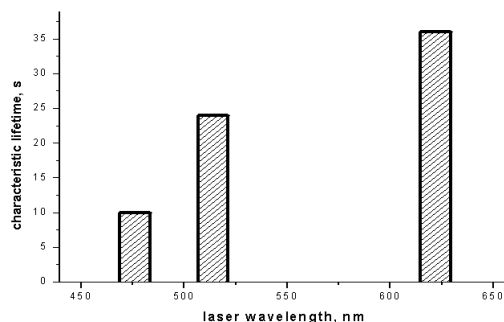
Figure 4.9: Dependence of the lifetime of the exoelectron emission from the laser wavelength at the fixed (25 mW) laser power.

An interesting question is the question on interrelation between thermally and optically stimulated relaxation processes. In view of this we performed experiments on the laser stimulated exoelectron emission with following heating. The samples were exposed to the laser light of variable power. After $600 - 700$ s when an intensity of the PSEE current goes to a noise level laser irradiation was completed. After that samples were heated with the constant rate 3.2 Kmin^{-1} from 7 to 45 K. The thermally stimulated yield of exoelectron emission (TSEE) was detected (Fig.4.10).
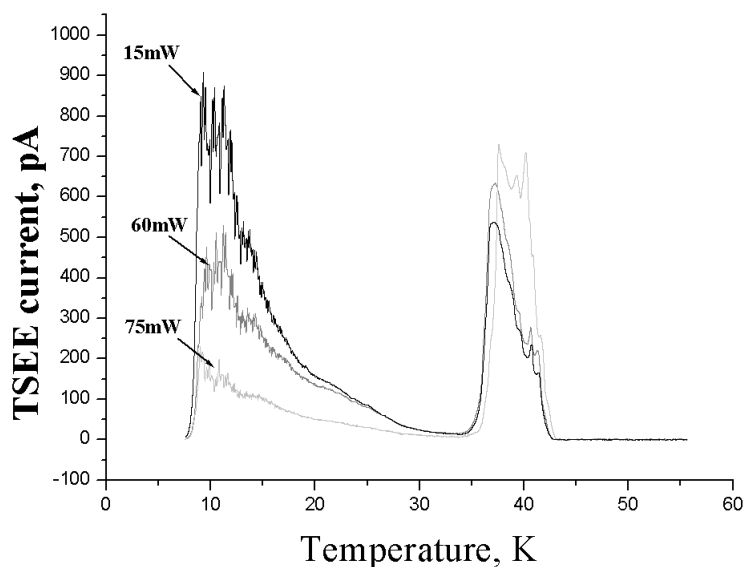
Figure 4.10: Bleaching of the low temperature peaks of the TSEE (from solid Ar pre-irradited first with an e-beam) and then irradiated with the laser light of different power at the fixed wavelength (514 nm).

Common features of the TSEE curves were similar to these registered in our pre-

vious study [133, 135, 136]. The origin of the peaks on this curve was discussed in these papers and briefly outlined below. The first peak at 12 K is caused by the de-trapping of electrons from the traps in the subsurface layer of the sample or from the grain boundaries [128, 133], the peak at 15 K is related to the radiation-stimulated defects. The shoulder at 23 K has quite not trivial origin [14, 138]. It was shown that at this temperature neutral oxygen atoms embedded into the matrix from the residual gases become mobile. Their diffusion results in the recombination of neutral O atoms and gives birth to O_2^* molecules. Their formation is followed by luminescence in the range of the well-known Herzberg progression. This chemiluminescence was considered as some kind of "internal" source of photons to release electrons from the traps [138]. In details origin of the peak at 23 K will be discussed in Section 4.3. In our experiments it was found that the intensity of these low temperature thermally stimulated peaks (LT TSEE) depends on the value of the laser power at the fixed wavelength, which was used before heating. Fig.4.10 shows this dependence.

Note that high temperature peaks around 40K are formed more likely due to charge transfer to the centers in deep layers containing more amount of residual gases which are evaporated when the sample lost its integrity.

The heating after the laser light irradiation with more powerful laser results in an effective bleaching of the LT TSEE peaks. It means that laser light with power of 75 mW at the 514 nm, for example, releases electrons from all kinds of shallow traps more effectively than laser light with power of 15 mW at the same wavelength. This causes the decreasing of the intensity of LT TSEE peaks. Dependence of the relative number of electrons forming LT TSEE to the number of photon-released electrons (PSEE) on the laser power is shown in Fig.4.11.

One can see that somewhere around 40 – 60 mW the relation of the number of LT TSEE electrons to the number of PSEE electrons become equal 1 and laser with more power releases most of electrons leaving less number of them for thermally stimulated channel.

It was supposed [134, 137] that laser light in a visible range can release electrons not only from deep, thermally disconnected traps such as a guest atoms of oxygen, for example, but also from shallow traps. The presented results on the bleaching of thermally stimulated exoelectron current peaks by laser light (514 nm) demonstrate that an increase in the laser power results in the more effective bleaching of LT TSEE. These findings give us a direct proof that shallow traps in the pre-irradiated solid Ar are effectively depopulated by photons of the visible range.

4.2.4   Conclusion

Using current activation spectroscopy method – PSEE in combination with cathodo-luminescence spectroscopy and photon-stimulated luminescence (PSL), we investigated the photon-induced relaxation processes in solid Ar which was pre-irradiated by a low energy electron beam. To avoid a possible contribution of thermally stimulated processes, the experiments were performed at low (6 K) temperature. A spectrally resolved VUV luminescence on the M-band of Ar stemmed from recom-
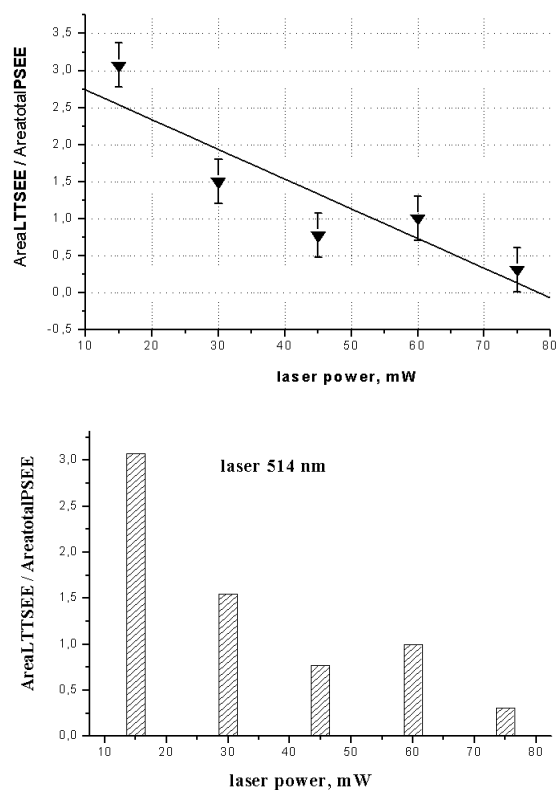
Figure 4.11: Dependence of the relative yield of exoelectrons (forming low temperature peaks) to the yield of photon-released electrons (before heating) on the laser power at the fixed wavelength (514 nm).

bination of STH and electrons was found to appear on exposure of pre-irradiated samples to laser light in visible range. This is a direct proof of stability of the intrinsic ionic centers Ar_2^+ at low temperatures and high efficiency of photon-stimulated radiative recombination of STHs of dimer configuration Ar_2^+ with electrons. The kinetics of their decay, in other words photo-bleaching of Ar_2^+ centers, under continuous laser emission is characterized by the long life-time of about 200 seconds at low laser power.

The experiments on PSEE from pre-irradiated solid Ar demonstrated efficiency of the second relaxation channel – photon-stimulated exoelectron emission. Its detail study yielded the new data on photo-bleaching of charged centers. Influence of the laser power and wavelength on the characteristic lifetime τ of PSEE was investigated. It was shown that an increase of the laser power causes a decrease of the lifetime. The increase of the wavelength of the laser light at fixed power results in an increase of the τ. These results are in a good agreement with the model of photon-stimulated processes [21] assuming that the lifetime τ is inversely proportional to the product of the density of photons irradiating the sample and the effective interaction cross-section of the photons and the electrons in the traps. It was found that

the characteristic lifetime τ appeared to be sensitive to the sample structure – as the sample structure becomes more perfect τ is shortened.

The study of bleaching of TSEE peaks by a pre-exposure to the laser emission have shown that the laser light effectively detraps electrons not only from deep but also from shallow traps in pre-irradiated solid Ar. From the experiments on the PSEE it was concluded that the increasing in photon density not only shortens characteristic relaxation time τ but more effectively bleaches LT TSEE peaks. The results obtained revealed a vital role of radiative processes in relaxation cascades.

The results presented in this section were published and approved at the conferences [appendixes: list of publications [9,15] and list of conferences].

4.3 Relaxation paths stimulated by "internal source" of light: key role of N radicals radiative decay forbidden transition ^{2}D → ^{4}S

4.3.1 Introduction

An exposure of doped rare-gas solids or RGS containing some guests to ionizing radiation results in generation not only of charged centers such as self-trapped/trapped charge carriers and structural defects but also to a formation of metastable neutral species like atoms and radicals. Spatially separated charge carriers and neutral species remain stable at low temperatures after completing irradiation. Some of these transient species are characterized by long lifetimes. Especially prominent appears to be nitrogen atom or N radical. Its radiative decay lifetime τ of the forbidden transition in Ne matrix is about 350 s and in Ar matrix τ is about 20 s [161]. With this in mind we focused on processes of relaxation occurring immediately after completed irradiation with an electron beam of Ar doped with nitrogen.

In this section we present new results: influence of internal source of visible light – afterglow from atomic nitrogen – on relaxation channels involving photon-stimulated radiative recombination (intrinsic and extrinsic) of charge centers with electrons in the VUV range and corresponding PSEE from doped Ar solids preliminary exposed to the low energy electron beam. Under electron bombardment N_2 molecules were fragmented and metastable atomic nitrogen was efficiently formed. The green afterglow from atomic nitrogen due to the well-known forbidden transition $^2D → {}^4S$ indicating the formation of N radicals was used as the "internal light source" for the stimulation of the relaxation.

It was found by our group that the characteristic lifetimes of the exoelectron emission and recombination luminescence of intrinsic and extrinsic charged centers were around 20 seconds, which is characteristic for the afterglow from atomic nitrogen in Ar matrix [161].

4.3.2 Experimental

General description of the experimental techniques was given in Chapter 3. Only essential points are mentioned here. For the purpose solid Ar (99.999%) was doped with N_2 (with a ratio 10^{-2}) and Xe (with a ratio 10^{-3}) to form not only intrinsic but also extrinsic charged centers and metastable ones. Samples were grown from the gas phase and the temperature was kept 6 K during deposition and measurements. Films were irradiated by an electron beam (500 eV) during deposition (30 min). Details of the sample preparation are given in the Section 3.2.

Photon-stimulated exoelectron emission as well as spectrally resolved VUV recombination luminescence of intrinsic Ar_2^+ and extrinsic Xe_2^+ centers with electrons (indicated by the radiative transitions of neutralized centers Ar_2^* and Xe_2^* to the ground state) were registered (see Section 3.3). In order to register the spectrally resolved charge recombination luminescence in the VUV range after irradiation we tuned the VUV monochromator to the wavelength of the M-band of solid Ar and Xe respectively. The luminescence intensity of the corresponding band was recorded immediately after shut down of the electron beam. Simultaneously with exoelectron emission from the doped solid Ar an afterglow in the visible range on the wavelength of $^2D \rightarrow {}^4S$ transition of N radicals was monitored.

4.3.3 Results and discussion

4.3.3.1 Relaxation mechanism

Electron-hole pairs are efficiently created in RGS under electron bombardment. Holes are self-trapped in the lattice within 10-12 s [158] due to electron-phonon interaction and become immobile at a low temperature forming ionic centers of dimer configuration Rg_2^+ [158]. Electrons in the Ar matrix can be trapped by pre-existing defects such as vacancies, vacancy clusters, pores because of a negative electron affinity of pure argon (-0.4 eV) [158] or by guest atoms with positive electron affinity [137]. Another kind of traps for electrons is produced under irradiation. It was found that Frenkel pairs – interstitials and vacancies – are created in an Ar matrix via excitation of the electronic subsystem by a low energy electron beam [128]. The energy stored by the pre-irradiated sample can be released thermally or optically. The trapped electron receives an additional part of energy and can be promoted into the conduction band. Holes have less mobility by a factor of $10^{-4} - 10^{-5}$ [158] and cannot be released in that way. The depth of a shallow trap for the electron was estimated to be about 12 meV [107]. The deep trap, so-called thermally disconnected trap, is a guest atom. The binding energy for an N atom taking into account the polarisation energy of the Ar matrix is 1.05 eV and for an O atom – 2.61 eV, for O_2 this value is 1.59 eV [137]. Note that the conduction band in solid argon is 2.35 eV [49].

Electrons in the conduction band have several possibilities: to escape the sample directly or to recombine radiatively with positively charged centers. These processes were detected and studied in our experiments [133, 135, 136, 138] and [62, 136, 138] correspondingly.

4.3.3.2   Photon-stimulated exoelectron emission

To check the possibility of direct escaping of electrons from the sample at low temperature (6K) we performed experiments on the exoelectron emission. A typical luminescence spectrum in the visible range recorded under electron beam is shown in Fig.4.12.
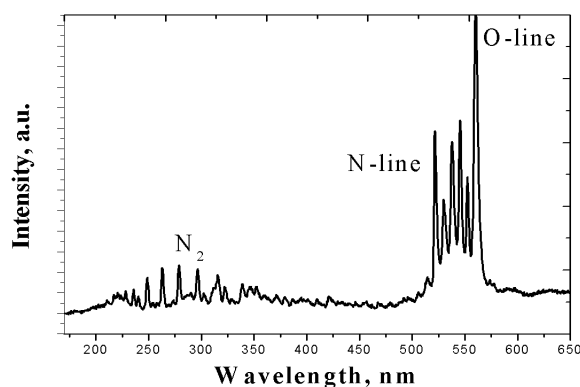

Figure 4.12: Cathodoluminescence spectrum of solid Ar doped with Xe and N$_2$ at 6 K.

In the range 240–340 nm one can see the Vegard-Kaplan bands $(A^3\Sigma_u^+ \rightarrow X^1\Sigma_g^+)$ [99]. The peak at 561 nm belongs to O atoms [99, 138] (^{1}S $\rightarrow$ ^{1}D transition). Note that this peak and the N$_2$ series have quite a short (less then 1s) lifetime. The main interesting feature is the peak at 523 nm – the well-known forbidden transition ^{2}D $\rightarrow$ ^{4}S indicating the formation of N atoms [137]. This is only one peak with long lifetime in the matrix.

After completing the irradiation, spectra in the range 170-1100 nm simultaneously with current were measured. In Fig.4.13(a) one can see clearly the exponential decay of the N line according to the expression:

$$g(t) = g_0 \exp\left(-\frac{t}{\tau}\right) \tag{4.5}$$

where g_0 is the initial concentration of excited N atoms and τ is the N line lifetime. τ extracted from that curve is about 20 ± 4 s in an Ar matrix and that is in good agreement with the results published in [161].

The energy of the ^{2}D $\rightarrow$ ^{4}S transition of 2.37 eV is sufficient to excite the trapped electrons into the CB stimulating electron transport followed by the exoelectron emission [137]. The yield of electrons from the sample was registered (Fig.4.13(b)) and one can clearly see a decay of the current.

That decay can be described by the following expression in the no-retrapping case [21]:

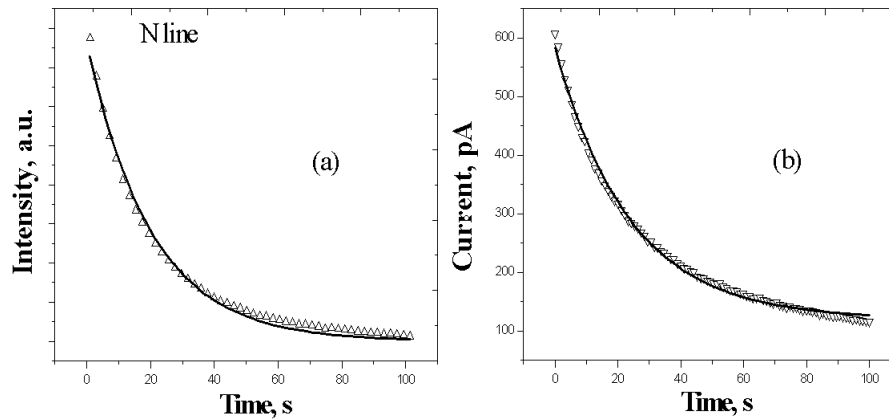$$N_c = N_0 g(t)\tau_c \exp(-gt) \tag{4.6}$$

Figure 4.13: Intensity of N-line (a) and exoelectron emission (b) recorded from the Ar doped with Xe and N_2 at 6 K after irradiation.

where g is the product of the density of photons irradiating the sample and the effective interaction cross-section of the photons and the electrons in the traps. τ_c is the effective lifetime of the electrons in the conduction band. N_0 – the initial concentration of electrons in the traps. In the special case the density of photons follows an exponential decay of afterglow $g(t) = g_0 \exp\left(-\frac{t}{\tau}\right)$ [99]. To estimate the characteristic lifetime $\tau = \frac{1}{g}$ we have to take into account that g is not constant now. In the range $t \sim \tau$ expression (4.6) is simplified and N_c decay will be described mainly by the exponent $g_0 \exp\left(-\frac{t}{\tau}\right)$. We received τ extracted from the curve (Fig.4.13(b)) of about 20 s. That characteristic time correlated well with the N line lifetime. During that characteristic time trapped electrons go into the conduction band and escape the sample directly without any barrier because of the negative electron affinity of Ar.

4.3.3.3 Photon-stimulated recombination luminescence

The experiment on PSL was made to monitor a charge recombination reaction. Xe was introduced to form extrinsic ionic centers. A cathodoluminescence spectrum is shown in Fig.4.14. The spectrum consists of the well-known molecular bands stemming from $^{1,3}\Sigma_u^+ \rightarrow {}^1\Sigma_g^+$ transitions – M-band for Ar at 9.8 eV and M-band for Xe_2^* at 7.2 eV and atomic band of Xe at 8.6 eV.

The intensity of the M-band for Ar and Xe recorded after completing the irradiation exhibits quite a long decay close to the lifetime of N atoms (around 20 s) in contrast with the intrinsic M-band lifetime – 1.8 ns for singlet and 1200 ns for triplet in Ar matrix [158]. Results are shown in Fig.4.15(a,b). In the no-retrapping case that decay can be described also by expression (4.6) because the rate of both processes – exoelectron emission and recombination luminescence – depends on the concentration of electrons in the conduction band.

The estimated characteristic lifetime is 24 s for the M-band of Xe and 19 s for
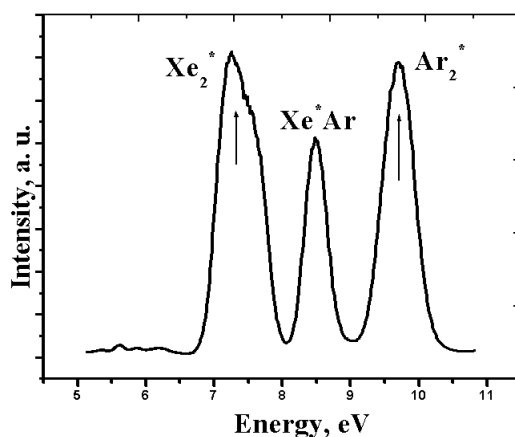
Figure 4.14: Luminescence of solid Ar doped with Xe under e-beam.
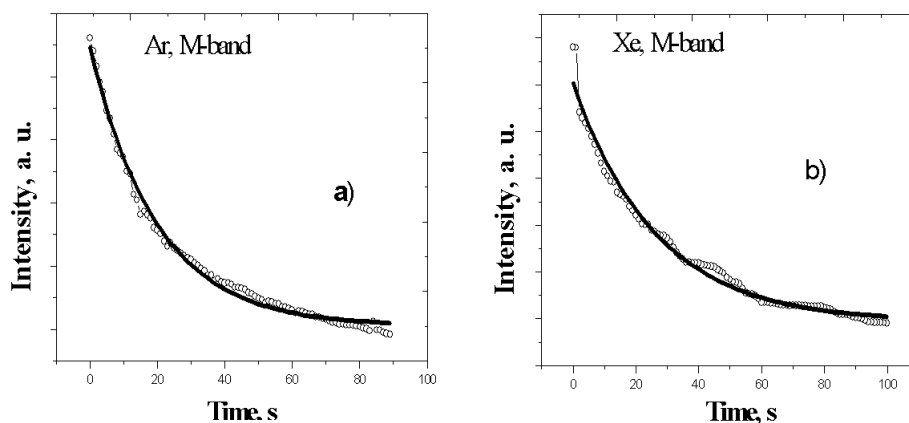
Figure 4.15: M-band for Ar (a) and Xe (b) detected after irradiation at 6K

the M-band of Ar respectively. Taking into account the estimation error we can say that both lifetimes are around 20 s. These values correlate with the lifetime of N atoms and current decay. It shows that Xe efficiently forms positively charged centers despite the positive electron affinity (+0.3 eV [158]).

4.3.4 Conclusion

The relaxation process in solid Ar pre-irradiated with a low-energy electron beam was studied. We used the activation spectroscopy method – PSL in combination with CL and PSEE. The information on photon-stimulated processes was obtained in the experiments with an "internal light source" – green afterglow from atomic nitrogen. The similar lifetimes for the N line decay, PSEE yield and intensities of the VUV recombination luminescence (intrinsic and extrinsic) give us a direct proof that the emission of exoelectrons and VUV recombination luminescence are stimulated by

the radiative transition of metastable N atoms – some kind of "internal photoeffect" followed by conversion of visible light into VUV photons.

The results presented in this section were published and approved at the conferences [appendixes: list of publications [3,14] and list of conferences].

4.4 Oxygen driven relaxation processes in pre-irradiated Ar solids: relaxation channels stimulated by chemiluminescence of O_2^*

4.4.1 Introduction

The electronic excitations in insulating materials induced by ionizing radiation initiate a sequence of relaxation processes involving both nuclear (atomic) and electronic subsystems. Very often electronic and atomic relaxation processes occurring in pre-irradiated solids are considered separately ignoring the interconnection between these channels of relaxation. Our recent studies demonstrated the fundamental importance of the interconnection between atomic and electronic processes in the formation and branching of relaxation paths [14, 64, 138].

In this section the role of oxygen atomic reactions in the relaxation cascades of pre-irradiated RGS is investigated. Oxygen is one of the most abundant elements in the universe that exhibits in many respects unique properties attracting considerable interest of scientists over many years. A.F. Prikhot'ko studied extensively elementary excitation of solid oxygen [52] and a lot of the credit must go to her research group, which discovered a number of novel phenomena in solid oxygen. The brilliant findings of A.F. Prikhot'ko inspired us when we went to the heart of the matter on the role of oxygen in the relaxation pattern of pre-excited cryocrystals.

Ar cryocrystals were chosen as matrices for several reasons: (i) because of a small atomic radius of oxygen (0.12 nm) it can be easily stabilized at low temperatures in Ar solids without any significant distortion of the lattice; (ii) solid Ar and O_2 have close sublimation temperatures (about 30 K); (iii) a high mobility and free-like behavior of electrons in solid Ar [158] together with a large electron escape depth of about 500 nm [61] enables one to gain information about relaxation processes in the bulk and at the surface; (iv) a negative electron affinity of solid Ar ($\chi = -0.4$ eV [158]) facilitates escaping the electrons from the surface.

In order to study simultaneously the relaxation in atomic and electronic subsystems we employed a combination of optical and current activation spectroscopy methods: TSL and TSEE. The findings of "real time-correlated activation spectroscopy" study of relaxation processes in pre-irradiated Ar solids doped with oxygen are presented.

We found that the thermally assisted diffusion of neutral atoms in the RGS lattice appeared to be primary process triggering electronic relaxation cascades – exoelectron emission and charge recombination reactions. The suggested mechanism

responsible for these relaxation channels is based on a chemiluminescent atom-atom recombination reaction. In a course of the experiments the origin of thermally stimulated peak at 23K in TSL and TSEE from pre-irradiated Ar solids was elucidated. A solid evidence of its origin due to O-O radiative recombination reaction is obtained.

4.4.2 Experimental

Thermally stimulated relaxation channels from pre-irradiated solid Ar doped with oxygen were investigated. The samples were grown in a standard way as was described in Section 3.2. The samples were doped with amounts of O_2 in a range $10^{-3} - 10^{-5}$. The deposition was performed under e-beam or samples were irradiated after deposition. The relaxation processes in the Ar samples were studied in the temperature range from 7 to 42K. To improve the sample structure series of experiments with annealed samples of Ar was performed. For the purpose after deposition under irradiation by e-beam the samples were warmed up to 25 K with a constant heating rate, then we kept them at 25 K during of about 5 min and then cooled down to 6 K and irradiated with e-beam again. After the procedure the substrate was turned to the position for measurements.

In earlier modification (see Section 3.3.3) of the experimental setup the luminescence spectra of the samples during irradiation, and their changes, were recorded in VUV and visible ranges. After the completed irradiation, we investigated the TSL of the samples, both the total yield and yields at the indicated wavelengths. TSEE measurements were done with the samples grown at the identical conditions following a standard procedure described in Section 3.3.4.

In a new modification of the experimental technique – the "real time-correlated activation spectroscopy" – presented in Section 3.4 we measured simultaneously at the same sample the yields of thermally stimulated exoelectron emission (TSEE) from the samples and spectrally-resolved thermally stimulated luminescence (TSL) in the visible range or the yield of TSL in the VUV range. The program developed by A.N. Ponomaryov permitted us to detect synchronously spectra over the entire operating range, TSEE current, temperature and pressure in the chamber simultaneously.

4.4.3 Results and discussion

The aim of our study presented in this Section is to reveal interconnection between atomic and electronic relaxation processes and elucidate possible mechanisms of such an interconnection. Primary process in the atomic subsystem under study is thermally stimulated diffusion of O atoms in pre-irradiated Ar matrix. The recombination of neutral O atoms is followed by an intense chemiluminescence. The response of other relaxation processes to oxygen atom-atom recombination was monitored by detection of intrinsic and extrinsic charge recombination reactions (TSL in the VUV range) and TSEE yields. In a course of study the origin and mechanism

of 23 K peak formation in TSL and TSEE yields from pre-irradiated solid Ar were cleared up.

All relaxation channels are quite sensitive to the structure of sample. That is why before main discussion we will show an influence of the sample structure on the thermally stimulated paths and briefly will describe an origin of thermally stimulated peaks in "glow curves" and "current curves" for thermally stimulated luminescence (TSL) and exoelectron emission (TSEE).

In order to clear up a part of pre-existing defects serving as electron traps a series of the experiments with measurements of TSL and TSEE yields from unannealed and annealed samples was performed. Typical "glow curves" and "current curves" are shown in Fig.4.16.
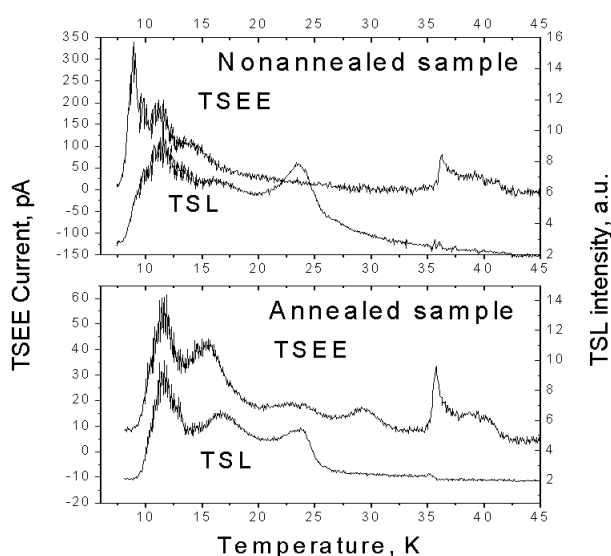

Figure 4.16: TSEE and TSL yields from unannealed and annealed Ar samples.

The yield of TSEE from unannealed samples is more than 5 times higher than that from annealed ones due to higher concentration of pre-existing defects. However, only some temperature peaks of TSEE correlate with peaks in the TSL yield. In low temperature range we observed strong peak at 8K which was not seen in TSL. The peak at 23K related to O atom recombination does not show up itself in the TSEE curve. High temperature features caused by impurity centers in deep layers are strongly enhanced in TSEE. The reason is that above 30K sublimation of sample occurs making possible exoelectron emission from deep layers of the sample. Clear correlation was found only for the 12K peak related to the subsurface layer. Note that radiation induced peak at 15K is seen as a shoulder of the TSEE curve.

Annealing of the sample at 27K resulted in essential changes especially in the TSEE curve. The yield of TSEE therewith shows a decrease in response to lowering the electron trap concentration. The curves of annealed sample exhibit pronounced structure. An interesting fact is the coincidence of nearly all peak positions. In view of negative electron affinity χ of solid Ar [158] exoelectron emission is appeared

to be the barrier-free process and the TSEE peaks emerge at the same temperature as the correspondent TSL peaks. Such a situation was considered theoretically [60] with definite set of parameters and χ of about $\chi = -0.5eV$. The peak at 15K stemmed from annihilation of radiation induced Frenkel pairs [10, 107] dominates in the spectrum as seen from a comparison of areas under the peaks. Yields of photons and exoelectrons look similar demonstrating correlation of these phenomena in annealed samples pre-irradiated with an electron beam. It means that the defects in the subsurface layer of an annealed sample are a continuity of the bulk defects and the TSEE yield carries the information not only on surface layer defects but also on more deep layers of the samples. This corroboration is consistent with quite a large electron escape depth (500nm) [61]. The special experiments were performed to estimate the TSEE active layer in pre-irradiated solid Ar. The samples of different thickness were deposited under electron beam to generate charge carriers through the entire sample and TSEE yield was measured as a function of sample thickness. The TSEE yield runs up to saturation in the range of thickness of about 1000nm while the TSL yield increases linearly. This dependence is shown in Fig.4.17.
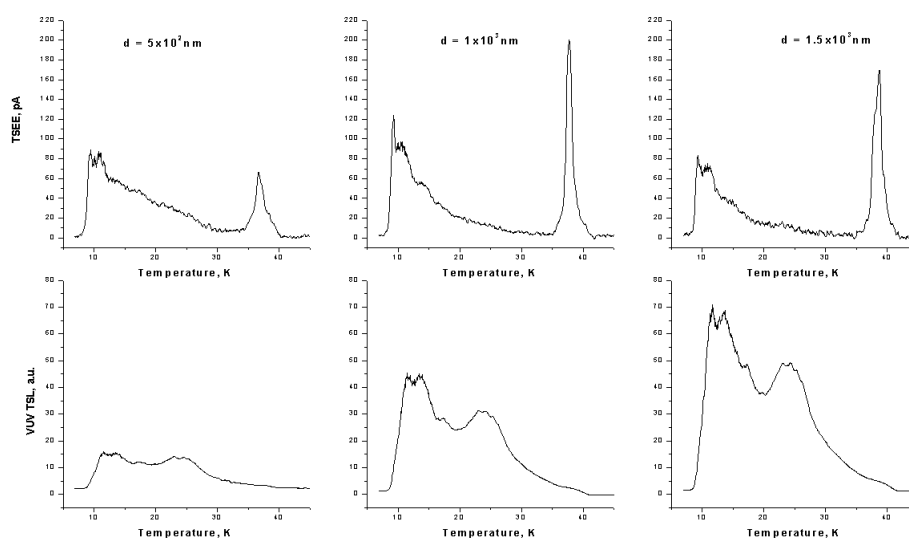
Figure 4.17: Dependence of the TSEE and VUV TSL yields from the sample thickness.

A competition between emission of photons and exoelectrons made itself evident also in the dose dependence of TSEE and TSL total yields from pre-irradiated samples as shown in Fig.4.18. This tendency is kept for both unannealed and annealed samples. TSEE clearly dominates for small irradiation doses.

Analysis of typical glow curves for annealed Ar samples is given below. Fig.4.19 shows typical curves of the yields of thermally stimulated exoelectron emission TSEE and recombination thermally stimulated luminescence TSL in the VUV range
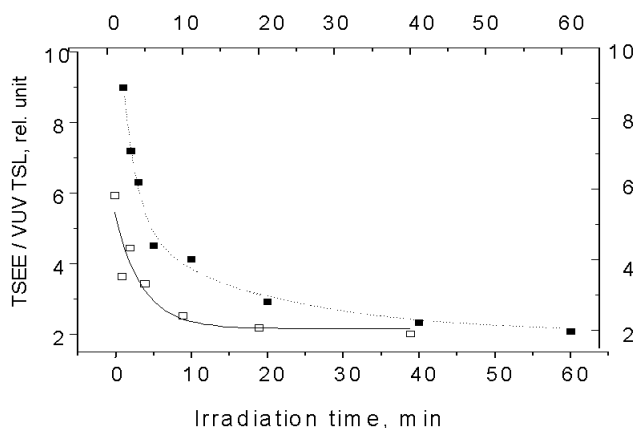
Figure 4.18: Dose dependence of relative TSEE and TSL yields for annealed (empty boxes) and unannealed (filled boxes) Ar samples

stemmed from the reaction:

$$\mathrm{Ar}_2^+ + \mathrm{e} \rightarrow \mathrm{Ar}_2^* \rightarrow \mathrm{Ar} + \mathrm{Ar} + \Delta E + h\nu\,(9.7\mathrm{eV}) \tag{4.7}$$
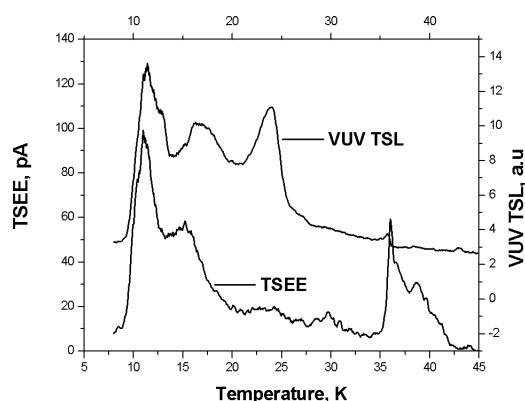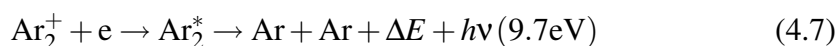
Figure 4.19: Yields of TSL in the VUV range and TSEE taken from the sample of Ar, which was annealed at 25 K and then irradiated at 7 K.

The measurements were performed simultaneously on the same sample in the temperature range 7 – 42 K using heating at a constant rate of 3.2 Kmin^{-1}. The clearly seen structure of the curves reasonably agrees with the previously measured yield of TSL detected in the M-band [82,128] and the yield of TSEE [133] with the only difference that the curves in Fig.4.19 show more distinct features.

The low temperature peak at 11.5 K is related to the electron traps in a sub-surface layer or at inner interfaces of the sample. The peak at about 15 K exhibiting the pronounce dose dependence was assigned to radiation-induced defects [107,128,133,150]. A rather strong TSEE maximum observed between 37 and 41 K

is presumably due to electrons trapped close to the substrate too deep in the sample to escape the surface at low temperatures, which are however released on the sample evaporation. The corresponding maximum in the VUV TSL turned out to be quite weak.

The origin of the broad 23 K peak in thermally stimulated phenomena was under discussion over 10 years. This peak was detected in the total yield of TSL [107, 133] and in intrinsic recombination emission – spectrally resolved TSL in the M-band [128] taken from Ar pre-irradiated by a 1 keV electron beam as well as from Ar pre-irradiated by X-rays [82]. Note that the peak at 23 K was also registered in the thermally stimulated conductivity [150] and in thermally stimulated exoelectron emission [133]. On the other hand, the intensity of this peak showed a clear connection with the presence of oxygen in the samples enhancing TSL and TSEE peaks at 23 K with increasing oxygen content. Monitoring of spectrally resolved TSL in the visible range taken from pre-irradiated Ar solids revealed the emergence of O_2^* emission near 23 K in oxygen-containing samples.

Different mechanisms of the 23 K peak formation were suggested to explain this puzzling behaviour of this peak in the yields of thermally stimulated phenomena in Ar solids. For instance it has been suggested in [150] that this peak is caused by recombination of O^- ions with neutral O atoms. It should be mentioned that in the experiments on TSC of doped Ar solids [150] the peak at 23 K was only one observed in TSL measured in the emission of O_2 (Herzberg bands). It was found that O atoms start to diffuse at about 20K to form molecular centers O_2 and this process of thermally stimulated atom diffusion results in recombination of neutral atoms yielding chemiluminescence. The authors of [150] observed also TSC at about 23 K in oxygen doped samples. It was explained by recombination of O^- ions with neutral O atoms followed by detachment of electron from O^-. Activation energy estimated for the 23 K peak is $E_t = 61$ meV [10]. The binding energy E_b of electron to O^- is defined by electron affnity E_a of oxygen atom $E_a = 1.461$ eV [93] and polarization energy E_p of Ar matrix $E_p = -1.15$ eV [96]: $E_b = E_a - E_p = 2.61$ eV. Because of a big difference in E_t and E_b the peak at 23 K clearly cannot be attributed to a direct process of thermally activated electron detachment. The other possibility suggested [150] is a thermal diffusion of O atoms and O^- ions. However, ions are characterized by short-range mobilities as it was demonstrated in the experiments on transmission of ions through rare-gas films [1]. In contrast with this neutral atoms in cryogenic solids yield long-range mobilities with migration length of 30 nm [18,30].

Another scenario was suggested and discussed in [136, 138]. It was supposed that neutral O atoms on heating started to diffuse through the Ar lattice forming oxygen molecules O_2^*. The radiative transition of O_2^* into the ground state was considered as a stimulating factor to electron detrapping which is the primary step of branching relaxation channels. In order to investigate an influence of oxygen impurities in Ar matrix on the relaxation processes and especially to clear up the mechanism of 23 K peak origin the series of experiments with pre-irradiated by low energy electron beam Ar samples doped with O_2 was performed.

The presence of O atoms was monitored by the luminescence spectra recording.

Fig.4.20 demonstrates the luminescence of O_2/Ar sample excited by an electron beam at T = 8 K. The line of atomic oxygen at 2.2 eV dominates in the spectrum and its intensity decreases with temperature rise that is in accordance with the data [13]. Along with this emission the spectrum exhibits a series of molecular luminescence bands of O_2^*. Some region of this progression (1.8 – 2.7 eV) is shown in Fig.4.20.
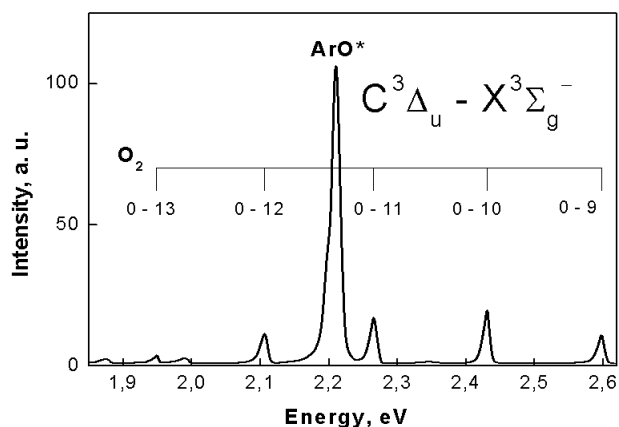

Figure 4.20: Luminescence spectrum of the O_2 doped solid Ar (1% of O_2). Ar films measured in the range of oxygen emissions at T=8K.

Experiments [55] with selective excitation of O_2 in Ar matrix and isotope analysis identifed this emission, attributed by some authors to A $\rightarrow$ X transition, as the $C_3\Delta_u \rightarrow X^3\Sigma_g^-$ transition (0-v bands). The emission bands reported in [55] and then in [13] are in general agreement with the bands observed in our experiments. TSL was measured at the wavelength of the (0-10) band. No TSL signal was observed at low temperatures up to 15 K. Beginning with this temperature the heating of the pre-irradiated sample gave rise to the TSL signal (curve 1 in Fig.4.21).

Two features were seen in the O_2^* emission – some shoulder at 18 K and pronounced maximum at 23 K. The emission was completely quenched at 28 K.

One may suggest that these two features in the TSL yield result from thermally induced diffusion of O atoms detrapped from different lattice sites followed by O_2^* formation. Comparison of the atomic diameter of oxygen with the size of trapping sites in fcc lattice of solid Ar [102] shows that O atoms can be trapped in substitutional (3.75 A) and in interstitial octahedral (1.56 A) sites.

In order to estimate activation energies needed for the detrapping we resorted to the so-called "cleaning technique" [169]. This technique is common in use when some material exhibits a multipeak TSL glow curve. All peaks at temperatures lower than the peak under study are removed by a proper thermal treatment or by high temperature irradiation. First the sample was irradiated at temperature T = 15 K and then the yield of the TSL was measured. A typical glow curve is shown in Fig.4.21 (curve 2). To isolate the most intensive peak the TSL yield was measured from the sample irradiated at 19 K (curve 3 in Fig.4.21). The Garlick-Gibson initial-
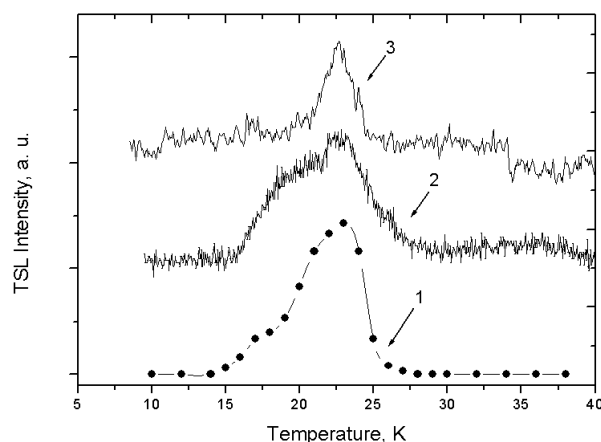
Figure 4.21: TSL of oxygen-containing sample (10^{-5}) recorded (1) at the wavelength of O_2^* emission, (2) from the sample pre-irradiated at 15K and (3) at 19K.

rise method [169], which is independent of the order of the kinetics, was applied to estimate the corresponding activation energies. In the initial portion of a glow curve the TSL intensity is proportional to $\exp(-E_{act}/kT)$. The analysis of several sets of glow curves measured as described above gave $E_{act} = 20 \pm 5$ meV for the first maximum and $E_{act} = 50 \pm 5$ meV for the second one. The TSL intensity is proportional to the rate of O_2^* formation due to O atom detrapping

$$I_{\text{TSL}} = -\frac{dN}{dt} \tag{4.8}$$

where N is the concentration of O atoms in traps.

In first order kinetics

$$\frac{dN}{dt} = -K(t)N \tag{4.9}$$

at the initial conditions $t = t_0$, $N = N_0$.

The solution of Eq.(4.9) is

$$N = N_0 \left(1 - \exp\left\{ -\int_{t_0}^{t} K(\tau)d\tau \right\} \right) \tag{4.10}$$

Assuming the Arrhenius form:

$$K(t) = s \exp\left(-\frac{E_{\text{act}}}{kT(t)} \right) \tag{4.11}$$

Here s is a frequency factor and in the case of $T = \beta t$ the intensity of TSL can be expressed by

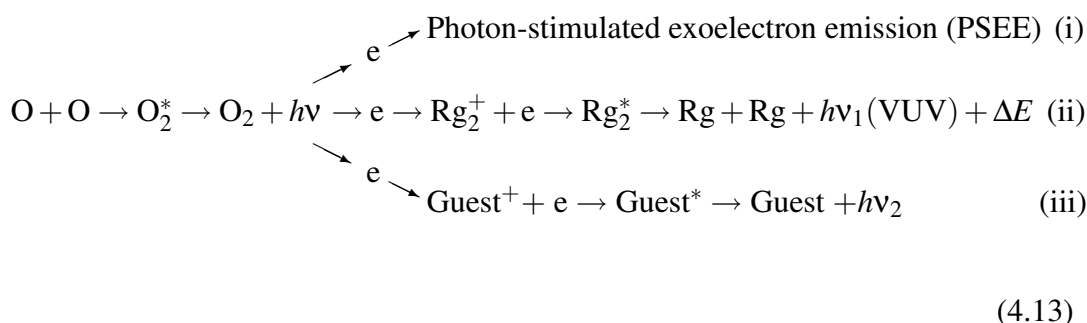$$I_{\text{TSL}} = N_0 s \, \exp\left(-\frac{E_{\text{act}}}{kT}\right) \exp\left[-\frac{s}{\beta} \int_{T_0}^{T} \exp\left(-\frac{E_{\text{act}}}{k\theta}\right) d\theta\right] \qquad (4.12)$$

Note that the recombination of neutral atoms is described by the same formalism as the recombination of charged carriers [30, 138, 169] and the estimated E_{act} are in a good agreement with E_{act}, obtained using curve-fitting technique for analysis of the total [82] and spectrally resolved [10] yields of TSL from solid Ar. While the main peak of the TSL in the visible range at 23 K is clearly due to thermally induced radiative recombination of neutral O atoms the peaks at the same temperature were also detected in TSEE from oxygen-containing samples grown at the similar conditions [134] and in spectrally resolved VUV TSL stemmed from recombination of self-trapped holes (Ar_2^+) [107] as well as ionic guests (CO^+) [10] with electrons. These observations provide impressive evidence that thermally induced atomic process diffusion of O species followed by their radiative recombination, has a dramatic impact on processes of electronic relaxation incorporating transport of electrons. If not explicitly mentioned, O atoms and O_2 molecules are effective electron traps with binding energies $E_b = 2.61$ eV for O^- and $E_b = 1.6$ eV for O_2^- as it was estimated taking into account the polarization energy of an Ar matrix [135]. The energy release in the nonradiative process of the vibrational relaxation of O_2^* species, that does not exceed the Debye energy 12 meV, cannot account for the electron detachment from these deep thermally disconnected traps. Suggestion on a thermal diffusion of negative ionic species O^- [150] is in contradiction with low mobility of ions in RGS [1].

We proposed the following scenario based on the key role of radiative electronic transitions in the relaxation cascade. O atoms generated in the matrix under irradiation and trapped in interstitial octahedral and in substitutional sites start to diffuse upon heating. Diffusion occurs most likely via interstitial sites for the former type of O atoms and by the vacancy mechanism for the latter ones. Note that the estimated energy of vacancy formation near a guest O atom in solid Ar is of 90 ± 30 meV, that is close to activation energy for 23K peak $E_{\text{act}} = 60$ meV [82]. Recombination of O atoms results in a formation of O_2^* molecule in the bound state. Direct measurements of O_2^* emission performed in this study permit to identify radiative transition responsible for the TSL as the $C^3\Delta_u \rightarrow X^3\Sigma_g^-$ transition. A subsequence of elementary processes of relaxation can be presented by following reactions:

$$O + O \rightarrow O_2^* \rightarrow O_2 + h\nu \rightarrow e \rightarrow Rg_2^+ + e \rightarrow Rg_2^* \rightarrow Rg + Rg + h\nu_1(\text{VUV}) + \Delta E \quad \text{(ii)}$$

Photon-stimulated exoelectron emission (PSEE) (i)

$$\text{Guest}^+ + e \rightarrow \text{Guest}^* \rightarrow \text{Guest} + h\nu_2 \quad \text{(iii)}$$

$$(4.13)$$

where Rg is a rare-gas atom.

The key process of this cascade is the photon-stimulated electron detrapping promoting electrons into the conduction band. Due to negative electron affinity E_a of solid Ar ($E_a = -0.4$ eV [158]) electrons occupying the bottom of the conduction band are at higher energy than the vacuum level, so there is no barrier for electron to escape from the surface that facilitates measurements of exoelectron emission from Ar films. Special experiments on PSEE performed with laser excitation [62, 64, 134, 135] at low temperatures and described in Section 4.2 provide strong evidence of proposed radiative mechanism of electron detrapping. Note that in the suggested scenario the chemiluminescent reaction is an initiating factor. Taking into account that an intense luminescence occurs in a variety of processes especially in cryogenic matrices, the considered mechanism seems to be of high importance.

To verify the discussed above [136, 138, 150] mechanisms of triggering relaxation cascades by recombination reactions we performed the experiments with synchronous measurements of thermally stimulated chemiluminescence of O_2^* stemmed from the diffusion-controlled atom-atom recombination reaction and TSEE yield as well as yields of TSEE and TSL in the VUV range originated from the intrinsic charge recombination reaction 4.7. The samples were doped with O_2 (10^{-3}) and the generation of O atoms under irradiation was monitored spectroscopically. Fig.4.22 shows a part of the luminescence spectrum in the visible range recorded under electron beam at low temperature (7 K). The molecular bands of oxygen (the $C^3\Delta_u \rightarrow X^3\Sigma_g^-$ transition) became relatively weak just after 10 min irradiation. The strongest feature in the spectrum belongs to the O atoms effectively formed in the sample under electron beam. An increase of the O line intensity with exposure time is illustrated in the insert.

In order to separate the 23 K peak – peak of interest – we "removed" all the peaks at temperatures lower than the temperature of emerging the peak under study. For the purpose we used the "cleaning technique" [169] described above and irradiated oxygen containing samples at 18K. On completing the irradiation we recorded the yield of TSEE and the TSL yield in the VUV range shown in Fig.4.23.

Both curves exhibit a maximum near 23 K thus demonstrating the correlation of the exoelectron emission and the emission of the VUV photons of the intrinsic charge recombination reaction (1). The VUV TSL curve turn out to be much broader than the TSEE curve which is to say that some additional electron traps are involved in the bulk recombination channel. The corresponding VUV TSL curve taken from
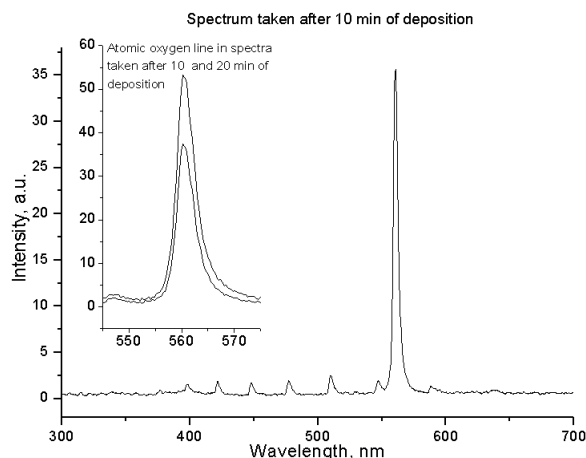
Figure 4.22: Luminescence spectrum of the Ar sample doped with O_2 (10^{-4}) recorded in the range of O_2 and O emissions. The spectrum was detected during deposition under electron beam. The O line detected after 10 (1) and 20 (2) min exposure is shown in the insert.
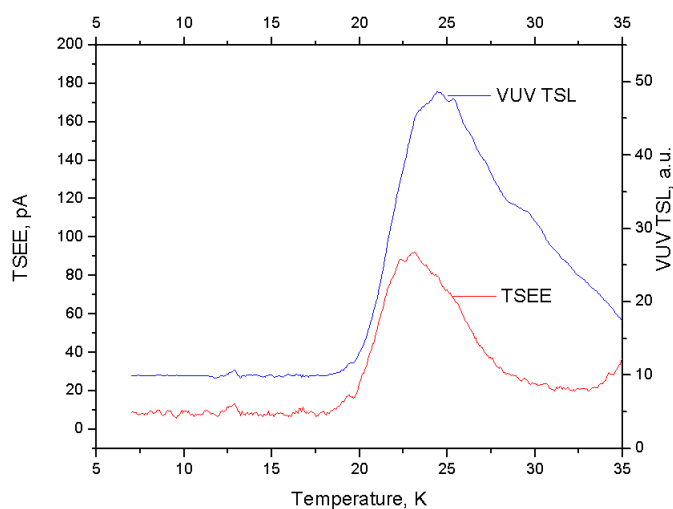
Figure 4.23: Yields of TSL in the VUV range and TSEE taken from the O_2^- containing sample pre-irradiated at 18 K.

the sample annealed at 25 K (Fig.4.19) exhibits more narrow peak which correlates with the 23 K peak in TSEE. At the same time the correlated in real time measurements of the TSEE yield and spectrally resolved TSL in the operating range of the spectrometer demonstrated in a conclusive way the correlation in the TSEE yield of the sample irradiated at 18K and the observed simultaneously photon emission of O_2^* (the $C^3\Delta_u \rightarrow X^3\Sigma_g^-$ transition).

The experiment with the linear heating (Fig.4.24) confirmed the correlation between the molecular oxygen emission and the yield of the TSEE current near 23K. In this case the oxygen containing sample of Ar was deposited at 18 K under 500eV electron beam.
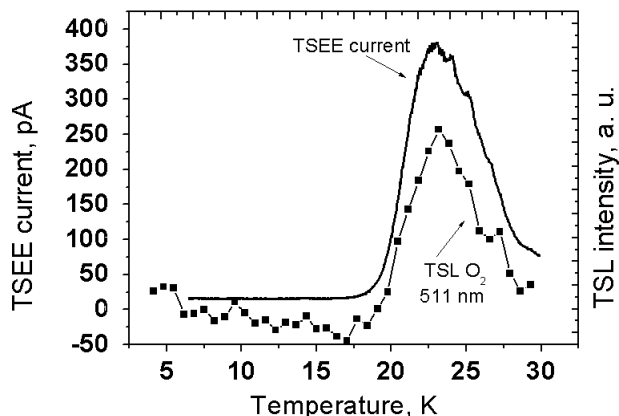

Figure 4.24: Yields of TSEE and O_2 emission in TSL taken from oxygen-containing Ar sample pre-irradiated at 18 K.

In Fig.4.24 one can see well correlated peaks in TSEE emission and TSL emission on the wavelength 511 nm which corresponds to the O_2^* emission.

Our experimental data especially taken in real time-correlated manner on relaxation processes in pre-irradiated Ar solids doped with oxygen enable us to restore and verify the following scenario to explain the relaxation pattern puzzling at first sight.

The charge recombination reactions in pre-irradiated rare-gas atomic cryocrystals are controlled by the mobility of electrons. The weakest bound in the traps electrons are mobilized at the lowest temperatures and escape the crystal or neutralize positive intrinsic (self-trapped holes) ions. These charge recombination reactions result in the appearance of the VUV emission. At a definite, higher temperature, the O atoms present also start to diffuse, and a complex sequence of events may take place. Recombination of neutral O atoms results in the formation of molecular O_2^* in bound excited electronic states. This is followed by a rapid relaxation, and eventually by radiative transition into the ground state. The emitted visible range photons, in turn, can be absorbed and provide the energy needed to detrap electrons from deeper traps promoting them to the conduction band, this is some kind of "internal photoeffect" followed by (i) ejection of exoelectrons from the surface, (ii) conversion of visible light into VUV photons via recombination of electrons with self-trapped holes by the reaction (1), or (iii) conversion of visible light into photons of other range via recombination of electrons with some extrinsic positively charged centers. All these electron-driven processes, which are outlined in the scheme (4.13) given above, were detected in our experiments.

The results obtained provide solid evidence for the electronic relaxation stimulation via chemiluminescent reactions. It is worthy of note that in contrast to the local energy release under nonradiative radical recombination the revealed radiative mechanism provides a long-range energy transfer for hundreds of lattice constants. Based on these results other radiative mechanisms of relaxation cascades triggering in pre-irradiated solids can be predicted, e.g. stimulation of relaxation by radiative transitions of metastable atoms or molecules. The first results demonstrating reliability of this mechnaism are presented in [63]. The experiments on stimulation of relaxation processes by laser light [14, 62, 64] provide an additional proof of the mechanisms discussed.

4.4.4   Conclusion

In the present study we explored an interconnection between atomic and electronic relaxation processes in preliminary irradiated by a low energy electron beam Ar solids with the focus on the role of chemiluminescent reactions in the thermally induced relaxation cascades involving charge carriers. Chemiluminescence was produced in thermally induced recombination reaction of neutral O atoms followed by O_2^* formation and its radiative decay. The main chemiluminescent peak was observed at 23K. In order to single out the peak of interest in TSEE yield and in the yield of intrinsic charge recombination reaction – TSL in the VUV range stemmed from recombination of self-trapped holes Ar_2^+ with detrapped electrons – "cleaning technique" was used. The samples were irradiated at elevated temperatures.

Clear correlation of the thermally induced relaxation process in the system of neutral particles with relaxation processes in the system of charge carriers was revealed. The spectrally resolved photon yield at the wavelength of O_2^* emission was demonstrated to correlate with the TSEE yield as well as the TSEE yield with the yield of charge recombination luminescence – TSL in the VUV range. The correlation is well-defined for annealed and then pre-irradiated samples. The chemiluminescence due to the recombination of neutral atoms is considered as an "internal photon source" promoting electrons to the conduction band and affecting the relaxation paths. Interesting feature of the mechanism suggested is a conversion of the visible range photons in high energy VUV photons.

Especially clear correlation, which points to the common primary process triggering all the relaxation cascades, was demonstrated in our most recent study based on synchronous measurements of spectrally resolved thermally stimulated luminescence (TSL) and exoelectron emission (TSEE) from pre-irradiated Ar solids doped with O_2. These real time-correlated measurements have given conclusive evidence in favour of the suggested mechanism of relaxation cascades stimulation via chemiluminescent reactions. The verified mechanism provides a long-range energy transfer and demonstrates the existence of a new relaxation channel (triggering of electronic relaxation processes by diffusion controlled atom-atom recombination reaction followed by light emission).

The results presented in this section were published and approved at a number of conferences (List of publications [2,5,10,13] and list of conferences are given in Appendixes).

4.5   A new post-irradiation phenomenon in Cryocrystals: anomalous low-temperature sputtering of solid Ar.

4.5.1   Introduction

Cryocrystals in particular RGS as it was mentioned are accepted as unique model solids for studying electronically induced phenomena and unveiling elementary steps of electronic excitation evolution due to their simple monoatomic lattice, weak Van der Waals interatomic forces along with a strong electron-phonon interaction. These features of RGS provide a high quantum yield of electronically stimulated processes facilitating a study of electronically induced phenomena and relaxation processes. Electronically induced phenomena on the surface, in particular electronically induced sputtering of the lattice atoms, so-called desorption induced by electronic transitions (DIET), have aroused considerable interest of researchers [42, 75, 117, 158, 174, 175] especially in view of new trends in current surface technologies. Very often desorption itself is used as an efficient tool for investigation of dynamical processes in solids, on their surfaces and interfaces.

Numerous experiments on electronically induced desorption from cryocrystals were performed under excitation with electron beam [7, 11, 12, 25, 37, 126, 160], fast ions [120, 155] and synchrotron radiation [3, 35, 41, 57, 87, 129]. The most reach spectrum of the desorbing particles was found for solid films of Ne and Ar. It was revealed that the desorption yield contains different particles – neutral atoms in the ground state, metastable atoms, short lived excited atoms, vibrationally hot molecules and ions. Several mechanisms were suggested to explain this reach spectrum of desorbing particles. The main mechanisms among them are as follows: (i) a "cavity ejection" mechanism and (ii) an "excimer dissociation" one. The "cavity ejection" mechanism [174] is based on negative electron affinity E_a of solid Ne and Ar resulting in prevailing repulsive forces between electron cloud of excited atom or molecule (self-trapped excitons) and surrounding matrix atoms. Behind the "excimer dissociation" mechanism [75, 174] is electronic transition of excited molecular dimer to the repulsive part of ground state potential curve. Both these mechanisms come into play at the final stage of a variety of relaxation paths. The case under study is the processes occurring after completing irradiation – the final stage of the relaxation.

Recently we found a new channel of relaxation of electronic excitations – anomalous sputtering of own matrix particles from the surfaces of pre-irradiated cryocrystals. A new effect – anomalous low-temperature desorption (ALTD) – was observed

in pre-irradiated Ar solids [135, 138]. As the sample temperature is increased, we registered in addition to photons and electrons emitted by the sample in a weak external electric field, also a sputtering of surface atoms.

We suppose that this desorption is caused by recombination of self-trapped holes with electrons released from their traps. Because the electronically induced defects play a decisive role in irradiated solids a question on their part in the stimulation of desorption is of clear importance. The key role of exciton-induced defects in anomalous low-temperature desorption (from pre-irradiated RGS) of the lattice atoms is demonstrated. Taking into account that the relaxation processes in pre-irradiated samples are strongly affected by a sample structure series of experiments with unannealed and annealed samples were done. It was shown that recombination events occurring in the bulk can contribute essentially to the ALTD yield.

In the present study we also explored in detail mechanisms of relaxation processes involving radiative electronic transitions in pre-irradiated solid Ar doped with oxygen acting as a deep trap for electrons. An influence of the dopant itself, which is a deep trap for electrons, and a role of radiative electronic transitions in stimulation of the low temperature desorption from Ar films pre-irradiated by an electron beam are discussed.

Relaxation processes were monitored using a combination of activation spectroscopy methods – thermally stimulated luminescence (TSL) and thermally stimulated exoelectron emission (TSEE) – with registration of the sputtering yields by measuring a pressure in the experimental chamber.

4.5.2   Experimental

Details of the experimental technique have been described in Chapter 3. High-purity (99.999%) Ar gas was used. The samples were grown [Section 3.2] from the gas phase, had a high optical quality and looked transparent. The base pressure in the sample chamber was $6 \cdot 10^{-8}$ mbar. Samples were prepared in two ways: (i) by deposition of a neutral gas with a following irradiation by an electron beam or (ii) with a concurrent deposition and irradiation by an electron beam to generate charge centers, lattice defects and metastable centers all over the whole sample. Electron bombardment provides suitable conditions for efficient excitation of the electronic subsystem and the generation of charged centers. We used slow electrons with the energy of 120eV in the case of concurrent irradiation and electrons with the energy of 1 keV in the case of irradiation of preliminary deposited neutral samples. Note that the energies we used are insufficient for the point defects producing via the knock-on mechanism. As was shown in [130] the irradiation by slow electrons guarantees a preference for the excitonic mechanism of defect formation in the lattice. The deposition temperature was 7 K and films of 50– 100µm thickness were grown. Oxygen was used as a dopant. The dopant to the Ar gas ratio was varied between 10^{-5} and 10^{-2}.

After completing irradiation we measured yields of the thermally stimulated exoelectron emission (TSEE) from the samples and thermally stimulated luminescence

(TSL). In most experiments we used a constant heating rate of 3.2 Kmin^{-1} for Ar samples. The Ar samples were studied in the temperature range from 7 to 45 K. Measurements details are described in Section 3.3.

To monitor the desorption yield from the preliminary irradiated samples we measured the pressure in the chamber as a function of sample temperature simultaneously with the exoelectron current detection and TSL measurements (see Section 3.4 and 3.3.5).

4.5.3 Results and discussion

Primary states of relaxation cascades observed under heating of the pre-irradiated samples are states of self-trapped holes (STH) and trapped electrons, as well as metastable levels of dopant and products of radiation-induced reactions. The thermally released and mobilized electrons recombine with the STH by the reaction

$$\text{Ar}_2^+ + \text{e} \rightarrow \text{Ar}_2^* \rightarrow \text{Ar} + \text{Ar} + h\nu\,(9.7\text{eV}) + \Delta E \qquad (4.14)$$
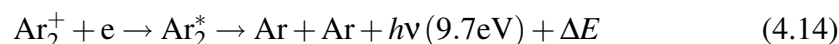
Energy stored by the self-trapped and trapped charge carriers is released via electronic transition of the recombination reaction product – "excimer" Ar_2^* – to the repulsive part of the ground state. The energy is released in the form of light (the well-known M band 9.7eV related to the $^{1,3}\Sigma_u^+ \rightarrow {}^1\Sigma_g^+$ transition) and kinetic energy of "hot" ground state Ar atoms. The excess energy about 1eV is distributed between the two Ar atoms. Already in earlier studies, e.g. [111, 112, 118, 155] this reaction was considered as a source of energy needed for the desorption of atoms from the surface under irradiation. Recombination-induced enhancement of the total desorption yield from solid Ar was observed under selective excitation above the energy gap E_g [107]. Thus one could expect to observe this effect in pre-irradiated solids.

Indeed we found new atomic process in pre-irradiated solid Ar – desorption induced by charge recombination under heating. First anomalous rise of a pressure at low temperature was recorded in experiment with pure pre-irradiated Ar under heating with constant rate 3.2 K/min [135]. The temperature dependence of pressure in the chamber, measured under heating of the sample exposed before to the electron beam shows clearly nonmonotonic behaviour (Fig.4.25).

An initial weak rise in the pressure was observed at T about 10 K and the first pronounced peak was recorded at $T = 15$ K that is much lower then the sublimation temperature Tsb of solid Ar ($T_{sb} = 30$ K) [158]. Then slow variations of the pressure were detected with maxima at about 20 and 35 K. The sharp decrease of the pressure at about 42 K is more likely due to cooling of the sample surface at intensive sublimation. Comparison of the pressure curve (Fig.4.25b) characterizing the yield of neutral atoms from the sample with the yield of electrons (Fig.4.25a) reveals a correlation in peak position that points to a common origin of effects underlying these phenomena. The peak at 15 K stems from levels of radiation induced defects. Formation of permanent Frenkel pairs stimulated by an excitation of elec-
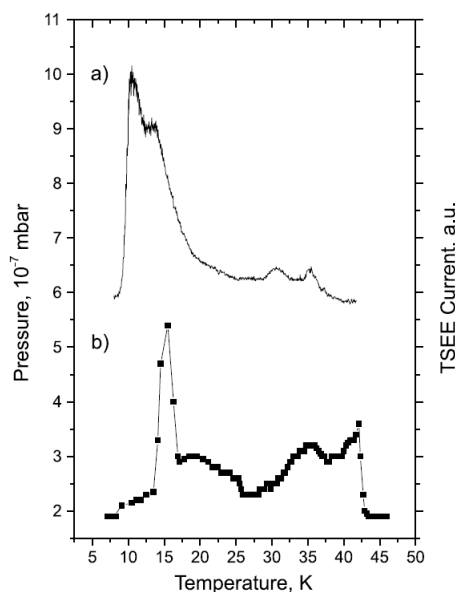
Figure 4.25: TSEE current from a standard film of pure Ar gas (a) and measured simultaneously pressure in the experimental chamber (b).

tron subsystem was observed experimentally [127, 130] and supported by theoretical study [47]. The most probable configuration of the defects is supposed to be the "dumb-bell" of $\langle 100 \rangle$ configuration. Because of negative electron affinity one can expect localization of electron at the vacancy. Note that despite of the common origin processes of electron emission and recombination are competitive and therefore recombination induced desorption depends on the interplay between these relaxation paths.

It is interesting that in our experiments we revealed branching of the relaxation paths even at the stage, which starts from thermalized electrons and self-trapped holes.

We suggested that a relaxation consists of 3 processes: exoelectron emission, anomalous low temperature desorption (ALTD) and recombination luminescence. A correlation between TSEE and ALTD was shown above in Fig.4.25. The experimental proof of common origin for recombination luminescence, anomalous low temperature desorption and exoelectron emission is given below.

The yield of desorption from solid Ar pre-irradiated with an electron beam up to dose about 10^{16}electrons/cm^2 is shown in Fig.4.26 as a plot of pressure dependence on temperature.

As it is examplified in Fig.4.25 the main desorption peak coincides in its position with the position of the second maximum of the TSEE measured from annealed and then irradiated at 6K film of solid Ar. At the same temperature we observed the peak in the total yield of TSL from the pre-irradiated sample (Fig.4.26) in agreement with our previous results [107, 133]. The absence of appreciable shift between
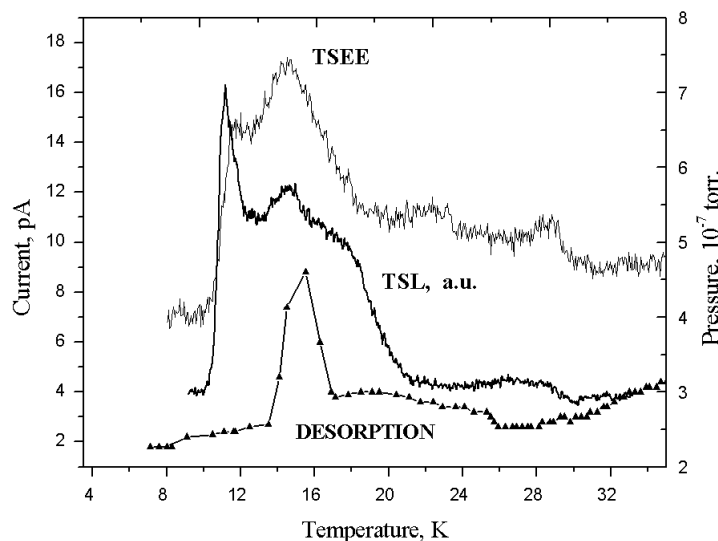
Figure 4.26: TSEE current, total yield of TSL from pre-irradiated with e-beam (120 eV) solid Ar and simultaneously measured pressure in the experimental chamber. The Ar sample was annealed and then irradiate at 6 K.

peaks in the TSEE and TSL is due to negative Ea of solid Ar ($E_a = -0.4$eV [158]) and as a consequence of absence of any barrier for electrons to escape. Note that the peak at 15K in solid Ar was also detected in a spectrally resolved TSL yields measured at the photon energies of the intrinsic recombination emission – in the M band of the molecular dimer Ar_2^* [128,133,136] in the extrinsic recombination emission (Cameron bands of CO in Ar matrix) [10, 136] and in the thermally stimulated current [150].

A correlation in the behaviour of TSEE, TSL and ALTD, which one can see from the Figs. 4.25 and 4.26, gives us an evidence that all these relaxation channels have a common underlying phenomenon: thermally stimulated release of trapped electrons results in radiative charge recombination followed by ALTD and direct escaping electrons from the sample.

Taking into account that before irradiation a primary own defects of matrix exist we performed experiments of thermally stimulated desorption from preliminary irradiated samples and samples without electron irradiation and examined an influence of a deposition temperature and radiation itself [138]. Fig.4.27 shows the desorption yield from the sample of Ar grown at $T = 7$ K recorded by the pressure measurement in the sample chamber before (curve 2) and after (curve 1) low temperature irradiation. The effect of irradiation itself is clearly seen in curve 3 (Fig.4.27).

The yield of the thermally stimulated desorption from nonirradiated sample is very weak. Nevertheless careful check performed at several samples revealed some shoulder at 11 K, clear peak at 15 K, wide features at about 20 and 35 K and peak near 40 K. Note that the similar features were observed in thermally stimulated des-
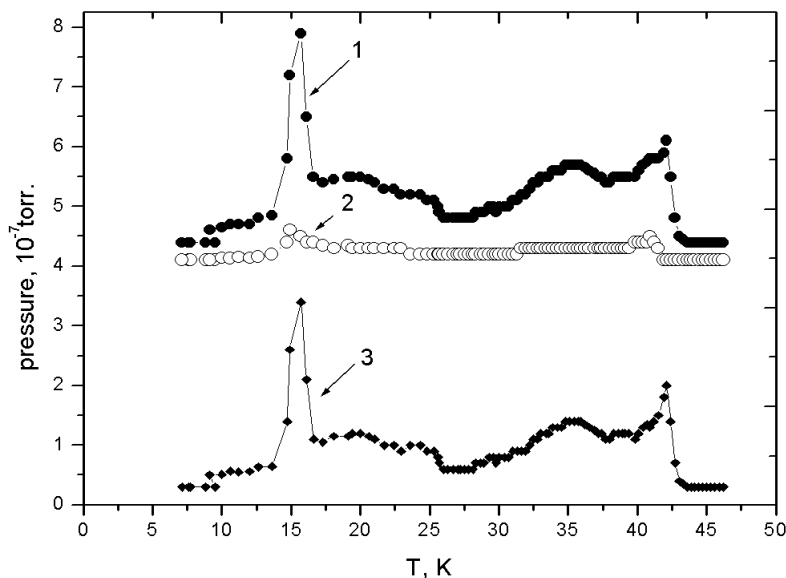
Figure 4.27: Temperature dependence of a pressure in the sample chamber with a standard Ar film grown at $T = 7$ K for nonirradiated (2) and irradiated (1) sample. Curve (3) shows the difference between (1) and (2).

orption from imperfect thin films (several monolayers) of Ar condensed on a Ru(0 0 1) substrate [148]. Because we recorded the desorption yield from thick samples (100 μm) grown on an Ag polycrystalline substrate these features cannot be related to the influence of a substrate and thought to be conditioned by properties of a condensed Ar. The yield of thermally stimulated desorption from preliminary irradiated samples increased dramatically. For the samples grown at 20 K no features were observed in the yield of thermally stimulated desorption. As a result of irradiation at $T = 7$ K again low temperature desorption emerged yielding the same features.

One can expect that creation in a matrix additional kind of traps for electrons will affect on the intensity of relaxation channels. Introducing a controlled amount of oxygen admixture during deposition the sample leads to the forming of deep thermally disconnected traps for electrons in Ar matrix.

That is why an atomic desorption from surfaces might be profoundly affected by impurities and this influence on the desorption under excitation was examined in a number of studies [12, 41, 118]. It was found [12, 57] that the DIET yields measured under excitation are higher for oxygen-containing samples than those for pure Ar. In contrast with these observations the yield of desorption from pre-irradiated samples of solid Ar doped with O_2 turns out to be much lower than that for pure Ar. Fig.4.28 shows a suppression of the desorption from pre-irradiated samples as oxygen concentration increased.

An enrichment of sample with O and O_2 causes redistribution of occupied electron traps in favor of deep ones. Being thermally disconnected these traps cannot be
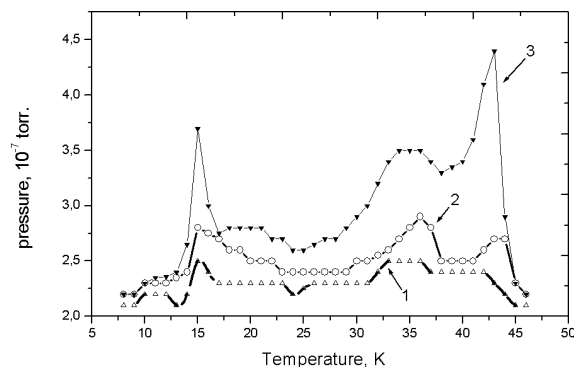
Figure 4.28: Temperature dependence of a pressure in the chamber for the Ar films containing 10^{-3} O_2 (curve 1), $5 \cdot 10^{-4}$ (2) and 10^{-4} O_2 (3).

emptied by following warm-up of the samples. Fig.4.29 demonstrates a correlation in the desorption yields and the TSEE currents from samples of Ar with different concentration of oxygen.

We checked the influence of oxygen on the desorption yield from Ar films under irradiation with an electron beam and from pre-irradiated solid Ar. Special interest to the influence of O_2 admixture on the desorption is caused by a number of reasons. O_2 is chemically active and serves an effective deep trap for electrons. On the other hand, oxygen centers can be easily stabilized in Ar matrix without significant distortion of the lattice. And what is important for the desorption study, O_2 and Ar have close sublimation temperatures about 30K [93].

Fig.4.30 demonstrates the effect of oxygen impurity on the desorption yield of short-lived excited atoms and vibrationally "hot" molecules from Ar film under irradiation by the electron beam.

The desorbing particles were detected by luminescence method. Wide W band related to the $^{1,3}\Sigma_u^{+(v)} \to {}^1\Sigma_g^+$ transition of the desorbing molecule increased in the intensity in the luminescence spectrum of the sample doped with O_2 (10^{-2}). Pronounced increase in the intensity was observed also for the atomic fraction of the desorption yield – atoms in the states $^3P_1$ (b line) and $^1P_1$ (a line). The c band stemmed from $^3P_2 \to {}^1S_0$ transition of Ar atoms at defect sites in the bulk decreased in the intensity in doped samples. Its reduction is caused by exciton trapping at dopant. Note that the bulk emission – M band (Fig.4.31) is efficiently quenched in O_2 doped samples.

This behaviour is similar to that observed in [12, 56, 111]. Taking into account that the reduction of another bulk band in the luminescence (c band) is not so pronounced one can speculate that at least partially reduction of the M band is caused by a suppression of the Ar_2^+ – electron recombination in a presence of O_2.
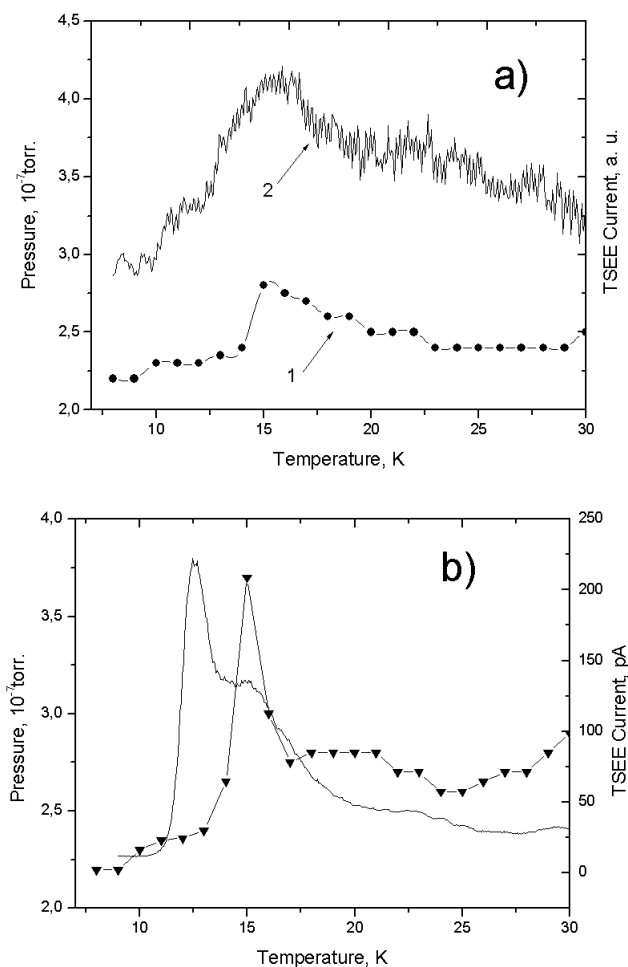
Figure 4.29: Comparison of TSEE current and recorded simultaneously pressure in the chamber for the Ar films with dopant to the Ar ratio $5 \cdot 10^{-4}$ (a) and 10^{-4} (b).

As expected the yield of desorption from pre-irradiated Ar samples doped with O_2 turns out to be much lower than for nominally pure Ar solids. Doping with quite small amount of O_2 (10^{-4}) strongly reduces the desorption yield as it is exemplified in Fig.4.32.

An increase in a number of deep electron traps prevents recombination events reducing the desorption yield. These traps are thermally disconnected and cannot be emptied by heating the sample. Binding energies E_b of electron for O^- and O_2^- centers in Ar matrix are estimated to be $E_b = 2.61\text{eV}$ and $E_b = 1.6\text{eV}$ correspondingly. Our experimental findings are in fair agreement with the time-of flight data [7, 160] on the influence of O_2 on the yields of Ar atoms from irradiated samples. According to these data the yield of slow atoms desorbed via "cavity ejection" mechanism was appreciably enhanced by doping, while the yield of fast atoms – mostly ground state atoms produced via "excimer" mechanism – appeared to be suppressed.
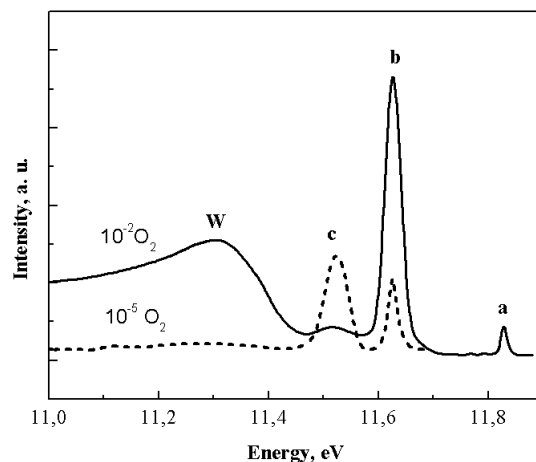
Figure 4.30: Spectrally resolved VUV luminescence from Ar films doped with different amount of oxygen impurities registered under electron bombardment (1 keV).
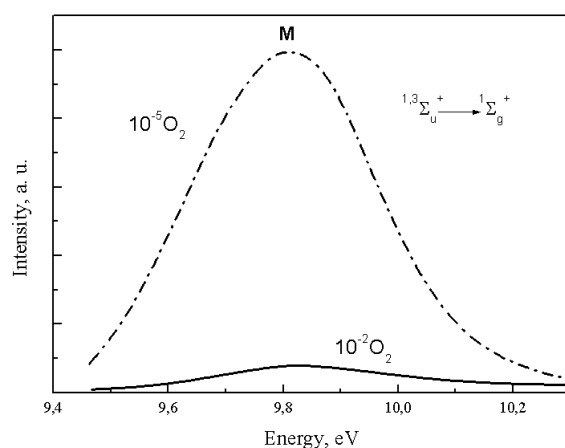
Figure 4.31: Cathodoluminescence spectrum of solid Ar doped with different concentration of oxygen.

We suggest that the "excimer" mechanism is a prinsipal mechanism in the scenario suggested for the anomalous low temperature sputtering. According to our experimental results introducing the oxygen impurities suppressed the low temperature desorption yield as shown in Fig.4.33

The whole set of data demonstrates prominent role of recombination processes in relaxation cascades.

It is worth to emphasize that the efficiency of ALTD is strongly affected by the sample structure. An annealing of samples before irradiation intensified the ALTD by several times as it shown in Fig.4.34 [49]. The annealing procedure was as
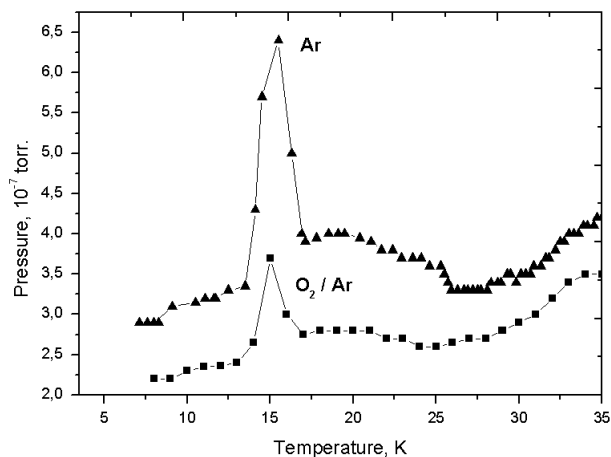
Figure 4.32: Pressure in the experimental chamber during heating of pre-irradiated samples of pure Ar and doped with oxygen (10^{-4}).
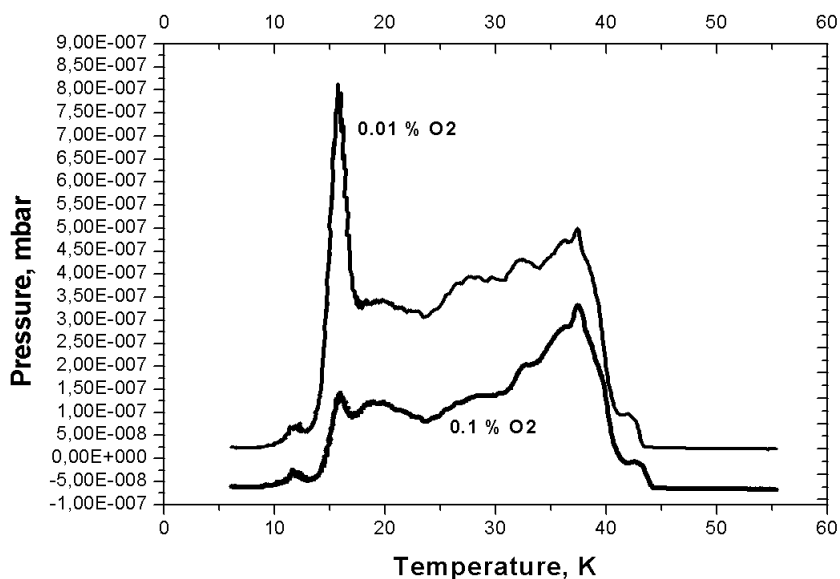
Figure 4.33: Pressure in the experimental chamber during heating of pre-irradiated samples of solid Ar doped with oxygen with different concentration.

follows: the sample deposited under e-beam irradiation was heated with a constant rate during 5 min up to 25K, kept at this temperature for 10 min and then slowly (during 5 min) cooled down to 7K. Then the sample was exposed to the e-beam again. The pressure curves were recorded after irradiation by 200 eV electron beam during 30 min.

Such a strong effect of annealing gives an evidence of an appreciable contribution of the bulk processes in the ALTD phenomenon. One could suppose that the

Figure 4.34: Sputtering yield under heating of pre-irradiated solid Ar for annealed (a) and unannealed (b) samples.

annealing causes an increase of the grain size in annealed sample and an improvement of the lattice structure. The evolution of the pressure curve with an increase of the exposure time is demonstrated in Fig.4.35. All the features of the pressure curve grow in their intensity. A small shift (0.5 K) of the low tempe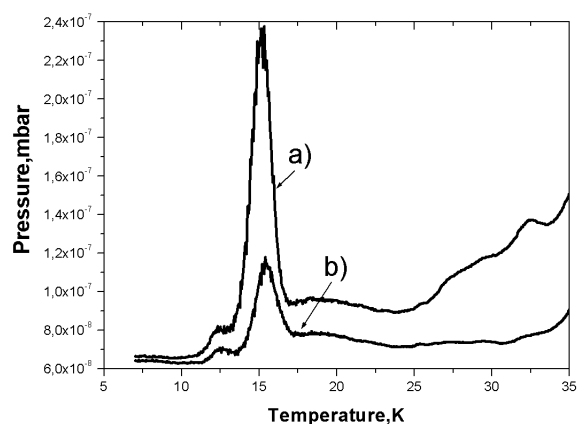rature peak positions to lower temperatures with increase of the radiation dose was observed in both – the pressure curve and the glow curve of the VUV TSL indicating accumulation of uncompensated negative space charge under irradiation.

Note that the accumulation of charge upon irradiation was observed in [5]. It is interesting to compare dose dependence for all registered yields: TSEE, VUV TSL and pressure. They are shown in Fig.4.36 for low temperature peaks.

All of them are characterized by non-linear behavior. The yield of TSEE grows more rapidly and after 20 min dose approach the saturation. The VUV TSL yield and pressure increase more slowly but also exhibiting a tendency to saturation. It is essential that the dose dependence of the VUV TSL and pressure correlate with each other also pointing to a common origin of effects underlying these phenomena.

While monitoring the pressure under electron beam we observed a sharp increase of the pressure when the beam was switched on as it shown in the insert in Fig.4.36. The level of pressure signal remained nearly constant under e-beam with abrupt drop upon switching off the beam. A constant level of the pressure signal under e-beam suggests quasi equilibrium conditions for the DIET under excitation. Taking into account data [112]] on the yield of Ar atoms under irradiation by 500 eV electrons (few atoms per incoming electron) we can roughly estimate the yield of DIET in our case. It consists of about 10^{15} at.s^{-1} [144]. The yield of ALTD depends strongly on the irradiation dose as it was illustrated in Fig.4.35 and the yield of ALTD is comparable with that of DIET (under e-beam) only at short exposures of order of 1 min.

These findings corroborates the recombination mechanism of atomic desorption from pre-irradiated Ar. The excess energy of the order 1 eV under radiative decay of
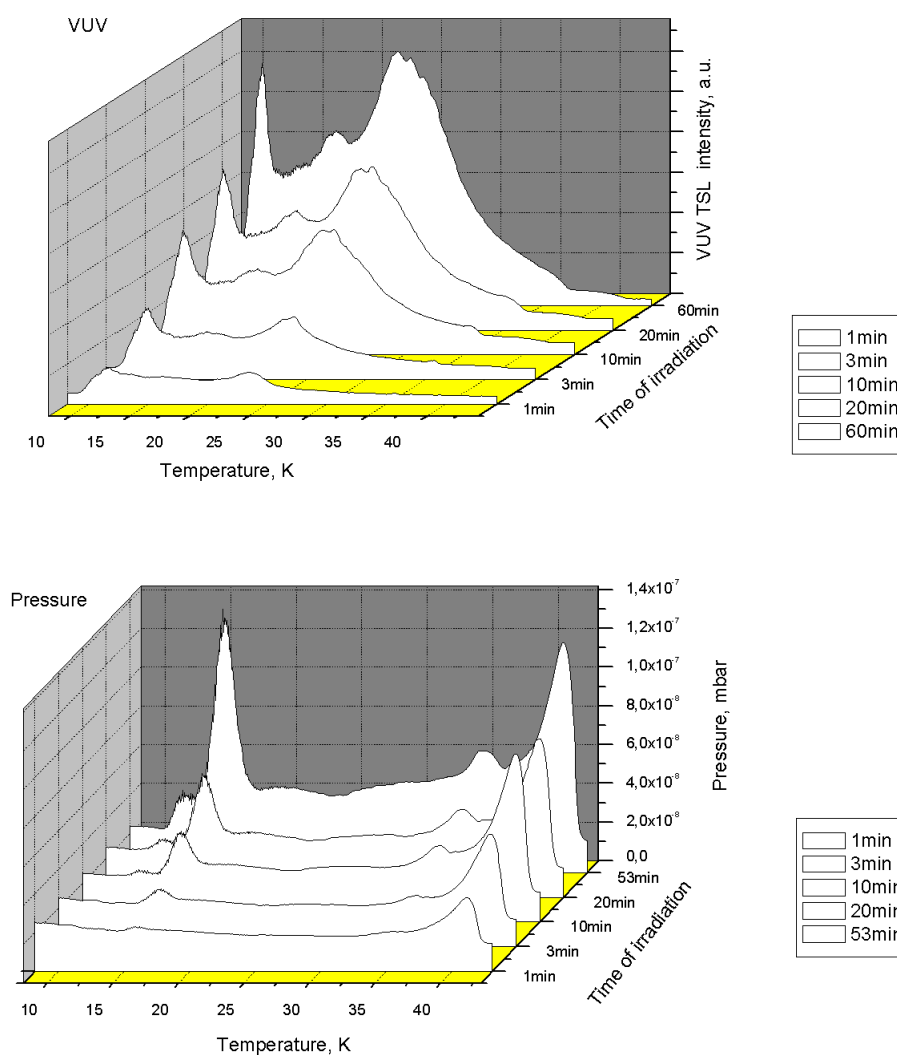
Figure 4.35: Dose dependence for pressure and total yield of VUV luminescence for irradiated with e-beam after deposition solid Ar.

Ar_2^* by reaction 4.14 can be transferred to the lattice atoms on the collision cascade.

The transfer of kinetic energy occurs preferentially along the close-packed $\langle 110 \rangle$ direction. The results of early simulations of electronically induced sputtering from rare-gas solids made by molecular dynamics methods are summed up in [75, 158, 174]. An appreciable yield of Ar atoms due to energy release was predicted from the depth up 6 atomic layers. It was found in the recent molecular dynamics study of energy transfer in solid Ar [23] that the energy can be transferred over large distances about 150 lattice constants. In view of this fact recombination events occurring in the bulk can contribute essentially to the desorption yield. This process can be described by a crowdion model. As it was shown in [104] crowdions – non-

Figure 4.36: Comparative dose dependence of total yield of VUV TSL, TSEE and pressure for irradiated after deposition Ar samples. The insert shows a pressure increase in the experimental chamber under electron bombardment.

linear solitary waves of displacements arising in close-packed atomic rows – exist in atomic Ar cryocrystals with a FCC lattice. One can see from the analysis of crowdion parameters: the crowdion width $\lambda/b = 2.76$ (b is the interatomic distance) and the crowdion effective mass $m = 0.3$ (in units of the atomic mass) that the interaction of the distinguished atomic row with the matrix surrounding is weak. The crowdion energy E_s is found to be quite large $E_s = 0.3$eV, however E_s is less than the energy transferred to the ground state Ar atoms in recombination reaction followed by the Ar_2^* dissociation at the radiative electronic transition to the ground sate. Taking into account that barriers for crowdion displacement usually are lower than the barriers for atom displacement one can expect substantial desorption of atoms via the crowdion mechanism both from irradiated and pre-irradiated RGS.

The scenario of the thermally stimulated relaxation cascades in pre-irradiated cryogenic solids verified in the present study can be presented by the following consecution of elementary processes:

$$\text{TE} + \Delta E_h \rightarrow \text{E(CB)} \rightarrow e \nearrow^{\text{TSEE} \quad (a)}_{\rightarrow \text{Rg}_2^+ + e \rightarrow \text{Rg}_2^* \rightarrow h\nu\,(\text{VUV}) + \quad (b)}$$
$$\text{Rg} + \text{Rg} + \Delta E \quad (c)$$

The key process of this cascade is the thermally stimulated electron detrapping promoting electrons into the CB. Energy absorbed during the irradiation and stored

by localized charge carriers is spend to initiate electron emission (TSEE), emission of photons (VUV recombination emission) and emission of "hot" lattice atoms, as shown in Fig.4.37.
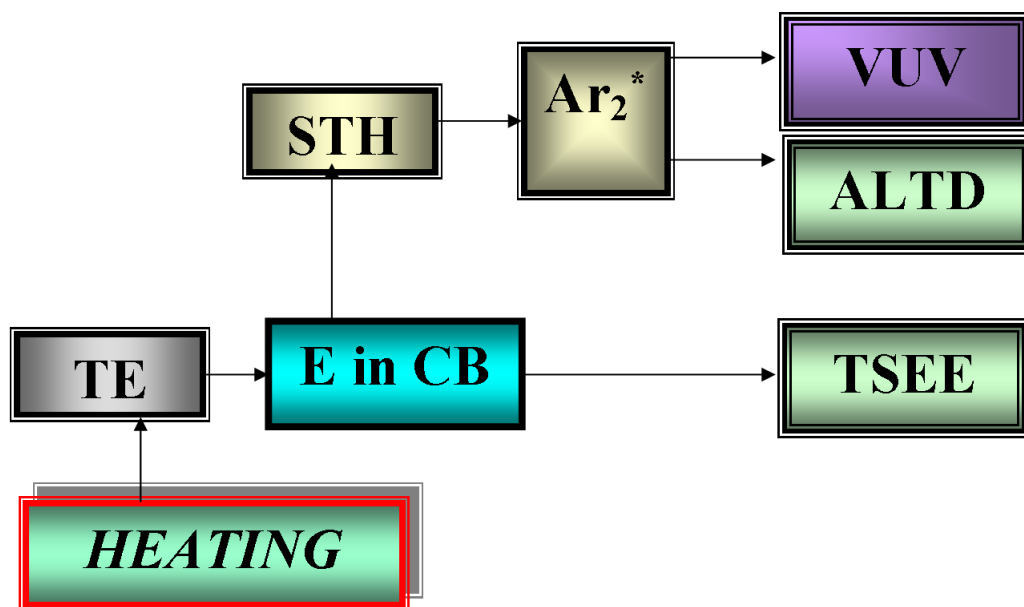

Figure 4.37: Schematic drawing of the relaxatian cascades, stimulated by heating.

4.5.4   Conclusion

A new phenomenon was found – sputtering of atoms from pre-irradiated solid Ar (ALTD) observed at low temperatures much below the characteristic sublimation temperature. Relaxation processes were monitored using a combination of activation spectroscopy methods – spectrally resolved thermally stimulated luminescence (TSL), thermally stimulated exoelectron emission (TSEE) – with measurements of the sputtering yields.

The temperature dependence of a pressure in the experimental chamber, measured under heating of the Ar sample exposed before to the electron beam shows clearly non-monotone behaviour. The most pronounced peak in the ALTD yield is related to annihilation of exciton-induced defects. Correlation in the peak positions of low temperature sputtering, TSL and TSEE was found suggesting common primary process of these relaxation channels: release of electrons from their traps upon heating of pre-irradiated solids. Stimulating factor for the desorption from pre-irradiated solid Ar is shown to be the recombination of the detrapped electrons with intrinsic ionic centers – self-trapped holes.

The results of experiments on sputtering of Ar atoms from the surface of nominally pure and O_2 doped solid Ar preliminary irradiated by an electron beam are

discussed. An oxygen impurity was used as a deep thermally disconnected electron trap. We found pronounced suppression of charge recombination reaction and decrease of the desorption yield from oxygen-containing pre-irradiated samples.

A strong effect of annealing gives an evidence of an appreciable contribution of the bulk processes in the ALTD phenomenon. It was found that the yield of ALTD depends strongly on the irradiation dose. The yield of ALTD was estimated and found to be comparable with that of DIET (under e-beam) only at short exposures of order of 1 min (10^{15} at.s^{-1}).

This correlation between TSEE, yield of total VUV luminescence and pressure indicates common processes underlying these phenomena and points out a key part of the exciton-induced defects in the studied postirradiation phenomena – anomalous low-temperature desorption from pre-irradiated RGS.

Possible models of the anomalous sputtering are discussed and the crowdion mechanism of an energy transfer followed by the atom ejection from the surface is proposed.

The results presented in this section were published and approved at the conferences [appendixes: list of publications [2,5,7,8,18,19] and list of conferences].

Outlook and Summary

When a solid material is exposed to high-energy radiation – VUV photons, electrons, or ions – part of the excitation energy may be stored in the crystal by various defects formed under exposure to radiation: ionic centers, electrons, radicals, lattice defects. Heating of a pre-irradiated sample or exposing it to photon flux triggers complex relaxation cascades involving both charged and neutral reactive species. The aim of this work is an elucidation of the fundamental processes of energy storage, relaxation, charge transfer, recombination reactions, medium effects, and dynamics of ionic centers in classical model materials – rare-gas solids. The investigations were focused on the relaxation cascades from pure and doped Ar solids, pre-irradiated with a low energy electron beam. Results of the thesis were published in [Appendix A: 2, 3, 5, 7–10, 13–15, 18, 19] and approbated at the conferences (see Appendix B).

In order to get reliable information, a set of activation spectroscopy methods (both optical and current) were employed – thermally stimulated luminescence (TSL) with measurements of total and spectrally resolved yields, thermally and photon-stimulated exoelectron emission (TSEE and PSEE), photon-stimulated luminescence (PSL). The main obtained results can be summarized as follows:

- A new experimental approach to study of relaxation cascades in RGS, pre-irradiated with low energy electron beam, was developed based on implementation of optical and thermal stimulation of relaxation processes. Using current and optical activation spectroscopy methods, along with spectrally resolved measurements of stimulated luminescence in a wide range from visible to vacuum ultraviolet, enabled us to discriminate reactions of ions from reactions of neutral reactive species, to find a nontrivial interconnections between atomic and electronic relaxation channels in doped RGS, and to suggest a new radiative mechanisms of electronic relaxation, triggered via atom-atom reactions, as well as to discover a new post-irradiation phenomenon – anomalous low temperature sputtering from pre-irradiated solids. It was established that relaxation cascades consist of several channels: (i) exoelectron emission from pre-irradiated Ar solids detected by TSEE and PSEE, (ii) radiative recombination of intrinsic and extrinsic positively charged centers with detrapped electrons, detected by TSL and PSL, and (iii) anomalous low temperature sputtering as post-irradiation phenomenon which was detected simultaneously with

channel (i) and (ii) by pressure measuring. Because detrapped electron can either recombine with positively charged center or escape a sample directly, the channel (i) competes with channel (ii). In doped solids, additional relaxation channel (iv) comes into play – diffusion-controlled reactions of neutral particles, e.g. radical recombination.

- Due to simultaneous monitoring of relaxation channels involving charged and neutral species, we were able to find interconnection between atom-atom recombination reaction followed by chemiluminescence (iv) and relaxation channels involving charged species (i) and (ii). This interconnection was revealed in the course of experiments on Ar solids doped with O_2. Irradiation by electron beam resulted in O radicals formation. Upon heating, O radicals became mobile in the temperature range about 20K and recombined forming O_2^* molecule. Its radiative decay appeared to be the stimulating factor for electron detrapping, followed by exoelectron emission (i) and recombination of positively charged ionic species (ii). The peak at 23K in "glow curve", measured at the wavelength of molecular oxygen emission, was demonstrated to correlate with the peak in TSEE yield and yield of charge recombination emission (TSL in the VUV range stemmed from recombination of Ar_2^+ with detrapped electrons). These experiments provided a convincing answer to the long-standing question on the origin of thermally stimulated peak in TSL at 23K as well as current yields (TSC).

- The role of optical stimulation was studied in details using an external photon source, tunable laser light, and unconventional "internal photon source", long-lifetime afterglow, stemmed from radiative decay of N radicals, formed in Ar matrix under electron beam. Both relaxation channels, recombination luminescence and exoelectron emission, for photon-stimulated relaxation path of pre-irradiated Ar matrix were investigated. A long-lifetime (in a range 10-100 s) kinetics for all relaxation channels was determined. It was found that current decay curves in nitrogen doped Ar matrix as well as decay curves for extrinsic (Xe_2^*) and intrinsic (Ar_2^*) M-band luminescence follow afterglow from N^* radicals with characteristic lifetime around 20 s for $^2D \rightarrow {}^4S$ forbidden transition in pre-irradiated Ar matrix. The experiments demonstrated that whole relaxation is caused by the N^* afterglow from pre-irradiated samples. One can consider this process as "internal photo-effect". As external source for the relaxation, the laser light in continuous mode was used, and dependence of lifetime on the parameter of the light source has been clarified.

- And behind the field of research, scientist can always find new phenomena. New one – anomalous low temperature desorption or sputtering (ALTD) from solid Ar, pre-irradiated with low energy electron beam – was found. Correlation of ALTD with current and recombination VUV luminescence curves was established and mechanism of the phenomenon was suggested – thermally

stimulated charge recombination reaction of Ar_2^+ with detrapped electron occurring near the surface. The transition of neutralized center Ar_2^* to a repulsive part of the ground state potential curve results in the energy release, which is spent for the ejection of matrix atom from the surface. Energy transfer is supposed to occur along close-packed rows of matrix via so-called "crowdion" mechanism. Influence of oxygen impurities acting as "electron scavengers" on the yield of ALTD was investigated and a strong dependence of the ALTD intensity yield on the sample structure was found.

The obtained results can give rise to novel experimental approach and studies in the field of physics and chemistry of metastable and ionic species. Let us mention some of them.

- The study of RGS with negative electron affinity invites to be extended to others with positive electron affinity. In this way, it will be probably possible to clear up the question of which kind of traps for electrons exist in these solids – an important issue for cryochemistry.

- The new complex approach to study of the relaxation channels from pre-irradiated solids may be developed employing combination of luminescence and current activation spectroscopy methods with synchronous direct measurements of sputtering yield by mass-spectrometer.

- The performed and suggested studies are of considerable interest both from the point of view of fundamental solid-state physics and chemistry, and in a number of important applications in material and life sciences, surface science, solid-state photochemistry, cryochemistry and related areas – astrophysics and space science. An employing of the new technique seems to be helpful for extension of investigations to more complex materials and nanostructures.

Acknowledgements

This thesis would have no chance to be written without kind support from people and organisations to whom I would like to express my deepest thanks.

First of all, I would like to extend my deep gratitude to my supervisor, Professor Vladimir E. Bondybey. Without his continual support, great ideas and critical advices, this work would not exist never. His sharp eyes for detail and perfect analytical skills have been instrumental in the success of this work. Over the years I know Vladimir as a sympathetic, with open mind and very nice person. His overlying enthusiasm and integral view on research are the sound foundation of this work. Due to his personal skills and the great team, which was created in PCII, the working atmosphere was very fruitful, cooperative and it was just a pleasure to work together.

My thankfulness dedicates to people with whom I started working at TUM:

Dr. Dieter Kraus and Dr. Bernhard Urban with their helpful discussion at the lunchtime.

Dr. Andreas Lammers, who made my first e-mail box in TUM in one moment as in fairy tale and saved us many times with all computer problems, system definitely knew who is working with computers.

My cordially deep thanks to our not only secretary but "first aid" for every problem – Sabine Kullick. Her support and helpful assistance with any problem was inestimable.

Dr. Martin Lorenz, Dr. Alice Smith-Gicklhorn, for their kind help and introducing into the "matrix isolation" lab.

Peter Kämmerer, for his helpful assistance with computer system and also with our gas-handling system.

Matthias Stecher, for his invaluable technical help in the lab, who keeps all system in a right conditions.

Dr. Martin Beyer, Dr. Brigitte Fox-Beyer, who made pleasant atmosphere in the lab and help us with every problem many times.

My special thanks to Dr. Marcin Frankowski with whom we have got a lot of inspiring results in the lab and spent a wonderful time together with his family. Without him, this thesis does not exist.

A lot of thanks to our co-worker Alexey Ponomaryov (soon a Doctor), who have made a new modification of our experimental Setup. He provides us with numerous measurements and makes every thing that we ask him about.

Appendices

APPENDIX A

List of publications

1. E.V. Savchenko, O.N. Grigorashchenko, A.N. Ogurtsov, V.V. Rudenkov, G.B. Gumenchuk, M. Lorenz, A. Lammers, and V.E. Bondybey, "Stability of Charge Centers in Solid Ar", J. Low Temp. Phys. 122 (2001) 379-387.

2. E.V. Savchenko, O.N. Grigorashchenko, A.N. Ogurtsov, V.V. Rudenkov, G.B.Gumenchuk, M. Lorenz, M. Frankowski, A.M. Smith-Gicklhorn, V.E. Bondybey, "Photo- and thermally assisted emission of electrons from rare gas solids", Surface Science 507-510 (2002) 754-761.

3. E.V. Savchenko, O.N. Grigorashchenko, G.B.Gumenchuk, A.N. Ogurtsov, M. Frankowski, A.M. Smith-Gicklhorn, and V.E. Bondybey, "Defect-related relaxation Processes in irradiated rare gas solids", Radiation Effects & Defects in Solids 157 (2002) 729-735.

4. E.V. Savchenko, O.N. Grigorashchenko, A.N. Ogurtsov, V.V. Rudenkov, G.B.Gumenchuk, M. Lorenz, A.M. Smith-Gicklhorn, M. Frankowski, and V.E. Bondybey, "Thermally assisted emission of electrons and VUV photons from irradiated rare gas solids", Surf. Rev. & Lett. 9 (2002) 353-358.

5. E.V. Savchenko, O.N. Grigorashchenko, G.B.Gumenchuk, A.G.Belov, E.M. Yurtaeva, M. Frankowski, A.M. Smith-Gicklhorn, and V.E. Bondybey, "Relaxation processes induced by radiative electronic transitions in preirradiated rare gas solids", Surface Science 528 (2003) 266-272.

6. M. Frankowski, E.V. Savchenko, A.M. Smith-Gicklhorn, O.N. Grigorashchenko, G.B.Gumenchuk, and V.E. Bondybey, "Thermally stimulated exoelectron emission from solid neon", J. Chem. Phys. 121 (2004) 1474-1479.

7. E.V. Savchenko, G.B.Gumenchuk, E.M. Yurtaeva, A.G.Belov, I.V. Khizhniy, M. Frankowski, M.K. Beyer, A.M. Smith-Gicklhorn, A.N. Ponomaryov, V.E. Bondybey, "Anomalous low-temperature desorption from preirradiated rare gas solids", J. Luminescence 112 (2005) 101-104.

8. E.V. Savchenko, O.N. Grigorashchenko, G.B. Gumenchuk, A.G. Belov, E.M. Yurtaeva, I.V. Khyzhniy, M. Frankowski, M. K. Beyer, A.M. Smith-Gicklhorn, and V.E. Bondybey, "Anomalous Phenomena on Surfaces of Preirradiated Cryocrystals", J. Low Temp. Phys. 126 (2005) 621-631.

9. G.B. Gumenchuk, M.A. Bludov, A.G. Belov, "Photon-induced recombination of self-trapped holes with electrons in preirradiated solid Ar", FNT, V. 31, N. 5, (2005), P. 237-240.

10. E.V. Savchenko, A.G. Belov, G.B.Gumenchuk, A.N. Ponomaryov, and V.E. Bondybey, "Oxygen-driven processes in pre-irradiated Ar cryocrystals", Fizika Nizkikh Temperatur (Low Temperature Physics), Special Issue on Low Temperature Spectroscopy and Optics, 32 (2006) 1417-1425.

11. E.V. Savchenko, I.V. Khyzhniy, G.B.Gumenchuk, A.N. Ponomaryov, M.K. Beyer, M. Frankowski, and V.E. Bondybey, "Photo- and thermally stimulated relaxation processes in pre-irradiated atomic solids", Radiation Physics and Chemistry, 76 (2007) 577-581.

12. A. Ponomaryov, G. Gumenchuk, E. Savchenko and V.E. Bondybey, Radiation Effects, "Radiation effects, energy storage and its release in solid rare gases", PCCP 9 (2007) 1329-1340.

13. E.V. Savchenko, I.V. Khyzhniy, G.B.Gumenchuk, A.N. Ponomaryov, and V.E. Bondybey, "Relaxation emission of electrons and photons from rare-gas solids: correlation and competition between TSL and TSEE", Phys. Stat. Sol (c) 4 (2007) 1088-1091.

14. G.B. Gumenchuk, A.M. Bludov, A.G. Belov, A.N. Ponomaryov, V.E. Bondybey and E.V. Savchenko,"Photon-stimulated charge recombination and exoelectron emission from pre-irradiated solid Ar", Phys. Stat. Sol. 4 (2007) 1151-1154.

15. G.B. Gumenchuk, A.N. Ponomaryov, A.G. Belov, E.V. Savchenko, and V.E. Bondybey, " Optically stimulated exoelectron emission from solid Ar irradiated by an electron beam", accepted to publication, FNT (Low Temperature Physics) 33 (2007).

16. A.N. Ponomaryov, E.V. Savchenko, G.B. Gumenchuk, I.V. Khizhniy, M. Frankowski, and V.E. Bondybey , "Thermoactivation spectroscopy of solid Ar doped with N2", accepted to publication, FNT (Low Temperature Physics) 33 (2007).

17. E.V. Savchenko, I.V. Khyzhniy, G.B. Gumenchuk, A.N. Ponomaryov, and V.E. Bondybey, "Relaxation channels and transfer of energy stored by pre-irradiated rare-gas solids", submitted to Radiation Measurements.

18. G.B. Gumenchuk, I.V. Khyzhniy, A.G. Belov, A.N. Ponomaryov, E.V. Savchenko, M. Bludov, S.A. Uyutnov, and V.E. Bondybey, "Desorption of "hot" molecules from pre-irradiated Ar solids", submitted to Surface Science.

19. E.V. Savchenko, G.B. Gumenchuk, I.V. Khyzhniy, A.N. Ponomaryov, and V.E. Bondybey, "Comparative study of electronically induced desorption from pre-irradiated solid Ar and Ar excited with an electron beam", submitted to Surface Science.

Conferences

Presentations at Scientific Conferences:

1. In Book of Abstracts of the 13th International Conference on Vacuum Ultra-violet Radiation Physics (VUV-13), Trieste, Italy, July 23-27 2001, p.Tu084.
   Savchenko E. V., Grigorashchenko O. N., Ogurtsov A. N., Rudenkov V. V., Gumenchuk G. B., Lorenz M., Smith-Gicklhorn A. M., Frankowsky M., Bondybey V. E.
   "Thermally assisted emission of electrons and VUV photons from irradiated rare gas solids."
   Poster

2. In Book of Abstracts Of the 20th European Conference On Surface Science (ECOSS-20), Krakow, Poland, Sept. 4-7, 2001, Volume29J, p. Th-P-83.
   Savchenko E. V., Grigorashchenko O. N., Ogurtsov A. N., Rudenkov V. V., Gumenchuk G. B., Lorenz M., Frankowsky M., Smith-Gicklhorn A. M., Bondybey V. E.
   "Photo- and thermally assisted emission of electrons from rare gas solids."
   Poster

3. In Book of Abstracts of the Euro-physical Conference on Defects in Insulating Materials (EURODIM-2002), Wroclaw, Poland, 1-5 July 2002, p. Tu-P.41.
   Savchenko E. V., Grigorashchenko O. N., Gumenchuk G. B., Ogurtsov A. N., Frankowsky M., Smith-Gicklhorn A. M., Bondybey V. E.
   "Defect-Related Relaxation Processes in Irradiated Rare Gas Solids."
   Poster

4. In Book of Abstracts of Fifth International Conference on Low Temperature Chemistry (LTC5), Berlin-Dahlem, Germany, 7-10 September 2004, p. 78.
   Gumenchuk G. B., Belov O. G., Bludov M. O.
   "Laser-induced recombination reaction of self-trapped holes with electrons in solid argon."
   Poster

5. In Book of Abstracts EURODIM 2006, 10th Europhysical Conference on Defects in Insulating Materials, July 10-14, 2006, Milano, University of Milano-Bicocca, Italy, p.343.
   E.V. Savchenko, G.B., Gumenchuk, M.O. Bludov, A.G. Belov, A.N. Ponomaryov, V.E. Bondybey
   "Photon-stimulated charge recombination and exoelectron emission from pre-irradiated solid Ar."
   Poster

6. In Book of Abstracts CC 2006, Sixth International Conference on Cryocrystals and Quantum Crystals, 3-7- September, Kharkov, Ukraine.P48, p.135.
   G.B. Gumenchuk, A.N. Ponomaryov, A.G. Belov, E.V. Savchenko, and V.E. Bondybey
   Optically stimulated exoelectron emission from solid Ar irradiated by an electron beam."
   Poster

7. In Book of Abstracts LUMDETR 2006 (6th European Conference on Luminescent Detectors and Transformers of Ionizing Radiation, June 19-23, Lviv, Ukraine, Tu-P25-DM, p.124.
   E.V. Savchenko, I.V. Khyzhniy, G.B. Gumenchuk, A.N.Ponomaryov, and V.E. Bondybey
   "Relaxation channels and transfer of energy stored by pre-irradiated rare-gas solids."
   Poster

8. In Book of Abstracts DIET XI International Workshop, 11-15 March 2007, Berlin, Germany, P17.
   G.B. Gumenchuk, I.V. Khyzhniy, A.G. Belov, A.N. Ponomaryov, E.V. Savchenko, M. Bludov, S.A. Uyutnov, and V.E. Bondybey
   "Desorption of "hot" molecules from pre-irradiated Ar solids."
   Poster

9. In Book of Abstracts DIET XI International Workshop, 11-15 March 2007, Berlin, Germany, P18.
   E.V. Savchenko, G.B. Gumenchuk, I.V. Khyzhniy, A.N. Ponomaryov, and V.E. Bondybey
   "Comparative study of electronically induced desorption from pre-irradiated solid Ar and Ar excited with an electron beam."
   Poster

Bibliography

[1]   *M. Akbulut, N.J. Sack, T. Madey*, Surf. Sci. Rep. 28 (1997) 177.

[2]   *V.A. Apkarian and N. Schwentner*, Chem. Rev. 99 (1999) 1481.

[3]   *I. Arakawa, T. Adachi, T. Hirayama, and M. Sakurai*, Low Temp. Phys. 29 (2003) 342.

[4]   *Balzer R. and Giersberg E-J*, Phys. Staus Solidi a 57 K141 (1980).

[5]   *R.A. Baragiola, M. Shi, R.A. Vidal, C.A.Dukes*, Phys. Rev. B58 (1998) 13212.

[6]   *C.S. Barret, L. Mayer*, J. Chem. Phys. 41, 1078 (1964).

[7]   *A.D. Bass, E. Vichnevetski, and L. Sanche*, Phys. Rev. B60 (1999) 14405.

[8]   *Becker, K.* Solid State Dosimetry C.R.C. Press, Boca Raton, Fla., 1973

[9]   *J. Becker, O. N. Grigorashchenko, A.N. Ogurtsov, M. Runne, E.V. Savchenko, G. Zimmerer*, J. Phys. D: Appl. Phys. 31 (1998) 749.

[10]   *J. Becker, O.N. Grigorashchenko, A.N. Ogurtsov, M. Runne, E.V. Savchenko, G. Zimmerer*, J. Phys. D: Appl. Phys. 31 (1998) 749.

[11]   *A.G. Belov, V.N. Svishchev, I.Ya. Fugol'*, Low Temp. Phys. 15 (1989) 61.

[12]   *A.G. Belov, E.M. Yurtaeva, I. Ya. Fugol'*, Low Temp. Phys. 26 (2000) 152.

[13]   *A.G. Belov, I.Ya. Fugol, E.M. Yurtaeva, O.V. Bazhan*, J. Lumin. 91 (2000) 107.

[14]   *V.E. Bondybey and E.V. Savchenko*, Phys. Stat. Sol., a 202, N 2, 221-227, (2005).

[15]   *V. E. Bondybey and T. A. Miller*, in Molecular Ions: Spectroscopy Structure and Chemistry, North-Holland Publishing Company, New York, 1983 pp.125-173.

[16]   *V.E. Bondybey, M. Räsänen, and A. Lammers*, Ann. Rep. Prog. Chem. C95, 331 (1999).

[17]   *Braunlich, P.* J. App. Phys., 1967 38, 1221, 2516.

[18]   *C. Bressler, M. Dickgiesser, N. Schwentner*, J. Chem. Phys. 107 (1997) 10268.

[19]   *Brian Brocklehurst and Georg C. Pimentel*, JCP 36, 2040 (1962).

[20]   *Brodribb J.D., Huges D.M. and Lewis T.J.,* Electrets, Charge Storage and transport in Dielectrics, ed. M.M. Perlman (Princeton, N.J.: Electrochemical Society) 1972.

[21]   *J.D.Brodribb, D. O'Colmain, and D. M. Hugers,* J. Phys. D: Appl. Phys. 8, 856 (1975).

[22]   *M.C. Castex*, in: Spectral Line Shapes, Vol. 4, ed. R.G. Exton (Deepak, Hampton, Virginia, 1987) p.289.

[23]   *A. Cenian and H. Gabriel*, J. Phys.: Condens. Matter 13 (2001) 4323.

[24]   *F. Coletti and J.M. Deveber*, J. Luminesc. 31 and 32 (1984) 927.

[25]   *F. Coletti, J.M. Debever, and G. Zimmerer*, J. Phys. Lett. 45, L-467 (1984).

[26]   *P.J. Le Comber, R.J. Loveland, W.E. Spear*, Phys. Rev. B11, 3124 (1975).

[27]   *Gerhard A. Cook*, Argon, Helium and the Rare Gases, Interscience Publishers by John Wiley & Sons, New-York, London, 1961.

[28]   *Daniels, F., Boyd, C.A., and Saunders, D.F.* Science, 1953, 117, 343.

[29]   *W.B. Daniels, G. Shirane, B.C. Frezer, H. Umebayashi, J.A. Leake*, Phys.Rev. Lett., 18, 548 (1967).

[30]   *A.V. Danilychev, V.A. Apkarian*, J. Chem. Phys. 99 (1993) 8617.

[31]   *R. Dersch, B. Herkert, M. Witt, H.-J. Stockmann, H. Ackermann*, Z. Phys. B: Condens. Matter 80 (1990) 39.

[32]   *O. Dossel, H. Nahme, R. Haensel, N. Schwentner*, J. Chem. Phys. 79, 665 (1983).

[33]   *V.D. M. Doyama, R.M.J. Cotterill*, Phys. Rev. 1 (1970) 832.

[34]   *S.D. Druger, R.S. Knox*, J. Chem. Phys. 50, 3143 (1969).

[35]   *G. Dujardin, L. P. M. Rose, T. Hirayama, M. J. Ramage, G. Comtet, and L. Hellner,* Appl. Phys., 1998, A66, 527.

[36]   *M.A. Elango*, Elementary Inelastic Radiation Induced Processes, American Institute of Physics, New York (1991).

[37] *O. Ellegaard, R. Pedrys, J. Schou, et. al.*, Appl. Phys. A46, 305 (1988).

[38] *Jussi Eloranta, Kari Vaskonen, Heikki Häkkänen, Toni Kiljunen, and Henrik Kunttu*, JCP 109, 7784 (1998).

[39] *L. Emery, K.S. Song*, J. Phys. C19, 2469 (1986).

[40] *M.E. Fajardo, V.A. Apkarian*, J. Chem. Phys. 89 (1988) 4124.

[41] *P. Feulner, T. Müller, A. Puschmann, and D. Menzel*, Phys. Rev. Lett. 59, 791 (1987).

[42] *P. Feulner and E.V. Savchenko (Eds.)*, Electronically induced phenomena: Low Temperature aspects, Low Temperature Physics 29 (2003) Special Issue 2.

[43] *J. Fournier, J. Deson, C. Vermeil, and G.C. Pimentel*, JCP 70, 5726 (1979).

[44] *M. Frankowscki*, Spectroscopy of Unstable and Charged Species in Cryogenic Solids, Dissertation, der Technische Universität München 2004.

[45] *M. Frankowski, E.V. Savchenko, A.M. Smith-Gicklhorn, O.N. Grigorashchenko, G. Gumenchuk, and V.E. Bondybey*, J. Chem. Phys. 121 (2004) 1474.

[46] *Frenkel Ja.*, On the transformation of light into heat in solids, II.- Phys. Rev., 1931, 37, p. 1279-1294.

[47] *Hun-rong Fu and K.S. Song*, J. Phys.: Condenc. Matter, 9 (1997) 9785.

[48] *I. Ya. Fugol'*, Adv. Phys. 27, 1 (1978).

[49] *I.Ya. Fugol' and E.V. Savchenko*, Excitons in Atomic Cryocrystals in "Cryocrystals", B.I. Verkin and A. Ph. Prikhot'ko (eds.), Naukova Dumka, Kiev (1983), p.360.

[50] *I.Ya.Fugol*, Adv. Phys., 37, 1 (1988).

[51] *Fukuda, Y., Tomita, A. and Takeushi, N.* Phys. Stat. Sol. (a), 1987, 99, K135.

[52] *Yu.B. Gaididei, V.M. Loktev, A.F. Prikhot'ko, L.I. Shanskii*, In Eds. B.I Verkin and A.F. Prikhot'ko Cryocrystals: Elementary excitations of solid oxygen, Naukova Dumka, Kiev, 1983, pp. 231-359.

[53] *Garlick, G.F.J., and Gibson, A.F.* Proc. Phys. Soc., 1948, 60, 574.

[54] *Gartia, R.K., Ratnam, V.V.* Ind. J. Pure Appl. Phys., 1975, 13, 82.

[55] *J. Goodman, L.E. Brus*, J. Chem. Phys. 67 (1977) 1482.

[56] *O.N. Grigorashchenko, S.A. Gubin, A.N. Ogurtsov, and E.V. Savchenko*, J Electron Spectroscopy & Related Phenomena 79 (1996) 107.

[57] *O.N.Grigorashchenko, A.N. Ogurtsov, E.V.Savchenko, J. Becker, M. Runne, and G. Zimmerer*, Surface Science 390 (1997) 277.

[58] *O.N. Grigorashchenko, O.M. Sokolov, E.V. Savchenko, J. Agreiter, N. Caspary, A. Lammers, V.E. Bondybey*, J. Rad. Effects and Defects in Solids 149 (1999) 197,

[59] *O.N. Grigorashchenko, V.V. Rudenkov, I.V. Khyzhniy, E.V. Savchenko, M. Frankowski, A.M. Smith-Gicklhorn, M.K. Beyer, and V.E. Bondybey*, Low Temp. Phys. 29 (2003) 876; FNT 29 (2003) 1147.

[60] *S. Guissi, R. Bindi, P. Iacconi, D. Jeambrun, and D. Lapraz*, J. Phys. D: Appl. Phys. 31, 137 (1998).

[61] *E. Gullikson*, Phys. Rev. B37, 7904 (1988).

[62] *G.B. Gumenchuk, M.A. Bludov, A.G. Belov*, Fiz. Nizk. Temp. 31,237 (2005) [Low Temp. Phys.] 31, 179 (2005).

[63] *G.B. Gumenchuk, A.M. Bludov, A.G. Belov, A.N. Ponomaryov, V.E. Bondybey and V.E. Savchenko*, Phys. Stat. Sol., (c) 4, 1151 (2007).

[64] *G.B. Gumenchuk, A.N. Ponomaryov, A.G. Belov, E.V. Savchenko, and V.E. Bondybey*, Fiz. Nizk. Temp. [Low Temp. Phys.] 33 (2007), accepted to publication.

[65] *Haering R.R. and Adams E.N.,* Phys. Rev., 1960, 117, 451.

[66] *S.S. Sai Halasz, A.J. Dahm*, Phys. Rev. Lett. 28, 1244 (1972).

[67] *Takato Hirayama, Akira Hayama, Takashi Adachi, Ichiro Arakawa, Makoto Sakurai*, Phys. Rev. B 63 (2001) 075407.

[68] *V. Hizhnyakov*, Phys. Rev. B 53 (1996) 13981.

[69] *Holzapfel, G., Krystek, M.* J. Phys. (Paris), 1976, 37, C-7-238.

[70] *Hoogenstraaten, W.* Philips Res. Rep., 1958, 13, 515.

[71] *A. Hoshino, T. Hirayama, and I. Arakawa,* Appl. Surf. Sci., 1993, 70&71, 308.

[72] *N.Itoh, A.M.Stoneham*, Materials Modification by Electronic Excitation, Cambridge University Press, Cambridge, 2001.

[73] *N. Itoh and A.M. Stonehman*, Radiation Effects & Defects in Solids 155, 277 (2001).

[74] *M. E. Jacox*, J. Mol. Spectr., 1985, 113, 286.

[75] *R.E. Johnson and J. Schou*, Mat. Fys. Med. K. Dan. Vidensk. Selsk. 43 (1993) 403.

[76] *R.E. Jonson, M. Inokuti*, Nucl. Instrum. Methods 206, 289 (1983).

[77] *R.E. Jonson, J. Schou, K. Dan*, Vidensk. Selsk. Mat. Phys. Medd. 43 (1993) 403.

[78] *M. Joppien, F. Grotelüschen, T. Kloiber, M. Legnen, T. Möller, J. Wörmer, G. Zimmerer, J. Keto, M. Kykta, M.C. Kastex*, J. Luminesc. 48-49 (1991) 601.

[79] *J. Jortner, L. Meyer, S.A. Rice et al.*, J. Chem. Phys. 42, N. 12, (1965) 4250-4253.

[80] *McKeever S.W.S., O'Colmain D. and Hugehes D.M.,* Procc. IEE Conf. On Dielectric Materials, Cambridge, 1975 (Stevenage:IEE).

[81] *L. Khriachtchev, M. Pettersson, S. Pehkonen, E. Isoniemi, M. Räsänen*, J. Chem. Phys. 11 (1999) 1650.

[82] *M. Kink, R. Kink, V. Kisand, J. Maksimov, M. Selg*, Nucl. Instr. and Meth. B 122 (1997) 668.

[83] *M. Kirm, H. Niedrais*, J. Luminesc. 60-61 (1994) 611.

[84] *Kittel C.*, Einfürung in die Festkörperphysik, 5 Auflage, Oldenburg Verlag, München (1980).

[85] *M.L. Klein, J.A. Venables*, Eds. Rare Gas Solids, vol.1, Academic, New York, 1976.

[86] *T. Kloiber*, Ph.D. Thesis University of Hamburg, Hamburg (1989).

[87] *T. Kloiber, and G. Zimmerer*, Phys. Scripta 41, 962 (1990).

[88] *F.V. Kusmartsev, E.I. Rashba*, Czech. J. Phys. B 32 (1982), 54.

[89] *Lampert M.A.,* Phys. Rev., 1956, 103, 1648.

[90] *M. Lanno, J.C. Bourgoin*, Point Defects in SemiconductorsII, Experimental Aspects, Springer Series in Solid-State Science, vol. 122, Springer, Berlin, 1981.

[91] *G. Leclerc, A.D. Bass, M. Michaud and L. Sanche*, J. Electron Spectr. Rel. Phenom. 52 (1990) 725.

[92] *G. Leclerc, A.D. Bass, A. Mann and L. Sanche*, Phys. Rev B 46 (1992) 4865.

[93]   *D.R. Lide (Ed.)*, Handbook of Chemistry and Physics, CRC Press, Boca Raton, FL 1993.

[94]   *R.J. Loveland, P.G. Le Comber, W.E. Spear*, Phys. Lett. A39, 225 (1972).

[95]   *Ch.B. Lushchik and A. Ch. Lushchik*, Decay of electronic excitations with defect formation in solids (Nauka, Moscow, 1989) (in Russian).

[96]   *L.E. Lyons, M.G. Sceats*, Chem. Phys. Lett. 6 (1970) 217.

[97]   *Marr G.V., West J.B.*, Absolute photoionisation cross section tables for Xe, Ne Ar and Kr in the VUV spectral regions, Atomic Data and Nucl. Data Tables, 1-76, V. 18, N. 2, p. 297-310.

[98]   *D. Menzel,* Appl. Phys., 1990, A51, 163.

[99]   *B. Meyer*, Low Temperature Spectroscopy, Elsevier, New York 1971.

[100] *L.S. Miller, S. Howe, W.E. Spear*, Phys. Rev. 166, 871 (1968).

[101] *C.E. Moore*, NBS Publication 467 (Washington, DC) Vol. 1, (1949), Vol. 2, (1952), Vol. 3, (1958).

[102] *M. Moskovits, G. Ozin (Eds.)*, Cryochemistry, John Wiley & Sons, New York, 1976.

[103] *V.D. Natsik, Y.I. Nazarenko*, Low Temp. Phys. 26 (2000) 210, FNT 26 (2000) 283.

[104] *V.D. Natsik, S.N. Smirnov, Y.I. Nazarenko*, Low Temp. Phys. 27 (2001) 958, FNT, 27, (2001) 1295.

[105] *Nicholas K.H. and Woods J.,* Br. J. Appl. Phys., 1964, 15, 783.

[106] *Nicholas K.H. and Woods J.,* Br. J. Appl. Phys., 1964, 15, 1361.

[107] *A.N. Ogurtsov, E.V. Savchenko, O.N. Grigorashchenko, S.A. Gubin, I.Ya. Fugol'*, Low Temp. Phys. 22 (1996) 922.

[108] *A. N. Ogurtsov, E. V. Savchenko, J. Becker, M. Runne, and G. Zimmerer,* J.Luminesc., 1998, 76&77, 478.

[109] *A.N. Ogurtsov*, Advances in spectroscopy of subthreshold inelastic radiation-induced processes in cryocrystals. In: E.C. Faulques et al. (eds.), Spectroscopy of Emerging Materials (NATO Science Series II. Mathematics, Physics and Chemistry – Vol. 165) Kluwer Academic Publishers, Dordrecht/-Boston/London (2004) 45–56.

[110] *Pedris R., Oostra D.J., Haring A. de Vries A.E. and Schou J.*, Nucl. Instr. Methods B33 (1988), 840.

[111] *R. Pedrys, D.J. Oostra, and A.E. de Vries*, in Desorption Induced by Electronic Trnasitions, DIET II, eds. W. Brenig and D. Menzel, Springer, Berlin, 1985, p.190.

[112] *R. Pedrys, D.J. Oostra, A. Haring, A.E. de Vries, and J. Schou*, Nucl. Instr. & Meth. Phys. Res. B 33 (1988) 640.

[113] *Pollack G.L.*, Rev. Mod. Phys. 36, 748 (1964).

[114] *A.N. Ponomaryov*, "NO TITEL YET", Dissertation, Technische Universität München 2007.

[115] *A.N. Ponomaryov, G. Gumenchuk, E. Savchenko and V.E. Bondybey*, Radiation Effects, "Energy Storage and its Release in Solid Rare Gases", PCCP 11 (2007).

[116] *Randall, J.T., and Wilkins, M.H.F.* Proc. Roy. Soc. Lond., 1945, 184, 366,390.

[117] *G. Raseev, G. Dujardin (Eds.),* Desorption Induced by Electronic Transitions DIET-9, North-Holland, Elsevier 2003.

[118] *C.T. Reimann, W.L. Brown and R.E. Johnson*, Phys. Rev. B 37 (1988), 1455.

[119] *C.T. Reimann, R.E. Jonson, and W.L. Brown*, Phys. Rev Lett. 53, 600 (1990).

[120] *C.T. Reimann, W.L. Brown, D.E. Grosjean, M.J. Nowakowski, W.T. Buller*, Phys.Rev. B45 (1992) 43.

[121] *D.G. Robbins*, J. Electrochem. Soc. 127 (1980) 2694.

[122] *U. Rössler*, Phys. Status Solidi 42, 345 (1970).

[123] *V. Saile*, Appl. Opt. 19, 4115 (1980).

[124] *E.V Savchenko, Yu.I. Rybalko and I.Ya. Fugol*, JETP Letters 42, (1985) 260.

[125] *E.V. Savchenko, Yu.I. Rybalko, I.Ya. Fugol*, Sov. J. Low Temp.Phys. 14 (1988) 220.

[126] *E.V. Savchenko, I.Ya. Fugol, O.N. Grigorashchenko, S.A. Gubin, A.N. Ogurtsov*, Low.Temp. Phys. 19 (1993) 418, (FNT, 19 (1993) 586).

[127] *E.V. Savchenko, A.N. Ogurtsov, O.N. Grigorashchenko, S.A. Gubin*, Chem. Phys. 189 (1994) 415-426.

[128] *E.V. Savchenko, A.N. Ogurtsov, O.N. Grigorashchenko, S.A. Gubin*, Low Temp. Phys. 22 (1996) 926; FNT 22 (1996) 1210.

[129] *E.V. Savchenko, T. Hirayama, A. Hayama, T. Koike, T. Koninobu, I. Arakawa, K. Mitsuke, M. Sakurai*, Surf. Sci. 390 (1997) 261.

[130] *E.V. Savchenko, A.N. Ogurtsov, O.N. Grigorashchenko*, Phys. The Solid State, V. 40, N. 5, (1998), 831.

[131] *E.V. Savchenko, N. Caspary, A. Lammers, V.E. Bondybey*, J. Low Temp. Phys. 111 (1998) 693,

[132] *E.V. Savchenko, O.N. Grigorashchenko, O.M. Sokolov, J. Agreiter, N. Caspary, A. Lammers, V.E. Bondybey*, J. Electron. Spectrosc. And Relat. Phenom. 101-103 (1999) 377.

[133] *E.V. Savchenko, O.N. Grigorashchenko, A.N. Ogurtsov, V.V. Rudenkov, G.B. Gumenchuk, M. Lorenz, A. Lammers, V.E. Bondybey*, J. Low Temp. Phys. 122 (2001) 379.

[134] *E.V. Savchenko, O.N. Grigorashchenko, A.N. Ogurtsov, V.V. Rudenkov, M. Lorenz, M.Frankowski, A.M. Smith- Gicklhorn, V.E. Bondybey*, J. Luminecence 94-95 (2001) 475.

[135] *E.V. Savchenko, O.N. Grigorashchenko, A.N. Ogurtsov, V.V. Rudenkov, G.B. Gumenchuk, M. Lorenz, M. Frankowski, A.M. Smith-Gicklhorn, V.E. Bondybey*, Surf. Sci. 507-510 (2002) 754.

[136] *E.V. Savchenko, O.N. Grigorashchenko, A.N. Ogurtsov, V.V. Rudenkov, G.B. Gumenchuk, M. Lorenz, A.M. Smith-Gicklhorn, M. Frankowski, and V.E. Bondybey*, "Thermally assisted emission of electrons and VUV photons from irradiated rare gas solids", Surf. Rev. & Lett. 9 (2002) 353-358.

[137] *E.V. Savchenko, O.N. Grigorashchenko, G.B. Gumenchuk, A.N. Ogurtsov, M. Frankowski, A.M. Smith-Gicklhorn, and V.E. Bondybey*, Radiation Effects & Defects in Solids 157, (2002), 729.

[138] *E.V. Savchenko, O.N. Grigorashchenko, G.B.Gumenchuk, A.G.Belov, E.M. Yurtaeva, M. Frankowski*, A.M. Smith-Gicklhorn, and V.E. Bondybey, Surface Science, 528 (2003) 266.

[139] *E.V. Savchenko, A.N. Ogurtsov, and G. Zimmerer*, Low Temp. Phys. 29 (2003) 270, (FNT 29 (2003) 356).

[140] *E.V. Savchenko, G.B. Gumenchuk, E.M. Yurtaeva, A.G.Belov, I.V. Khizhniy, M. Frankowski, M.K. Beyer, A.M. Smith-Gicklhorn, A.N. Ponomaryov, V.E. Bondybey*, "Anomalous low-temperature desorption from preirradiated rare gas solids", J. Luminescence 112 (2005) 101-104.

[141] *E.V. Savchenko, O.N. Grigorashchenko, G.B. Gumenchuk, A.G. Belov, E.M. Yurtaeva, I.V. Khyzhniy, M. Frankowski, M.K. Beyer, A.M. Smith-Gicklhorn, and V.E. Bondybey*, "Anomalous Phenomena on Surfaces of Pre-irradiated Cryocrystals", J. Low Temp. Phys. 126 (2005) 621-631.

[142] *Elena Savchenko, Alexander Ogurtsov, Ivan Khyzhniy, Gregory Stryganyuk, Georg Zimmerer*, Phys. Chem. Chem. Phys. 7 (2005) 785.

[143] *E.V. Savchenko, A.G. Belov, G.B.Gumenchuk, A.N. Ponomaryov, and V.E. Bondybey*, ”Oxygen-driven processes in pre-irradiated Ar cryocrystals”, Fizika Nizkikh Temperatur (Low Temperature Physics), Special Issue on Low Temperature Spectroscopy and Optics, 32 (2006) 1417-1425.

[144] *E.V. Savchenko, G.B. Gumenchuk, I.V. Khyzhniy, A.N. Ponomaryov, and V.E. Bondybey*, ”Comparative study of electronically induced desorption from pre-irradiated solid Ar and Ar excited with an electron beam”, Surface Science, accepted to publication.

[145] *E.V. Savchenko, I.V. Khyzhniy, G.B.Gumenchuk, A.N. Ponomaryov, M.K. Beyer, M. Frankowski, and V.E. Bondybey*, ”Photo- and thermally stimulated relaxation processes in pre-irradiated atomic solids”, Radiation Physics and Chemistry, 76 (2007) 577-581.

[146] *E.V. Savchenko, I.V. Khyzhniy, G.B. Gumenchuk, A.N. Ponomaryov, and V.E. Bondybey*, ”Relaxation channels and transfer of energy stored by pre-irradiated rare-gas solids”, submitted to Radiation Measurements.

[147] *E.V. Savchenko, I.V. Khyzhniy, G.B. Gumenchuk, A.N. Ponomaryov, and V.E. Bondybey*, ”Relaxation emission of electrons and photons from rare-gas solids: correlation and competition between TSL and TSEE”, Phys. Stat. Sol (c) 4 (2007) 1088-1091.

[148] *H. Schlichting*, Die Dissertation, Technische Universität München, 1990.

[149] *J. Schou*, Nucl. Instr. And Meth. B27 (1987) 188.

[150] *A. Schrimpf, C. Boekstiegel, H.-J. Stockman, T. Bornemann, K. Ibbeken, J. Kraft, B. Herkert*, J. Phys. Condens. Matter 8 (1996) 3677.

[151] *K.W. Schwarz*, Phys. Rev. A6, 837 (1972).

[152] *N. Schwentner, F.J. Himpsel, V. Saile, M. Skibowski, W. Steinmann, E.E. Koch*, Phys. Rev. Lett. 34, 528 (1975).

[153] *N.Schwentner, E.E. Koch, and J. Jortner*, Electronic Excitation in Condensed Rare Gases, v. 107 Tracts Mod. Phys, Springer, Berlin, 1985.

[154] *D.J.O'Shaughnessy, J.W. Boring, S. Cui, R.E. Jonson*, Phys. Rev. Lett. 61, 1635 (1988b).

[155] *D.J. O'Shaugnessy, J.W. Boring, S. Cui, and R.E. Johnson*, Phys. Rev. Lett. 61 (1988) 1635.

[156] *Richard R. Smardzewski*, JCP 68, 2878 (1978).

[157] *K.S. Song*, Can. J. Phys. 49, 26 (1971).

[158] *K.S. Song and R.T. Williams*, Self-Trapped Excitons, Springer Series in Solid-State Sciences, Springer Verlag, Berlin (1996), Vol. 105.

[159] *Spurny, Z. and Kaambre, H.* in: Techniques of Radiation Dosimetry (k. Manesh and D.R. Vij, Eds.) (John Wiley, Chichester), 1985, p.281.

[160] *Hudel E. Steinacker E. and P. Feulner*, Phys. Rev. B 44 (1991), 8972.

[161] *D.S. Tinti and G.W. Robinson*, J. Chem. Phys. 49, (1968), 3229.

[162] *Tomita, A. Hirai, N., and Tsutsumi, K.* Jpn. J. App. Phys., 1976, 15, 1899.

[163] *Townsend, P.D.* Radiat. Meas., 1994, 23, 341.

[164] *Uchrin, G.* Radiat. Prot. Dosim., 1993, 47, 595.

[165] *M. Ueta, H. Kanzaki, K. Kobayashi, Y. Toyozawa, E. Hanamura*, Excitonic Processes in Solids, Springer Ser. Solid-State Sci., vol. 60, (Springer, Berlin, Heidelberg 1986) Chap.5.

[166] *M. Umechara*, Phys.Rev. B 33, 4237, (1986).

[167] *Urbach, F.* Wiener Berichte, 1930, 139, 363.

[168] *T. Vaness*, Nachweis und Characterisierung von Elektronenfallen in festen Edelgasen, Disssertation, der Universität Hamburg 1990.

[169] *D.R. Vij*, Thermoluminescence, in: D.R. Vij (Ed.) Luminescence of Solids, Plenum Press, New York, (1998).

[170] *Wannier G.H.*, The structure of electronic excitation levels in insulating crystals. Phys. Rev., 1937, 52, p. 191-197.

[171] *P. Wiethoff, B. Kassühlke, D. Menzel, and P. Feulner*, Low Temp. Phys. 29 (2003) 266, (FNT, 2003, v. 29, No. 3, 351).

[172] *J.M. Ziman*, Principles of the Theory of Solids, Cambridge University Press 1972.

[173] *G.Zimmerer*, Creation, Motion and Decay of Excitons in Rare-Gas Solids, in: Excited-State Spectroscopy in Solids, Ed. by U.M.Grassano and N.Terzi, North-Holland, Amsterdam (1987) p. 37.

[174] *G. Zimmerer*, Nucl. Instrum. & Methods, Phys. Res. B91, 601 (1994),

[175] *G. Zimmerer*, J Low Temp. Phys. 111 (1998) 629.